Analytical and Experimental Analyses of Isotropic and Anisotropic Magnetoactive Elastomers

Alireza Beheshti Kisomi

A Thesis

In the Department

of

Mechanical, Industrial and Aerospace Engineering

Presented in Partial Fulfillment of the Requirements

For the Degree of

Doctor of Philosophy (Mechanical Engineering) at

Concordia University

Montreal, Quebec, Canada

March 2020

CONCORDIA UNIVERSITY

SCHOOL OF GRADUATE STUDIES

This is to certify that the thesis prepared

By: Alireza Beheshti Kisomi

Entitled: Analytical and Experimental Analyses of Isotropic and Anisotropic Magnetoactive Elastomers

and submitted in partial fulfillment of the requirements for the degree of

Doctor of Philosophy (Mechanical Engineering)

complies with the regulations of the University and meets the accepted standards with respect to originality and quality.

Signed by the final examining committee:

_____ Chair
Dr. William E. Lynch

_____ External Examiner
Dr. Ruxandra Botez

_____ External to Program
Dr. Khaled Galal

_____ Examiner
Dr. Waiz Ahmed

_____ Examiner
Dr. Muthu Packirisamy

_____ Thesis Supervisor
Dr. Ramin Sedaghati

_____ Thesis Supervisor
Dr. Subhash Rakheja

Approved by _____
Dr. Ali Dolatabadi Chair of Department or Graduate Director

April 15, 2020 _____
Dr. Amir Asif, Dean Faculty of Engineering and Computer Science

ABSTRACT

Analytical and Experimental Analyses of Isotropic and Anisotropic Magnetoactive Elastomers

Alireza Beheshti Kisomi, Ph.D.

Concordia University, 2020

Magnetoactive elastomers (MAEs) are emerging smart materials, which exhibit rapid and reversible variations in the viscoelastic properties under an applied magnetic field. While response behaviors of these novel materials have been widely studied using phenomenological based approaches, only a few studies have attempted the physics based analyses of MAEs. The main aim of the present thesis research is to develop a continuum based formulation considering the magneto-elastic coupling for predicting the quasi-static behavior of both the isotropic and anisotropic MAEs undergoing small and finite deformations. Firstly, the constitutive magneto-mechanical equations for an isotropic magnetoactive medium are formulated considering the principle of material objectivity. A stored energy density function has been introduced with respect to the invariants of the Cauchy-Green deformation tensor and the magnetic field induction vector. The proposed function is subsequently used to develop a material model for finite deformation analysis of the isotropic MAEs. A linearization scheme has also been implemented to formulate a small-deformation theory for the isotropic material.

In the second part, a novel energy density function for an incompressible transversely-isotropic deformable magnetic solid has been presented in terms of some invariants based on both the mechanical and magnetic anisotropy. The proposed energy density function is effectively used to formulate a coupled magneto-elastic model of the transversely-isotropic MAEs.

The validity of the proposed models is demonstrated through comparisons of the model responses with the laboratory measured characteristics. For this purpose, the isotropic and transversely-isotropic cylindrical MAEs were fabricated in the laboratory by mixing silicon rubber with micron-sized carbonyl iron particles (15% volume fraction). The mixture was cured in the absence and presence of the external magnetic field, respectively, to realize isotropic and anisotropic structures. An experimental set-up was designed to accurately measure the relative permeability of the isotropic and anisotropic samples. The torsion-deflection characteristics of the MAEs were also measured under varying applied magnetic field by utilizing a magneto-rheometer.

The measured data were used to examine validity of the proposed models and to identify parameters of constitutive equations for both the isotropic and anisotropic MAEs. The comparison revealed reasonably good agreements between the analytical and experimental results. The proposed models could thus serve as essential tools for designing MAE-based devices for noise and vibration control applications.

ACKNOWLEDGMENT

First and foremost, I must appreciate guidance, support and mentorship of my doctoral dissertation advisors, Professor Ramin Sedaghati and Professor Subhash Rakheja.

I would like also to thank all my friends and colleagues for their support and assistance in completing the PhD thesis at Concordia University.

TABLE OF CONTENTS

LIST OF FIGURES

LIST OF TABLES

NOMENCLATURE

t	time
$\mathbf{x}$	spatial position vector
$\boldsymbol{\varphi}$	deformation function
$\mathbf{X}$	material position vector
$\mathbf{u}$	displacement vector
$\mathbf{F}$	deformation gradient tensor
$\mathbf{C}$	right Cauchy-Green deformation tensor
I_1	first invariant of $\mathbf{C}$
I_2	second invariant of $\mathbf{C}$
I_3	third invariant of $\mathbf{C}$
$\mathbf{E}$	Green-Lagrange strain tensor
$\mathbf{G}$	left Cauchy-Green deformation tensor
$\mathbf{R}$	orthogonal rotation tensor
$\mathbf{U}$	right stretch tensor
$\mathbf{V}$	left stretch tensor
λ_i	principal stretches
$\mathbf{v}$	velocity vector
$\mathrm{d}v$	spatial volume element
$\mathrm{d}V$	reference volume element
J	determinant of deformation gradient tensor
$\mathrm{d}a$	spatial area element
$\mathrm{d}A$	material area element

$\mathbf{n}$	spatial normal unit vector
$\mathbf{N}$	material normal unit vector
G	shear modulus or Lamé's second parameter
λ	Lamé's first parameter
$\mathbf{A}$	unit chain vector of a transversely isotropic medium
$\mathbf{a}$	deformed chain vector
I_4	first mixed invariant of a transversely isotropic material
I_5	second mixed invariant of a transversely isotropic material
G_T	transverse shear modulus
G_L	longitudinal shear modulus
E_L	longitudinal Young's modulus
$\mathbf{I}$	identity tensor
$\boldsymbol{\sigma}$	Cauchy stress tensor
$\mathbf{B}$	magnetic field induction in rigid-body state
$\mathbf{H}$	magnetic field strength in rigid-body state
$\mathbf{M}$	magnetization vector in rigid-body state
μ_0	permeability in vacuum
$\boldsymbol{\mu}^{\mathrm{r}}$	relative permeability tensor
$\boldsymbol{\chi}$	susceptibility tensor
μ^r	relative permeability of an isotropic material
χ	susceptibility of an isotropic material
M_s	saturation magnetization
δ	scaling factor

ρ	spatial density
$\mathbf{t}^{(\mathbf{n})}$	traction vector
$\mathbf{f}$	magnetic body force
$\overline{\mathbf{f}}$	mechanical body force
$\mathbf{l}$	magnetic body couple
u	internal energy per unit mass
ϕ	magnetic energy
$\mathbf{b}$	Eulerian magnetic field induction
$\mathbf{h}$	Eulerian magnetic field strength
$\mathbf{m}$	Eulerian magnetization
$\boldsymbol{\eta}$	dual of magnetic couple
ε_{ijk}	permutation symbol
μ	permeability of an isotropic material
$\boldsymbol{\sigma}^{S}$	magnetic stress tensor
$\mathbf{P}$	nominal stress tensor
ρ_0	referential density
U^T	total internal energy
W	stored energy function
$\tilde{\mathbf{B}}$	Lagrangian magnetic field induction
I_6	first mixed magneto-mechanical invariant
I_7	second mixed magneto-mechanical invariant
I_8	third mixed magneto-mechanical invariant
G^*	nominal shear modulus

λ^*	nominal Lamé's first parameter
$\hat{\mathbf{b}}$	variational magnetic field induction
$\hat{\mathbf{h}}$	variational magnetic field strength
$\hat{\mathbf{m}}$	variational magnetization
$\mathbf{e}$	infinitesimal strain tensor
θ	angle of rotation
κ	angle of twist per unit length
T	applied torque
$\mathbf{e}_i$	Eulerian Cartesian unit base vectors
$\mathbf{E}_i$	Lagrangian Cartesian unit base vectors
I_9	first mixed magneto-mechanical invariant related to anisotropy
I_{10}	second mixed magneto-mechanical invariant related to anisotropy
$\mathbf{Q}$	orthogonal rotation tensor

CHAPTER 1

INTRODUCTION

1.1 Motivation

The elastomers are typically treated as hyperelastic materials capable of undergoing large deformation elastically and returning to the original configuration upon removal of the load [1]. Based on the definition, the main characteristic of elastomeric materials is their high elongation and flexibility or elasticity, versus failure. When iron particles are dispersed in an elastomeric matrix, the final medium is generally called the particle-reinforced elastomer [2]. Furthermore, the medium enriched by iron particles becomes a magnetoactive elastomer (MAE), when subjected to an external magnetic field. It should be noted that magnetorheological elastomers (MREs) are basically magnetoactive materials (MAEs) in which the host elastomeric medium behaves as a viscoelastic material. The term MAEs and MREs are commonly used interchangeably in the literature such as the work of Rudykh and Bertoldi [3], in which the iron-particles reinforced medium under the influence of the magnetic field is referred to as the MRE without consideration of the viscous effect. Generally two physics-based approaches are adopted in the deformation analysis of magnetoactive elastomers, namely, the continuum-based (or macro-mechanical) and micro-mechanical methods. In the continuum-based approach, the role of micron sized particles embedded in the matrix is incorporated in an implicit manner. In the micromechanical scheme, however, the behavior of the MAEs is evaluated considering the microstructure of the medium.

As the dynamic characteristics of MAEs can be continuously and adaptively changed under the applied magnetic field, they can be effectively utilized for design of adaptive systems and devices for control of noise and vibration under a wide range of frequencies and varying environmental conditions [4]. Furthermore, the coupled magneto-mechanical properties of MAE render them suitable for sensors and actuators applications [5].

This dissertation research is concerned with quasi-static analyses of isotropic and transversely isotropic MAEs undergoing mechanical and magnetic loadings using the continuum-based approach. Firstly, the constitutive equations for a deformable magnetic solid are treated for an isotropic medium in terms of some invariants and laboratory experiments are undertaken on the fabricated samples in order to characterize magnetic properties and torque-twist responses of the MAE. The second part of the thesis focuses on treatment and development of magneto-mechanical constitutive models of transversely isotropic MAEs.

In this chapter, a review of the relevant studies is presented to build essential knowledge on the methods of analyses and to construct the scope of thesis. The essential fundamentals of nonlinear elasticity are presented together with widely used hyperelastic models for the isotropic and transversely isotropic elastomers. The principles associated with the magnetic materials are presented, and the frameworks and formulations related to finite deformations of the electro-magneto-mechanical solids are discussed. The scope of the thesis research and the objective are presented subsequently.

1.2 Review of Literature

The fundamental aspect of the finite elasticity of the solids is first discussed. This is then followed by reviewing studies addressing developments of constitutive equations of elastomers and MAEs.

1.2.1 Finite Elasticity of Solids

Reported studies on finite deformation of solids have provided essential insight into common hyperelastic models implemented for isotropic and transversely isotropic elastomers. These are briefly discussed below.

1.2.1.1 Kinematics

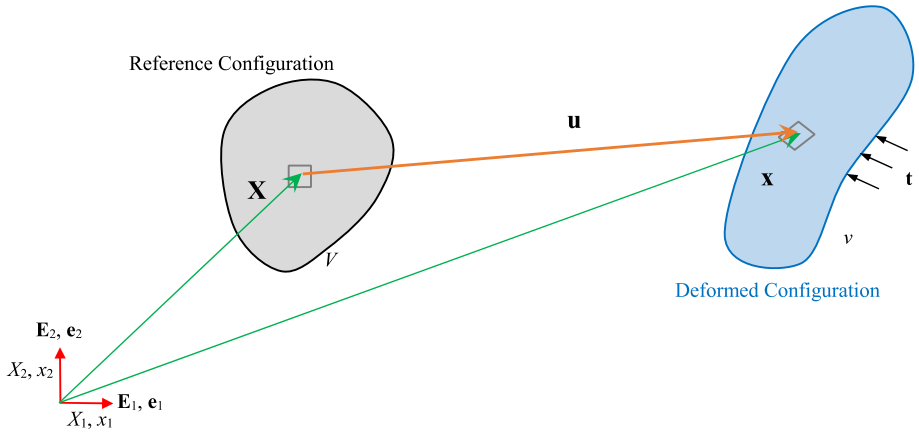

Figure 1-1. Deformed and undeformed configurations of a body.

In solid mechanics, two configurations are generally defined involving deformed (spatial) and reference (material) configurations to formulate governing equations for finite deformation analysis of a medium [6, 7]. The former is associated with the state of the body after application of the loading and the latter is concerned with the undeformed state of body at time $t = t_0$. Referring to Figure 1-1, let $\mathbf{X}$ define the position vector of a particle of the body in the undeformed configuration, and vector $\mathbf{x}$ describe the position of the same particle in the deformed configuration. Moreover, let the deformed and undeformed bodies occupy the domains v and V, respectively. There exists a one-to-one map between two configurations and the deformation function $\boldsymbol{\varphi}$ can be defined as:

$$\mathbf{x} = \boldsymbol{\varphi}(\mathbf{X}, t) \tag{1.1}$$

In addition, the displacement vector for the particle can be expressed as:

$$\mathbf{u} = \mathbf{x} - \mathbf{X} \tag{1.2}$$

The basic kinematic tensor in solid mechanics is described by the deformation gradient $\mathbf{F}$, defined as the gradient of the deformation function, such that:

$$\mathbf{F} = \frac{\partial \boldsymbol{\varphi}}{\partial \mathbf{X}} = \boldsymbol{\varphi} \nabla_{\mathbf{X}} \tag{1.3}$$

Assuming that the material line element $d\mathbf{X}$ deforms to the spatial line element $d\mathbf{x}$ after the application of a deformation, the deformation of the line element can be estimated from the deformation gradient as [6]:

$$d\mathbf{x} = \mathbf{F}.d\mathbf{X} \tag{1.4}$$

The large magnitude deformation of solids are generally analyzed using the right Cauchy-Green deformation tensor, **C**. Since the base vectors of this tensor are delineated with respect to the material frame (reference coordinate), it is referred to as the material tensor and defined as:

$$\mathbf{C} = \mathbf{C}^T = \mathbf{F}^T.\mathbf{F} \tag{1.5}$$

where the superscript T denotes transpose. The constitutive equations for hyperelastic materials are generally formulated using invariants of the right Cauchy-Green deformation tensor which are given by [6]:

$$I_1(\mathbf{C}) = tr(\mathbf{C}) \tag{1.6}$$

$$I_2(\mathbf{C}) = \frac{1}{2}[tr(\mathbf{C})^2 - tr(\mathbf{C}^2)] \tag{1.7}$$

$$I_3(\mathbf{C}) = \det(\mathbf{C}) \tag{1.8}$$

Subsequently, the Green-Lagrange strain tensor, **E**, is defined as [6]:

$$\mathbf{E} = \frac{1}{2}(\mathbf{C} - \mathbf{I}) \tag{1.9}$$

The left Cauchy-Green deformation tensor, **G**, is also related to the deformation gradient as [6]:

$$\mathbf{G} = \mathbf{G}^T = \mathbf{F}.\mathbf{F}^T \tag{1.10}$$

It is noted that since the base vectors of left Cauchy-Green deformation tensor are generally defined with respect to the spatial frame, it is referred to as the spatial or Eulerian tensor.

Additionally, it can be shown that the right and left Cauchy-Green deformation tensors have the same invariants, given by [6]:

$$I_1(\mathbf{C}) = I_1(\mathbf{G}) = tr(\mathbf{G}) \tag{1.11}$$

$$I_2(\mathbf{C}) = I_2(\mathbf{G}) = \frac{1}{2}[tr(\mathbf{G})^2 - tr(\mathbf{G}^2)] \tag{1.12}$$

$$I_3(\mathbf{C}) = I_3(\mathbf{G}) = \det(\mathbf{G}) \tag{1.13}$$

It is feasible to decompose the deformation gradient multiplicatively into two parts involving an orthogonal tensor **R**, describing a rigid rotation, and a right or left stretch tensor, denoted by **U** or **V**, respectively, such that [6]:

$$\mathbf{F} = \mathbf{R}.\mathbf{U} = \mathbf{V}.\mathbf{R} \tag{1.14}$$

From the definition of **C** and **G**, it can be shown that the relations $\mathbf{C} = \mathbf{U}^2$ and $\mathbf{G} = \mathbf{V}^2$ hold due to the orthogonally of the tensor **R** [6]. A study has formulated a model based on the eigenvalues of the material and spatial stretch tensors, **U** and **V** [8]. The eigenvalues for the two tensors are identical, often denoted as principle stretches, and expressed by λ_i.

The velocity vector of a particle of the body can be obtained from time derivative of the deformation function as:

$$\mathbf{v} = \frac{d}{dt}\boldsymbol{\varphi}(\mathbf{X}, t) = \dot{\boldsymbol{\varphi}}(\mathbf{X}, t) \tag{1.15}$$

Considering the hyperelasticity, it is preferable to express relations with respect to the reference configuration. The spatial volume and surface elements are related to the corresponding material pairs through the following relations:

$$dv = JdV \tag{1.16}$$

$$da\ \mathbf{n} = J\ dA\ \mathbf{F}^{-T}.\mathbf{N} \tag{1.17}$$

where $J = \det(\mathbf{F})$, and **n** and **N** are unit normal vectors to the spatial and material surfaces, respectively. The relation given in Eq. (1.17) is also known as Nanson's formula, which is used to convert the material area of an element to its corresponding spatial one and vice versa.

1.2.1.2 Isotropic Hyperelastic Models

A number of material models have been reported for finite deformation analyses of incompressible elastomers. The modified forms of the models have been applied to generate stress tensor for MAEs [9, 10]. The reported constitutive equations for elastomers have provided essential basis for deriving suitable stored energy functions from the stress-strain characteristics. The large deformation under the application of an external load within the elastic regime constitutes the primary features of rubbers. Moreover, the loading and unloading paths are ideally the same for pure hyperelastic materials and more importantly there is no residual deformation, which distinguishes them from other solids such as plastics [11, 12]. The vast majority of models proposed to predict the rubber behavior are based on nonlinear stress-strain characterizations. Generally, the reported studies have employed two different methods for developing the constitutive equations of elastomers, namely, the macro-mechanics and micro-mechanics approaches [13]. In the macro-mechanics or continuum-based approach, one

essentially deals with the problem without addressing constituents of the material. In other words, the continuum-based approach is concerned with the global behavior of the material in macro-scale. In the micro-mechanics approach, the focus is on the microscopic features of the medium. In other words, the role of polymer chains network and statistical schemes are considered for deriving the constitutive equations [14-16]. Since the present dissertation research is focused on the finite deformation analysis using the continuum approach, the following discussions are limited only to the continuum methods.

Rubbers may also exhibit viscoelastic behavior particularly under loading at relatively high strain rates, which would necessitate consideration of the dissipation of energy properly. The natural rubbers, however, exhibit relatively small damping, generally considered negligible [17, 18]. Even for high damping rubbers, in which the deformation is reversible but the loading and unloading paths are not same, the hyperelastic models can be applied for characterizing stress-strain characteristics during the loading [19]. Treloar [19] conducted various experiments on rubbers including two-dimensional extension, simple elongation, pure shear and combined shear and elongation. A number of hyperelastic material models have evolved during the past decades [8, 14]. These have employed the experimental data identification and verifications of various material models proposed for rubbers [20].

Rubbers are used as a matrix in the fabrication of magnetoactive elastomers. Pure rubbers may be categorized into two main groups, namely, natural and latex rubbers [19]. While the natural rubbers exhibit negligible dissipation of the energy, the latex rubbers exhibit notable rheological features [17], which are adequately described by a rate-dependent constitutive equation. In this case, the free energy density is a function of the strain tensor and its derivative with respect to time. For the cases in which a latex rubber is used as the matrix in the production of MAEs, it is crucial to take the damping property of the matrix into account. The main step in the visco-hyperelasticity is the decomposition of the deformation gradient into two parts including the elastic and viscous constituents. A few studies have suggested that the modified version of the generalized Maxwell model for analysis of finite deformations can also describe the behavior of the latex rubbers [21].

The building block in the formulation and development of constitutive equations for hyperelastic materials is the free strain energy density function. The simplest and well-known

model for the analysis of the hyperelastic materials is the Kirchhoff-Saint Venant model which is basically the modified version of the Hooke's law and is obtained by replacing the so-called infinitesimal strain tensor with the Green-Lagrange strain tensor [6]. In this model, the strain energy function, W, is described as [22]:

$$W = \lambda[tr(\mathbf{E})]^2 / 2 + G\mathbf{E} : \mathbf{E} \tag{1.18}$$

where G and λ are called the Lame's constants.

It should be noted that the models based on the invariants of the Cauchy-Green deformation tensor or the principal stretches are considered to be more suited for finite deformation analyses of rubber-like materials [8, 14]. The most practical material models are grouped into three categories, namely, involving I_1-based model, I_1 and I_2-based model, and a model in terms of the principle stretches. These are briefly described below.

We begin with the neo-Hookean material model which is specified in terms of the first invariant of the tensor **C** and the associated stored energy is [13]

$$W = C_{10}(I_1 - 3) \tag{1.19}$$

where $C_{10} = G/2$ considering the consistency with the linear elasticity. The model was firstly elaborated using the micromechanical approach, whose the material constant is estimated from microscopic information of the material. Owing to its simplicity, the I_1-based model has been widely used during the past few decades. It has been shown that the neo-Hookean model provides reasonably accurate model properties for medium level strains (<150%) [13].

Building upon the micro-mechanical approach, Arruda and Boyce [14] developed a model considering the following five terms in the strain energy function:

$$W = \sum_{i=1}^{5} \frac{C_i}{N^{i-1}} (I_1^i - 3^i) \tag{1.20}$$

where C_i are material constants and N stands for the number of segments per unit polymer.

Yeoh [23] characterized large deformation of elastomers using the following energy density:

$$W = \sum_{i=1}^{3} C_i (I_1 - 3)^i \tag{1.21}$$

Additionally, the following strain energy function was proposed by Gent [24]:

$$W = -J_m \frac{G}{2} Ln(1 - \frac{I_1 - 3}{J_m}) \tag{1.22}$$

where J_m is a material constant.

Similarly, Lopez-Pamies [25] proposed a material model considering the first invariant of Cauchy-Green deformation tensor as:

$$W = \sum_{i=1}^{N} \frac{3^{1-\alpha_i}}{2\alpha_i} G_i (I_1^{\alpha_i} - 3^{\alpha_i}) \tag{1.23}$$

It is noted that the above model is very close to Arruda-Boyce model presented in Eq. (1.20). The exponent of I_1 in the reported model is considered as an integer varying from 1 to 5. Among the above-stated I_1-based models, the Lopez-Pamies model exhibits relatively more flexibility.

The general form of a material model originated by Rivlin and Saunders [26] on the basis of the first and the second invariants of the deformation tensor for incompressible materials is expressed as:

$$W = \sum_{i=0,=0}^{\infty} C_{ij} (I_1 - 3)^i (I_2 - 3)^j, \qquad C_{00} = 0 \tag{1.24}$$

where C_{ij} are material unknowns. It is worth noting that many hyperelastic models are indeed a simplification of the model in Eq. (1.24).

Mooney [27] proposed a model for rubber-like materials in which the free energy function is described as:

$$W = C_{10}(I_1 - 3) + C_{01}(I_2 - 3) \tag{1.25}$$

The two constants C_{10} and C_{01} are identified by comparison of theoretical results with the experimental data. In the literature, this material model is frequently known as the Mooney-Rivlin model. Furthermore, for moderate strains up to 250%, the Mooney-Rivlin material model is known to yield accurate prediction of the material behaviour in an efficient manner [13]. Moreover, the I_1-based neo-Hookean model can be derived from the Mooney-Rivlin model, by letting C_{01}=0.

Gent and Thomas [28] also proposed an I_1 and I_2-based model for describing the energy function as:

$$W = C_1(I_1 - 3) + C_2 Ln(I_2 / 3) \tag{1.26}$$

where C_1 and C_2 are the unknowns of this material model.

Ogden [29] proposed a material model using the principle stretches in place of the invariants, and demonstrated its validity through experiments. The model is widely used for different elastic materials, and is known to yield accurate prediction, particularly under large strains. The Ogden model states the energy function, as:

$$W = \sum_{i=1}^{N} \frac{G_i}{\alpha_i} (\lambda_1^{\alpha_i} + \lambda_2^{\alpha_i} + \lambda_3^{\alpha_i} - 3) \tag{1.27}$$

where G_i and α_i are material constants, λ_k ($k = 1, 2, 3$) are principle stretches. The above model employing three terms of the expansion is generally considered as the standard model (N=3) [29].

As stated earlier, the Ogden or standard model yields accurate predictions of the responses of hyperelastic materials for large strain deformations. This model, however, incorporates six material constants, which must be estimated through the experiments.

For compressible rubbers the determinant of the deformation gradient, $J = \det(\mathbf{F})$, may be different from the unity value obtained for incompressible rubbers. For this class of materials, the strain energy density function may be decomposed into two parts including the volume-preserving component and the volume-changing component. The volume-preserving component utilizes the traditional incompressible material model, while the latter part is expressed as a function of J. The compressible material models have thus been realized by introducing a term that is a function of the third invariant of the deformation tensor, $I_3 = J^2$, to incompressible models [29-32]. The rubbers, however, are generally considered as incompressible.

1.2.1.3 Transversely Isotropic Hyperelastic Models

In order to find a material model for transversely isotropic magnetoactive elastomer, it is crucial to gain insight into the conventional constitutive equations adopted for the anisotropic hyperelastic materials. The finite deformation analyses of transversely isotropic elastomers, generally, involve considerations of two additional invariants, I_4 and I_5, defined with respect to the right Cauchy-Green deformation tensor and fiber unit vector, **A**, apart from the three invariants of the deformation tensor [33, 34]. The material model of this class of hyperelastic materials is developed assuming that the energy density function is composed of two constituents

one of these components is described by the isotropic hyperelasticity model, while the second component employs the term defined with respect to I_4 and/or I_5 to account for the deformation attributed to the transversely isotropic media. The reported anisotropic constitutive equations may be grouped into three classes namely I_4-based, I_5-based and I_4 and I_5-based models. A number of studies have established that only the last class, based on I_4 and I_5, is permissible due to its consistency with the linear elasticity [33]. The first class of models (I_4-based) includes those reported by Weiss et al. [35], Qiu and Pence [36], Merodio and Ogden [34, 37, 38], Horgan and Saccomandi [39], Kassianidis et al. [40], Horgan and Murphy [41, 42], Destrade et al. [43], Destrade et al. [44] and Hamdaoui et al. [45]. The models reported by Polignone and Horgan [46], Merodio and Ogden [34] and Horgan and Saccomandi [39] pertain to the second category (I_5-based) of the models. Lu and Zhang [47], Feng et al. [48], Murphy [33], Destrade et al. [44], Horgan and Murphy [49] and Moreira and Nunes [50] considering combination of I_4 and I_5 proposed hyperelastic models for transversely isotropic materials. Murphy [33] investigated the consistency of the transversely isotropic hyperelasticity with the linear elasticity and established that the energy density function can be adequately described using the combination of both I_4 and I_5.

A number of alternate models have also been developed for analyses of orthotropic and transversely isotropic hyperelastic materials and soft tissues. These employ the energy density which is not composed of a traditional isotropic hyperelastic model and an anisotropic part expressed with respect to the invariants, I_4 and/or I_5 [38, 51-55].

The material models developed for finite deformation of incompressible transversely isotropic elastomers, however, are most widely being used for analyses of anisotropic rubbers and MAEs. These have evolved from the basic so-called neo-Hookean material model, where the invariant I_4 and I_5 are expressed in terms of Cauchy-Green deformation tensor $\mathbf{C}$, as [33, 34]:

$$I_4 = \mathbf{A}.\mathbf{C}.\mathbf{A} \tag{1.28}$$

$$I_5 = \mathbf{A}.\mathbf{C}^2.\mathbf{A} \tag{1.29}$$

The majority of reported models on anisotropic hyperelasticity express the energy density into the isotropic and anisotropic components such that [33, 34]

$$W = W^*(I_1, I_2, I_3) + W^\dagger(I_4, I_5) \tag{1.30}$$

where the first and the second terms in the right hand side of above equation related to the isotropic and transversely isotropic energy density, respectively.

Polignone and Horgan [46] appended an expression in terms of I_5 to neo-Hookean material model to express the energy density function as:

$$W = \frac{G}{2}[(I_1 - 3) + a(I_5^2 - 2I_5 + 1)] \tag{1.31}$$

which G and a are two material constants in this model.

Qiu and Pence [36] proposed anisotropic energy as a function of I_4 with G and γ being the unknowns, such that:

$$W = \frac{G}{2}[(I_1 - 3) + \gamma(I_4 - 1)^2] \tag{1.32}$$

Similarly, Merodio and Ogden [34] introduced a relation with respect to I_1 and I_5 as:

$$W = \frac{G}{2}[(I_1 - 3) + \gamma(I_5 - 1)^2] \tag{1.33}$$

Horgan and Saccomandi [39] proposed the anisotropic energy functions W^I, W^{II}, W^{III} and W^{IV} building on I_4, I_5 and the neo-Hookean isotropic model, as follows:

$$W^I = \frac{G}{2}(I_1 - 3) - G^I J_m^I((I_4 - 1) + J_m^I \ln(1 - \frac{I_4 - 1}{J_m^I})) \tag{1.34}$$

$$W^{II} = \frac{G}{2}(I_1 - 3) - \frac{G^I}{2} J_m^{II} \ln(1 - \frac{(I_4 - 1)^2}{J_m^{II}}) \tag{1.35}$$

$$W^{III} = \frac{G}{2}(I_1 - 3) - G^{II} J_m^{III} \ln(1 - \frac{(I_5 - 1)^2}{J_m^{III}}) \tag{1.36}$$

$$W^{IV} = \frac{G}{2}(I_1 - 3) - \frac{G^{IV}}{n} J_m^{IV} \ln(1 - \frac{(I_4 - 1)^n}{J_m^{IV}}) \tag{1.37}$$

where G, G^I, G^{II}, G^{IV}, J_m^I, J_m^{II}, J_m^{III}, J_m^{IV} and n are material unknowns.

Murphy [33] established that both I_4 and I_5 must be incorporated in the energy density function to ensure the consistency of nonlinear models with the transversely isotropic linear elasticity. The study proposed the following relations for the energy density:

$$W = \frac{G_T}{2}(I_1 - 3) + \frac{G_T - G_L}{2}(2I_4 - I_5 - 1) + \frac{E_L + G_T - 4G_L}{32}(I_5 - 1)^2 \tag{1.38}$$

$$W = \frac{G_T}{2}(I_1 - 3) + \frac{G_T - G_L}{2}(2I_4 - I_5 - 1) + \frac{E_L + G_T - 4G_L}{16}(I_4 - 1)(I_5 - 1) \tag{1.39}$$

$$W = \frac{G_T}{2}(I_1 - 3) + \frac{G_T - G_L}{2}(2I_4 - I_5 - 1) + \frac{E_L + G_T - 4G_L}{8}(I_4 - 1)^2 \tag{1.40}$$

where G_T, G_L and E_L are unknowns of the incompressible material models, which are also the constants of the linear anisotropic elastic materials proposed by Spencer [56].

It is a known fact in the reference configuration, see Figure 1-1, the energy density and the stress tensor are zero, such that [33]

$$W|_{\mathbf{F}=\mathbf{I}} = 0, \qquad \boldsymbol{\sigma}|_{\mathbf{F}=\mathbf{I}} = \mathbf{0} \tag{1.41}$$

Considering $\mathbf{F} = \mathbf{I}$, it is further concluded that $I_1 = I_2 = 3$ and $I_3 = I_4 = I_5 = 1$ in the material or reference configuration. Apart from these, the following requirements must be met to ensure consistency with the linear elasticity [33]:

$$2\frac{\partial W}{\partial I_1}|_{\mathbf{F}=\mathbf{I}} + 2\frac{\partial W}{\partial I_2}|_{\mathbf{F}=\mathbf{I}} = G_T \tag{1.42}$$

$$\frac{\partial W}{\partial I_4}|_{\mathbf{F}=\mathbf{I}} + 2\frac{\partial W}{\partial I_5}|_{\mathbf{F}=\mathbf{I}} = 0 \tag{1.43}$$

$$2\frac{\partial W}{\partial I_5}|_{\mathbf{F}=\mathbf{I}} = G_L - G_T \tag{1.44}$$

$$4\frac{\partial^2 W}{\partial {I_4}^2}|_{\mathbf{F}=\mathbf{I}} + 16\frac{\partial^2 W}{\partial I_4 \partial I_5}|_{\mathbf{F}=\mathbf{I}} + 16\frac{\partial^2 W}{\partial {I_5}^2}|_{\mathbf{F}=\mathbf{I}} = E_L + G_T - 4G_L \tag{1.45}$$

It must be emphasized that the strain energy functions proposed by Murphy [33], specially the components connected with anisotropy, (Eqs. (1.38)-(1.40)) are in compliant with the above conditions. Moreover, it must be emphasized that Murphy [33] proved that it is obligatory to write the energy density in terms of both I_4 and I_5 for satisfying the above-stated requirements by taking advantage of the above conditions.

Feng et al. [48] also emphasized the significance of both invariants, I_4 and I_5, in their model and subsequently proposed the following energy density as a function of I_4 and I_5 [57]:

$$W = \frac{G}{2}[(I_1 - 3) + \zeta(I_4 - 1)^2 + \phi I_5^*] \tag{1.46}$$

with $I_5^* = I_5 - {I_4}^2$, and G, ζ and ϕ are the material unknowns in the model.

1.2.2 Continuum-Based Approach for Finite Deformation of a Magnetic Medium

The continuum-based approaches and the constitutive relations developed for hyperelastic isotropic and transversely isotropic materials have also been applied for deformation analyses of MAEs. The fundamentals of magnetism are briefly reviewed so as to gain insight into fundamental relations for the magnetic active materials.

Let **B** describe the magnetic field induction (or magnetic flux density) and **H** be the magnetic field strength. For a medium, which is magnetized under the application of a magnetic field, the magnetic flux density **B** is related to the magnetic field strength **H** and the magnetization **M**, as [58]:

$$\mathbf{B} = \mu_0(\mathbf{H} + \mathbf{M}) \tag{1.47}$$

where $\mu_0 = 4\pi \times 10^{-7}\ N/A^2$ is the permeability in vacuum.

The above relationship in the free space can be expressible as:

$$\mathbf{B} = \mu_0 \mathbf{H} \tag{1.48}$$

The governing differential equations for a nonconductive magnetic body in accord with the Maxwell's equations can be stated as [58]:

$$\nabla . \mathbf{B} = 0 \tag{1.49}$$
$$\nabla \times \mathbf{H} = \mathbf{0} \tag{1.50}$$

The above are valid for both the isotropic or anisotropic media. For rigid magnetic materials, two tensors, relative permeability tensor $\boldsymbol{\mu}^r$, and susceptibility tensor $\boldsymbol{\chi}$, are used to describe **B** and **M**, respectively, such that [59]:

$$\mathbf{B} = \mu_0 \boldsymbol{\mu}^r . \mathbf{H} \tag{1.51}$$
$$\mathbf{M} = \boldsymbol{\chi} . \mathbf{H} \tag{1.52}$$

The above relations are also referred to as constitutive relations for magnetic materials, where $\boldsymbol{\mu} = \mu_0 \boldsymbol{\mu}^r$ defines the magnetic permeability of the material.

For linear isotropic materials, Eqs. (1.51) and (1.52) can be simplified as [58]:

$$B_i = \mu_0 \mu^r H_i \tag{1.53}$$
$$M_i = \chi H_i \tag{1.54}$$

where B_i and M_i are the magnetic flux density and magnetization, respectively, of the linear isotropic material. μ^r and χ are the relative permeability and the susceptibility of a magnetic material, respectively. The above relations also yield $\mu^r = \chi + 1$. Moreover, the above linear relations are considered valid within the working domain of the magnetic field, prior to saturation of the magnetic material.

For a transversely isotropic magnetic material, linear relations among **B**, **H** and **M** are expressed , as [59]:

$$B_1 = \mu_0 \mu_{11}^r H_1, \qquad B_2 = \mu_0 \mu_{11}^r H_2, \qquad B_3 = \mu_0 \mu_{33}^r H_3 \tag{1.55}$$

$$M_1 = \chi_{11} H_1, \qquad M_2 = \chi_{11} H_2, \qquad M_3 = \chi_{33} H_3 \tag{1.56}$$

where subscript i = 1, 2, 3 refers to every axis of the coordinate system, and x_3 is aligned with the symmetry axis of a transversely isotropic material.

The first effort towards the formulation of an electro-sensitive medium under electro-mechanical fields was developed by Toupin [60]. Toupin [61] subsequently reported the dynamic version of his formulations. That is, a framework for electro-mechanical materials was developed by combining classical mechanics with the theory of electromagnetism. Subsequently, Tiersten [62, 63] presented a boundary value problem for large deformation analysis of a medium that is nonconductive and magnetically saturated. The formulations were developed using the laws of electronic spin continuum and lattice continuum. Jordan and Eringen [64] formulated analysis of isotropic elastic solids undergoing finite deformations subjected to electromagnetic and thermal fields. Maugin and Eringen [65] conducted a study into the nonlinear behavior of elastic solids under constant magnetic field and proposed a new constitutive equation. For linear static and dynamic analysis of a soft ferromagnetic material, a framework was proposed by Pao and Yeh [66] and Hutter and Pao [67]. Additionally, Pao [58] developed two frameworks for the dynamics of an electromagnetic deformable body undergoing large deformation and proposed an energy density in the form of a polynomial function with respect to the Green-Lagrange strain tensor and magnetic and electric fields . One of these formulations is currently being used for analysis of MAEs. Tiersten and Tsai [68] also derived governing equations for the finite deformation analysis of a medium subject to electromagnetic and thermal fields. Brown [69] conducted a detailed study on magneto-mechanics and rigorously elaborated a unique formulation for deformable magnetic materials. Additionally, valuable

information on the magneto-mechanics could also be found in detail in the works of Eringen and Maugin [70] and the text book on electromagnetic theory by Kovetz [71]. Two important frameworks, which have been widely used during the past few decades for finite deformation of magnetoactive materials, are described below.

As mentioned before, Pao [58] elaborated two frameworks for the finite deformation analysis of a medium with magnetic and electric features involving the two-dipole formulation reported in [72] and the dipole-current circuit formulation. In the dipole-current circuit formulation, the free energy is expressed as a function of the deformation gradient **F**, electric field intensity **E**, magnetic field induction **B** and the temperature T. Many studies reporting the energy density in terms of invariants rather than the corresponding tensors, have employed the latter framework of Pao [58]. For instance, Eringen and Maugin [70], Dorfmann and his coworkers [10, 73-76] and Bustamante and his colleagues [77-82] modified the latter formulation of Pao [58] to conduct static analysis of magnetoactive elastomers. These studies, however, did not attempt model verification via experiments. Further, building upon the work of Dorfmann and Ogden [74], Saxena et al. [83] proposed a formulation for visco-magneto-hyperelastic materials. Additionally, one underlying point that must be raised herein is that the Lagrangian counter part of Maxwell equations, by taking advantage of the pull-back operation, are used by Dorfmann and Bustamante, whereas the approach was not implemented by Pao. That is, Pao [58] took advantage of material magnetic fields just for the purpose of the material objectivity of constitutive equations. Pao [58] constructed the constitutive equations related to the dipole-current circuit model building upon the Eulerian form of the second law of thermodynamics. Eringen and Maugin [70], on the other hand, developed the corresponding equations with respect to the material form of the law (Lagrangian form). The validity of the formulations, however, was not attempted.

Kankanala and Triantafyllidis [9] defined MAEs as rubbers enriched by ferromagnetic particles and derived constitutive equations for the isotropic elastomers along with a boundary value problem with respect to the material and spatial descriptions. Unlike the formulations of Pao [58], the study developed relations based on the deformation gradient **F** and the magnetization **M**. The idea of the work was initially proposed by Brown [69], but it was never implemented. Essentially, Kankanala and Triantafyllidis [9] reformulated the framework using the energy approach together with the unconstrained minimization of the potential energy

functional. Furthermore, this framework combines the Mooney-Rivlin model for hyperelastic materials with some magnetic terms. Two major formulations have been widely implemented for large deformation analysis of magnetoactive materials were presented by Dorfmann and Ogden [10, 74] and Kankanala and Triantafyllidis [9]. While the works of Dorfmann and Ogden [10, 74] were based on the original formulation of Pao [58], the fundamental element in [9] was based on the works of Brown [69] and Kovetz [71].

In the context of continuum-based formulations for the anisotropic MAEs, significance of the reported studies have emphasized nonlinear constitutive equations for MAEs with chains of iron particles. For instance, Bustamante [79] developed a material model for transversely isotropic magnetoactive elastomers by modifying the formulation by Dorfmann and Ogden [74] and expressing the energy density as a function of the magnetic field strength in place of the magnetic field induction. Later, Danas et al. [84] investigated the anisotropic MAEs theoretically and experimentally by using the framework proposed by Kankanala and Triantafyllidis [9]. The material constants were identified from the experimental data acquired from uniaxial and simple shear tests for various orientations of the particle's chains. The energy density function was based on invariants expressed by the right Cauchy-Green deformation tensor, the magnetization vector and the transversely isotropy unit vector. Magneto-viscoelasticity of polymers with chains of iron particles under finite deformation was modelled by Saxena et al. [85] using the framework of Dorfmann and Ogden [74]. Among the three models reported for transversely isotropic magnetoactive elastomers [79, 84, 85], the model validity was attempted via experiments only by Danas et al. [84].

1.2.3 Magnetic Properties of MAEs

MAEs comprise two primary constituents, namely, a rubbery matrix and iron particles. The unique behavior of the magnetoactive elastomers is attributed to the presence of the iron particles in the matrix, which exhibits significant mechano-magnetic interactions under the application of the external magnetic field. Soft carbonyl iron powder (CIP) is commonly used as magnetizable iron particles in fabrication of MAEs. Figure 1-2 exhibits the relation between magnetization and magnetic field induction for the CIP in the x_1-direction. The figure suggests nearly linear relation between $\mathbf{B}$ and $\mathbf{M}$ for $-0.5\ T \leq B \leq 0.5\ T$. Based on the reported experimental data, the

following nonlinear and linear relations between the components of magnetization and the magnetic field have been proposed [86]:

$$M_k = M_s \tanh(\delta J_1)\frac{B_k}{J_1} \qquad \text{with} \qquad k \in \{1,2,3\} \tag{1.57}$$

$$M_k = \chi B_k \qquad \text{with} \qquad k \in \{1,2,3\} \tag{1.58}$$

where M_s, δ, χ and $J_1 = \sqrt{B_k B_k}$ are the saturation magnetization, the scaling parameter, the magnetic susceptibility and the norm of the magnetic field induction vector, respectively.

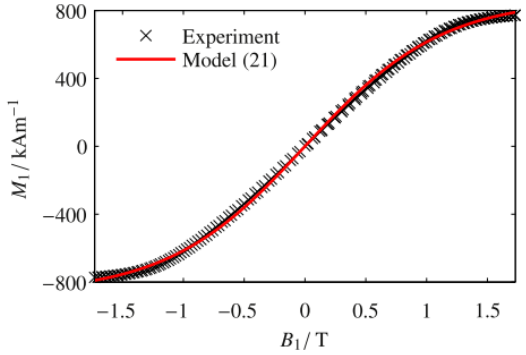

Figure 1-2. Magnetic behavior of the carbonyl iron particles [87].

In MAEs, the size, distribution and volume fraction of the iron particles in the matrix play a key role in their performance. Typically, the sizes of the iron particles and the volume fraction range from 0.1 μm to 10 μm, and 10% to 50%, respectively [88]. Using very fine particles with a low volume fraction generally leads to a very poor response. Soft particles made of materials such as, iron, cobalt and their oxides [89-91], are generally used as ferromagnetic particles in elastomeric medium [92] due to their high magnetic permeability, large magnetic saturation, and zero residual magnetization. It is worth noting that the hard particles made of materials such as $BaFe_{12}O_{19}$ or $SrFe_{12}O_{19}$ are of less interest due to their relatively high residual magnetization [5, 93]. The matrix material of the MAE, on the other hand, can be conductive or non-conductive, and solid or porous.

The magnetic saturation for pure iron is around 2 Tesla [94]. The magnetization of the media varies only negligibly as the external magnetic field exceeds 2 T leading to saturation of the interactions among the particles [88]. The carbonyl iron particles are most commonly used in magnetoactive materials due to their high magnetic permeability, low residual magnetization and high saturation magnetization. MAEs or MARs made of carbonyl iron particles thus exhibit high

magnetic interactions, strong magnetic effects, and insignificant remanence or residual magnetism upon removal of the magnetic field [95]. Furthermore, the iron particles have very low magnetostriction (the deformation of the material under the influence of a magnetic field) [96]. In MAEs, the degree of magnetostriction is dependent on a number of factors, including the stiffness of the matrix, the volume fraction and orientation of magnetic field and it mainly occurs at relatively high magnetic fields [84, 97]. The magnetic properties in MAEs directly depend on the volume fraction of iron particles as shown in Figure 1-3 [88]. The results suggest that increasing the volume fraction yields relatively higher permeability and saturation.

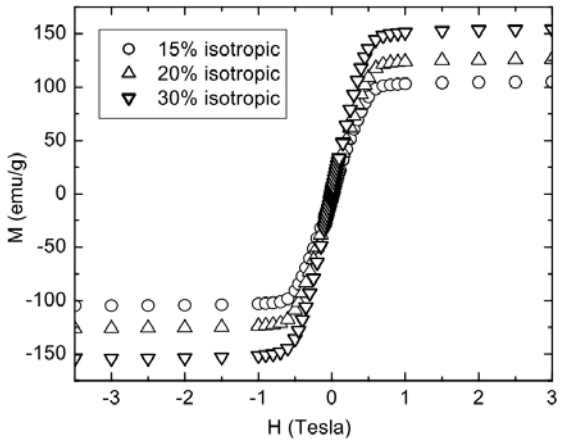

Figure 1-3. Magnetic behavior of MAEs [88].

The role of the particles distribution is also significant and it yields the isotropic or anisotropic medium. In this regard, MAEs can be classified into two main groups on the basis of distribution of the iron particles, namely, isotropic and transversely isotropic. In the former, the iron particles are randomly distributed in the matrix, whereas in the latter group the particles are arranged in chain-like structure, as shown in Figure 1-4 (a) and (b). The anisotropic MAE can be obtained by applying the magnetic field during the curing process [98], which leads to formation of particles' chains and consequently the mechanical and magnetic anisotropic behavior [99-101]. Upon the application of an external magnetic field, the particles align themselves along the direction of the applied magnetic field which would alter the dynamic characteristics such as stiffness and damping of the material.

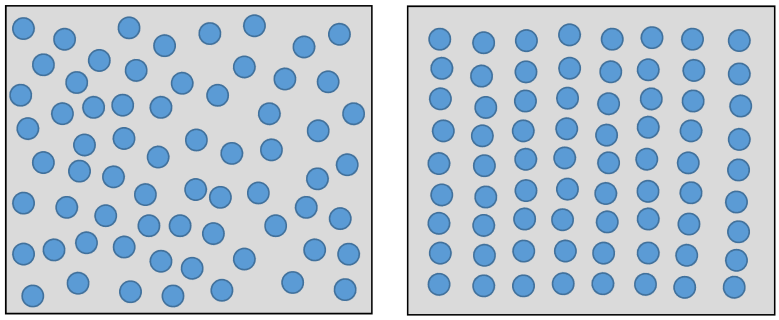

(a) (b)

Figure 1-4. Schematic of microstructure of (a) isotropic (b) transversely isotropic MAE.

1.2.4 Experimental Studies on MAE

A number of studies have experimentally investigated the properties of MAEs considering different mechanical loading (strain and strain rate) and magnetic flux density. The measured data have provided significant insight into the properties of MAEs and the effects of magnetic field, apart from facilitating identification of material unknowns in the constitutive equations. When a ferromagnetic body is under influence of an external magnetic field, it becomes magnetized, and consequently generates an additional magnetic field in the material in addition to the original external field. The deformation of the body also affects the magnetic field inside the material. One of pioneering works in experimental characterization of MAEs has been conducted by Jolly et al. [102]. In this study, the mechanical behavior of MAEs with different volume fractions was investigated under dynamic double-lap shear tests. In order to evaluate magneto-active (MA) effects, Lokander and Stenberg [95] conducted experiments on isotropic MAEs made of various types of iron powder and rubber matrix using a tensile machine and a rheometer. The authors subsequently identified design factors to improve the MA effects [91]. Varga et al. [103] studied the impact of a magnetic field on elastic modulus based on the compression mode of the both isotropic and the anisotropic MAEs under different orientations of the magnetic field. Farshad and Benine [99] conducted quasi-static tests including tension/compression of a cylindrical MAE and a cantilever beam under the influence of a magnetic field to determine MA effects of the isotropic and transversely isotropic MAE samples. Bellan and Bossis [104] conducted tension/compression tests on structured and unstructured

MAE samples. Additionally, Bodelot et al. [105] experimentally evaluated magneto-mechanical responses of cylindrical samples of isotropic and anisotropic MAEs under uniaxial tests. The vast majority of the experimental works have reported stress-strain characterizations and elastic or shear moduli of MAEs as functions of the applied magnetic field. Apart from these MA effects, it is also vital to fully characterize the induced magnetic field inside the material, for developing reliable material models. Only limited efforts, however, have been reported for measuring the magnetic field inside the MAEs [84]. This is likely due to lack of reliable methods for measuring the field strength inside the medium.

1.3 Objectives

Considerable efforts have been reported on the formulations and theoretical frameworks for analysis of finite deformations of hyperelastic isotropic and transversely isotropic MAEs. These have provided governing constitutive relations and material models. The validity of the reported models for MAEs, however, is lacking. Furthermore, there exists a lack of experimental data on the response behavior of the MAEs that can be used for estimation of the material constants associated with the constitutive equations of MAEs. Accordingly, the objectives of the present research study are as follows:

1. Formulate a framework for isotropic MAEs based on some invariants and propose a material model allowing for the objectivity principle and estimating the associated material constants using experimental characterizations obtained from a magneto-rheometer.
2. Propose a small-deformation constitutive equation for isotropic MAEs by decomposing the magnetic parameters into two parts including rigid-body and perturbed states, and demonstrate validity of the model with the measured data.
3. Derive formulations for the transversely isotropic magnetoactive elastomers comprising a novel invariant-based energy density, and estimate the material unknowns using the experimental data acquired from finite torsion of a cylindrical MAE sample.

1.4 Outline

The remainder of the thesis is as follows. Chapter 2 is concerned with finite deformation of the isotropic magnetoactive elastomers. The governing mechanical and magnetic equations are

presented and the constitutive equations are derived. The processes associated with the fabrication of isotropic MAE and the experimental methods are also presented for characterizing the magnetic constants and mechanical behavior of the MAE via torsion test under varying magnetic fields. A linear form of the constitutive relations is further developed for small-deformation analysis of a magnetic solid. The effectiveness of the proposed material model is demonstrated by comparing the model result with the measured data. Chapter 3 presents the theory of transversely isotropic MAEs and design of experiments. The constitutive equations are derived for the compressible and incompressible MAEs, and a unique energy density function is proposed to obtain the stress tensor. Laboratory experiments are performed to identify the permeability and torque-twist response of the anisotropic medium under various magnetic fields. The analytical response of a right cylindrical sample made of MA elastomer is obtained and compared with the experimental data to show the model validity and to find model constants. The major contributions and conclusions of the study are summarized in chapter 4 together with recommendations for future works in the area.

CHAPTER 2

FINITE DEFORMATION OF ISOTROPIC MAGNETOACTIVE ELASTOMERS

2.1 Introduction

Isotropic MAEs consist of randomly distributed iron particles in the rubbery matrix, which leads to isotropic mechanical and magnetic behavior of the medium. This chapter is aimed at developing formulations for small and large deformation analysis of magnetoactive elastomers. The dipole current-circuit framework proposed by Pao [58] has been employed and revisited based on the invariant form of the energy density function for nonlinear deformations. The governing equations are also linearized by decomposing the magnetic parameters, as proposed by Pao and Yeh [66].

Firstly, the governing differential equations are formulated for the spatial configuration. Constitutive equations are subsequently developed using the stored energy density function defined with respect to the invariants of the right or left Cauchy-Green deformation tensor and the magnetic field induction vector for finite deformations of the isotropic magnetoactive elastomers (MAEs). An isotropic magnetoactive sample with 15% iron particle volume fraction was fabricated in the laboratory and an experiment was designed to measure its magnetic permeability. Using an advanced magnetorheometer, quasi-static tests were carried out on circular cylindrical MAE samples to measure the torque-twist response under various magnetic fields. Subsequently, a linearization scheme is adopted to formulate a constitutive equation for small deformation analysis of MAEs by decomposing the magnetic parameters into two constituents involving the rigid-body and perturbation states. The unknown parameters of the proposed linear and nonlinear material models are identified using the experimental data. The accuracy of the proposed constitutive model in predicting the response behavior of the MAE is then demonstrated through comparison of theoretical results with those obtained experimentally.

2.2 Basic Equations

In this section, the governing equations associated with a medium exhibiting both the mechanical and magnetic properties are formulated for coupled mechanical-magnetic analysis of the isotropic MAEs.

2.2.1 Governing Relations

In the first step, the global forms of the basic laws in the continuum mechanics are presented. More precisely, the laws associated with mass, linear momentum, angular momentum and energy balance for a medium occupying the volume v with the bounding surface s, respectively, may be expressed as [58]:

$$\frac{d}{dt}\int_v \rho dv = 0 \tag{2.1}$$

$$\frac{d}{dt}\int_v \rho \mathbf{v} dv = \oint_s \mathbf{t}^{(\mathbf{n})} ds + \int_v \mathbf{f} dv + \int_v \bar{\mathbf{f}} dv \tag{2.2}$$

$$\frac{d}{dt}\int_v (\mathbf{x}\times\rho\mathbf{v}) dv = \oint_s (\mathbf{x}\times\mathbf{t}^{(\mathbf{n})}) ds + \int_v (\mathbf{l} + \mathbf{x}\times(\bar{\mathbf{f}} + \mathbf{f})) dv \tag{2.3}$$

$$\frac{d}{dt}\int_v (\frac{1}{2}\rho\mathbf{v}.\mathbf{v} + \rho u) dv = \oint_s \mathbf{t}^{(\mathbf{n})}.\mathbf{v} ds + \int_v (\mathbf{f}.\mathbf{v} + \bar{\mathbf{f}}.\mathbf{v} + \phi) dv \tag{2.4}$$

where ρ, $\mathbf{t}^{(\mathbf{n})}$, $\bar{\mathbf{f}}$, $\mathbf{f}$, $\mathbf{l}$, u and ϕ are, respectively, the spatial density, traction vector, mechanical body force, magnetic body force, body couple, internal energy per unit mass and magnetic energy.

For a magnetic medium exclusively, the global form of the Maxwell equations can be written as [9]:

$$\int_s \mathbf{n}.\mathbf{b} ds = 0 \tag{2.5}$$

$$\int_c \mathbf{h}.d\mathbf{c} = \mathbf{0} \tag{2.6}$$

where vectors $\mathbf{b}$ and $\mathbf{h}$ are the Eulerian magnetic induction and the magnetic field strength, respectively. In addition, s is a spatial surface and c is a smoothed closed curve in the deformed body and $\mathbf{n}$ is the outward normal vector to the boundary surface. The former and the latter are indeed the Gauss's and Ampère's law.

In the development of the basic formulations for solids from the continuum point of view with respect to the local equations rather than the global equations, two integral transformations are commonly used involving the divergence and Stokes theorems, such that

$$\oint_s \mathbf{n}.\mathbf{K}ds = \int_v \nabla_{\mathbf{x}}.\mathbf{K}dv \tag{2.7}$$

$$\int_s \mathbf{n}.\nabla_{\mathbf{x}} \times \mathbf{K}ds = \oint_c \mathbf{K}.d\mathbf{c} \tag{2.8}$$

where c is a closed curved, $d\mathbf{c}$ is an element on the curve and $\mathbf{K}$ is an arbitrary tensor and $\mathbf{n}$ is the unit normal vector to the surface s.

With the aid of the integral transformations in Eqs. (2.7) and (2.8), the local forms of conservation of mass, linear momentum, angular momentum and energy can be accomplished from the respective global forms. These are obtained as:

$$\frac{\partial \rho}{\partial t} + \nabla_{\mathbf{x}}.(\rho \mathbf{v}) = 0 \tag{2.9}$$

$$\nabla_{\mathbf{x}}.\boldsymbol{\sigma} + \mathbf{f} + \overline{\mathbf{f}} = \rho \frac{d\mathbf{v}}{dt} \tag{2.10}$$

$$\frac{1}{2}(\boldsymbol{\sigma} - \boldsymbol{\sigma}^T) + \boldsymbol{\eta} = \mathbf{0} \tag{2.11}$$

$$\rho \frac{du}{dt} = \boldsymbol{\sigma} : \nabla_{\mathbf{x}}\mathbf{v} - \mathbf{m}.\frac{d}{dt}(\mathbf{b}) \tag{2.12}$$

where $\boldsymbol{\sigma}$ is the Cauchy stress tensor, $\boldsymbol{\eta}$ is the dual of the magnetic body couple $\mathbf{l}$ and $\mathbf{m}$ is the magnetization vector. Furthermore, the stress tensor is related to the internal traction via $\mathbf{t}^{(\mathbf{n})} = \mathbf{n}.\boldsymbol{\sigma}$, and the relation $l_i = \varepsilon_{ijk}\eta_{jk}$ or $\varepsilon_{ijk}\sigma_{jk} = -l_i$ holds, where ε_{ijk} is the permutation symbol. It should be noted that despite the purely mechanical analysis with a nonpolar medium, the Cauchy stress tensor is not symmetric and it is a coupled magneto-mechanical tensor.

In a similar manner, the local forms of the Gauss' law and Ampère's law (Maxwell's equations) are obtained from Eqs. (2.5) and (2.6), as:

$$\nabla_{\mathbf{x}}.\mathbf{b} = 0 \tag{2.13}$$

$$\nabla_{\mathbf{x}} \times \mathbf{h} = \mathbf{0} \tag{2.14}$$

The magnetic quantities in the above relations, however, are related, such that

$$\mathbf{b} = \mu_0(\mathbf{h} + \mathbf{m}) \tag{2.15}$$

where $\mathbf{m}$ is the magnetization vector and $\mu_0 = 4\pi \times 10^{-7}\ N/A^2$ is the permeability in the vacuum.

Generally the relation between the magnetization and the magnetic field is nonlinear, particularly as the magnetization approaches saturation. Soft ferromagnetic materials generally exhibit approximately linear b-h relationship for $b \leq 0.5\ T$ [87]. As stated in section 1.2.2, the assumption of linearity in magnetization-magnetic-field relation for a rigid body yields:

$$\mathbf{m} = \chi \mathbf{h} \tag{2.16}$$

where χ is the magnetic susceptibility. Equations (2.15) and (2.16) yield the following relationship between **b** and **h**:

$$\mathbf{b} = \mu_0 (1+\chi)\mathbf{h} = \mu_0 \mu^r \mathbf{h} = \mu \mathbf{h} \tag{2.17}$$

where μ^r and μ are the relative permeability and permeability of a magnetic material, respectively. The above relation is considered valid, provided that the magnetostriction in the medium is negligible.

Previously, in the introduction of the conservation laws, i.e. Eqs. (2.10) and (2.11), the non-mechanical body force and the body couple were deemed in the formulation. For a medium with magnetic properties, these two quantities can be introduced based on the magnetic parameters. For the dipole-current circuit model presented by Pao [58], these are expressed as:

$$\mathbf{f} = (\nabla_{\mathbf{x}} \mathbf{b}).\mathbf{m} \tag{2.18}$$

$$\mathbf{l} = \mathbf{m} \times \mathbf{b} \tag{2.19}$$

where, as mentioned before, **f** and **l** are the magnetic body force and the magnetic body couple per unit volume, respectively.

The mechanical and magnetic boundary conditions are defined considering a pillbox on the bounding surface of the body together with Eqs. (2.2), (2.5) and (2.6) such that [58, 71]:

$$\mathbf{n}.[\![\boldsymbol{\sigma} + \boldsymbol{\sigma}^S]\!] = \mathbf{0} \tag{2.20}$$

$$\mathbf{n}.[\![\mathbf{b}]\!] = 0 \tag{2.21}$$

$$\mathbf{n} \times [\![\mathbf{h}]\!] = \mathbf{0} \tag{2.22}$$

where the symbol $[\![q]\!] = q^+ - q^-$ describes the jump in the quantity q in the vicinity of the surface (just above and below of the surface). In the above relations, the stress tensor, $\boldsymbol{\sigma}^S$, is introduced as [58]:

$$\boldsymbol{\sigma}^S = (\mathbf{m}.\mathbf{b} - \frac{\mathbf{b}.\mathbf{b}}{2\mu_0})\mathbf{I} + \frac{\mathbf{bb}}{\mu_0} - \mathbf{bm} \tag{2.23}$$

where $\mathbf{I} = \delta_{ij}\mathbf{e}_i\mathbf{e}_j$ is the identity tensor and δ_{ij} is the Kronecker delta. It can be demonstrated that the divergence of the stress tensor in the above relation is the magnetic body force, such that [58]

$$\nabla.\boldsymbol{\sigma}^S = \mathbf{f} \tag{2.24}$$

It is noted that in the case of finite deformation in solid mechanics which involves both material and geometric nonlinearities, the governing equations are usually stated with respect to the reference configuration (Lagrangian approach) [6]. This is mainly due to the fact that the spatial configuration is not known, while the geometric information in the reference configuration is fully known. Thus, it is required to define a stress tensor which can be expressed relative to the reference (material) configuration in contrast to the Cauchy stress, which is defined relative to the spatial configuration. This can be achieved by defining a virtual stress tensor, denoted as the nominal stress, **P**, as [6]:

$$\mathbf{t}^{(\mathbf{n})}da = d\mathbf{a}.\boldsymbol{\sigma} = \mathbf{P}.d\mathbf{A} \tag{2.25}$$

with

$$\mathbf{P} = J\left(\mathbf{F}^{-1}.\boldsymbol{\sigma}\right)^T \qquad \text{or} \qquad \boldsymbol{\sigma} = J^{-1}\mathbf{F}.\mathbf{P}^T \tag{2.26}$$

The above are obtained using the relation between the spatial and the material surface elements, presented in Eq. (1.17)

For this stage, it is convenient to compute the stress power in terms of $\boldsymbol{\sigma}$ and $\mathbf{P}$. It must be pointed out that the first term in the right hand side of the conservation of energy, Eq. (2.12), is the stress power related to the Cauchy stress tensor.

$$P_s = \boldsymbol{\sigma} : \nabla_{\mathbf{x}}\mathbf{v} = \left(\mathbf{F}^{-1}.\boldsymbol{\sigma}\right)^T : \dot{\mathbf{F}} = J^{-1}\mathbf{P} : \dot{\mathbf{F}} \tag{2.27}$$

Using the above relation, the conservation of energy stated in Eq. (2.12) can be expressed in the following form:

$$\rho\frac{\mathrm{d}u}{\mathrm{d}t} = J^{-1}\mathbf{P} : \dot{\mathbf{F}} - \mathbf{m}.\frac{d}{\mathrm{d}t}(\mathbf{b}) \tag{2.28}$$

and equivalently

$$\rho_0\frac{\mathrm{d}u}{\mathrm{d}t} = \mathbf{P} : \dot{\mathbf{F}} - \frac{\rho_0}{\rho}\mathbf{m}.\frac{d}{\mathrm{d}t}(\mathbf{b}) \tag{2.29}$$

where $\rho_0 = J\rho$ is the reference density of the material.

In a similar manner, using Eq. (2.26), the conservation of linear momentum in the reference state can be expressed as:

$$\nabla_{\mathbf{X}}.\mathbf{P}^{T} + J\mathbf{f} + J\overline{\mathbf{f}} = \rho_0 \frac{d\mathbf{v}}{\mathrm{d}t} \tag{2.30}$$

2.3 Constitutive Equations

In this section, the constitutive equations for a deformable magnetic medium are formulated. For this purpose, relations are developed using the tensors, and the governing equations are rewritten with respect to some invariants rather than the corresponding tensors for compressible or incompressible MAEs.

2.3.1 General Equations

Using Eq. (2.4) together with Eq. (1.16), the total internal energy can be described as:

$$U^{T} = \int_{v} \rho u dv = \int_{V} \rho_0 u dV = \int_{V} W dV \tag{2.31}$$

where $W = \rho_0 u$ is the stored energy function evaluated in the referential volume. It must be pointed out that for the large deformation analysis of solids the stored energy function plays a key role in the formulation of the problem. Furthermore, Eq. (2.29) implies that the stored energy is a function of the deformation gradient and the magnetic field induction, such that

$$W = W(\mathbf{F}, \mathbf{b}) \tag{2.32}$$

By employing Eq. (2.29) and taking derivative of the energy density with respect to **F** and **b**, respectively, the nominal stress tensor and the magnetization vector are accomplished as:

$$\mathbf{P} = \frac{\partial W(\mathbf{F}, \mathbf{b})}{\partial \mathbf{F}} \tag{2.33}$$

$$\frac{\rho_0}{\rho}\mathbf{m} = -\frac{\partial W(\mathbf{F}, \mathbf{b})}{\partial \mathbf{b}} \tag{2.34}$$

By allowing for Eq. (2.26), the Cauchy stress tensor with respect to the energy density can be obtained as:

$$\boldsymbol{\sigma} = J^{-1}\mathbf{F}.[\frac{\partial W(\mathbf{F}, \mathbf{b})}{\partial \mathbf{F}}]^{T} \tag{2.35}$$

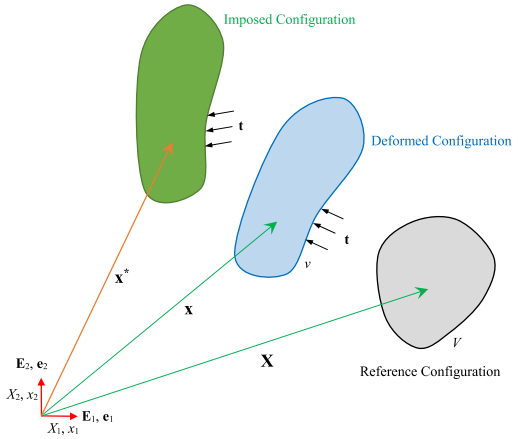

Figure 2-1. Imposed configuration to the deformed configuration.

In the development of constitutive equations for the hyperelastic materials, there exits one fundamental principle called the material objectivity or material frame indifference, which should be incorporated in the analysis. The principle states that the rigid rotation of the deformed body does not affect the stored energy function, see Figure 2-1. Let the superscript asterisk * denote the parameters in the configuration associated with the rigid rotation. The new position vector in the imposed configuration with respect to the orthogonal rotation tensor $\mathbf{Q}^{-1} = \mathbf{Q}^{T}$ about the origin is thus expressed as [6]:

$$\mathbf{x}^{*} = \mathbf{Q}.\mathbf{x} \tag{2.36}$$

Using the definition of the deformation gradient in Eq. (1.3) as well as the above-stated imposed position vector, the deformation gradient tensor can be expressed in the following form:

$$\mathbf{F}^{*} = \mathbf{Q}.\mathbf{F} \tag{2.37}$$

where indicates that $\mathbf{F}$ is not an objective tensor. Further, in order to find the magnetization vector in the imposed configuration, the orthogonal rotation tensor is applied, which yields:

$$\mathbf{b}^{*} = \mathbf{Q}.\mathbf{b} \tag{2.38}$$

As can be seen, the magnetization vector is not objective under the imposed rotation, similar to the deformation gradient. It must be remarked that the objective tensors do not change by the application of the aforestated transformation.

By inserting the imposed deformation gradient in Eq. (1.5), the right Cauchy-Green deformation tensor with respect to the imposed configuration may be obtained as follows:

$$\mathbf{C}^{*} = \mathbf{F}^{*T}.\mathbf{F}^{*} = \mathbf{F}^{T}.\mathbf{Q}^{T}.\mathbf{Q}.\mathbf{F} = \mathbf{C} \tag{2.39}$$

The above relation indicates that the right Cauchy-Green deformation tensor is unchanged under the imposed rotation and more precisely it is an invariant. Considering the relation $\mathbf{C} = \mathbf{U}^2$, it is concluded that the right stretch tensor is an invariant as well.

Now, let us focus on the objectivity of energy density function. Under the rigid motion described above, the function must be unchanged to satisfy the material objectivity. Applying the aforementioned transformation to the stored energy yields:

$$W = W(\mathbf{F}, \mathbf{b}) = W(\mathbf{Q}.\mathbf{F}, \mathbf{Q}.\mathbf{b}) \tag{2.40}$$

As discussed above, neither the deformation gradient nor the magnetic field vector are invariant under the transformation associated with the orthogonal rotation tensor. Accordingly, the above function in which the deformation gradient and magnetic field are independent variables does not meet the objectivity requirement.

Considering the polar decomposition of the deformation gradient addressed in Eq. (1.14) and arbitrariness of the orthogonal rotation tensor so that $\mathbf{Q} = \mathbf{R}^{T}$ the stored energy can be rewritten as [7, 72]

$$W = W(\mathbf{F}, \mathbf{b}) = W(\mathbf{Q}.\mathbf{F}, \mathbf{Q}.\mathbf{b}) = W(\mathbf{U}, \mathbf{U}^{-T}.\mathbf{F}^{T}.\mathbf{b}) \tag{2.41}$$

where $\mathbf{U}$ is invariant under the transformation, as stated earlier. Furthermore, it can be shown that the term $\mathbf{F}^{T}.\mathbf{b} = \tilde{\mathbf{B}}$ is also an invariant under the transformation as follows:

$$\tilde{\mathbf{B}}^{*} = \mathbf{F}^{*T}.\mathbf{b}^{*} = \mathbf{F}^{T}.\mathbf{Q}^{T}.\mathbf{Q}.\mathbf{b} = \mathbf{F}^{T}.\mathbf{b} = \tilde{\mathbf{B}} \tag{2.42}$$

where $\tilde{\mathbf{B}}$ is called the Lagrangian magnetic field induction.

Finally, considering $\mathbf{U} = \sqrt{\mathbf{C}}$, the energy density can be rewritten as:

$$W = W(\mathbf{C}, \tilde{\mathbf{B}}) \tag{2.43}$$

It must be pointed out that the Lagrangian magnetic field vector is not independent of the deformation gradient tensor and consequently the right Cauchy-Green deformation tensor.

Using the formulations in Eqs. (2.33), (2.34) and (2.43), the Cauchy stress and the magnetization tensors can be expressed as follows:

$$\boldsymbol{\sigma} = \frac{2}{J}\mathbf{F}.\frac{\partial W}{\partial \mathbf{C}}.\mathbf{F}^T - \mathbf{mb} \tag{2.44}$$

$$\mathbf{m} = -J^{-1}\mathbf{F}.\frac{\partial W}{\partial \tilde{\mathbf{B}}} \tag{2.45}$$

It must be noted that the first term in the right hand side of Eq. (2.44) is a symmetric expression, whereas the second one is non-symmetric. This fact is consistent with asymmetry of the Cauchy stress tensor. It can thus be deduced that the Cauchy stress tensor is a combination of a symmetric tensor and a non-symmetric tensor.

Additionally, given the definition of the Green-Lagrange strain tensor in Eq. (1.9), Eq. (2.44) can be rewritten as

$$\boldsymbol{\sigma} = \frac{1}{J}\mathbf{F}.\frac{\partial W}{\partial \mathbf{E}}.\mathbf{F}^T - \mathbf{mb} \tag{2.46}$$

2.3.2 Compressible Deformable Magnetic Medium

In the previous section, the constitutive equations were expressed with respect to some tensors. In the present section, the invariants are used to define the stored energy function. More precisely, the stored energy can be delineated in accord with three invariants of the right Cauchy-Green deformation tensor, I_1-I_3, presented in Eqs. (1.6)-(1.8), in addition to the three invariants associated with $\tilde{\mathbf{B}}$ and $\mathbf{C}$, which are given by:

$$I_6 = \tilde{\mathbf{B}}.\mathbf{C}^{-1}.\tilde{\mathbf{B}} = \mathbf{b}.\mathbf{b}, \tag{2.47}$$

$$I_7 = \tilde{\mathbf{B}}.\tilde{\mathbf{B}} = \mathbf{b}.\mathbf{G}.\mathbf{b}, \tag{2.48}$$

$$I_8 = \tilde{\mathbf{B}}.\mathbf{C}.\tilde{\mathbf{B}} = \mathbf{b}.\mathbf{G}^2.\mathbf{b} \tag{2.49}$$

Accordingly, the stored energy function is expressed as a function of the invariants, as [60]

$$W = W(I_1, I_2, I_3, I_6, I_7, I_8) \tag{2.50}$$

Upon substituting for the above energy density function in Eqs. (2.35) and (2.34), and performing some mathematical manipulations, the Cauchy stress tensor and the magnetization vector are obtained as:

$$\boldsymbol{\sigma} = 2J^{-1}([\frac{\partial W}{\partial I_1} + \frac{\partial W}{\partial I_2} I_1]\mathbf{G} - \frac{\partial W}{\partial I_2}\mathbf{G}^2 + \frac{\partial W}{\partial I_3} I_3\mathbf{I} + \frac{\partial W}{\partial I_7}(\mathbf{G}.\mathbf{b})\mathbf{b} + \frac{\partial W}{\partial I_8}[(\mathbf{G}^2.\mathbf{b})\mathbf{b} + (\mathbf{G}.\mathbf{b})(\mathbf{b}.\mathbf{G})]) \tag{2.51}$$

$$\mathbf{m} = -2J^{-1}[\frac{\partial W}{\partial I_6}\mathbf{b} + \frac{\partial W}{\partial I_7}\mathbf{G}.\mathbf{b} + \frac{\partial W}{\partial I_8}\mathbf{G}^2.\mathbf{b}] \tag{2.52}$$

The above equations are derived using the following relations:

$$\frac{\partial I_1}{\partial \mathbf{C}} = \mathbf{I}, \tag{2.53}$$

$$\frac{\partial I_2}{\partial \mathbf{C}} = I_1\mathbf{I} - \mathbf{C} \tag{2.54}$$

$$\frac{\partial I_3}{\partial \mathbf{C}} = I_3\mathbf{C}^{-1} \tag{2.55}$$

$$\frac{\partial I_6}{\partial \mathbf{F}} = \mathbf{0}, \tag{2.56}$$

$$\frac{\partial I_7}{\partial \mathbf{F}} = 2\mathbf{b}\tilde{\mathbf{B}}, \tag{2.57}$$

$$\frac{\partial I_8}{\partial \mathbf{F}} = 2\mathbf{b}(\tilde{\mathbf{B}}.\mathbf{C}) + 2(\mathbf{F}.\tilde{\mathbf{B}})\tilde{\mathbf{B}} \tag{2.58}$$

and

$$\frac{\partial I_6}{\partial \mathbf{b}} = 2\mathbf{b} \tag{2.59}$$

$$\frac{\partial I_7}{\partial \mathbf{b}} = 2\mathbf{G}.\mathbf{b} \tag{2.60}$$

$$\frac{\partial I_8}{\partial \mathbf{b}} = 2\mathbf{G}^2.\mathbf{b} \tag{2.61}$$

Next, by making use of the Cayley-Hamilton theorem stating that every second-order tensor, such as **G**, satisfies its characteristic equation:

$$\mathbf{G}^3 - I_1\mathbf{G}^2 + I_2\mathbf{G} - I_3\mathbf{I} = 0 \tag{2.62}$$

which is also equivalent to:

$$\mathbf{G}^2 = I_1\mathbf{G} - I_2\mathbf{I} + I_3\mathbf{G}^{-1} \tag{2.63}$$

an alternate form of Eq. (2.51) may also be obtained as:

$$\boldsymbol{\sigma} = 2J^{-1}([\frac{\partial W}{\partial I_2} I_2 + \frac{\partial W}{\partial I_3} I_3]\mathbf{I} + \frac{\partial W}{\partial I_1}\mathbf{G} - \frac{\partial W}{\partial I_2} I_3 \mathbf{G}^{-1} + \frac{\partial W}{\partial I_7}(\mathbf{G}.\mathbf{b})\mathbf{b} + \frac{\partial W}{\partial I_8}[(\mathbf{G}^2.\mathbf{b})\mathbf{b} + (\mathbf{G}.\mathbf{b})(\mathbf{b}.\mathbf{G})]) \tag{2.64}$$

For convenience, the above relation can be expressed in the following form:

$$\boldsymbol{\sigma} = \beta_1 \mathbf{I} + \beta_2 \mathbf{G} + \beta_3 \mathbf{G}^{-1} + \beta_7 (\mathbf{G}.\mathbf{b})\mathbf{b} + \beta_8 [(\mathbf{G}^2.\mathbf{b})\mathbf{b} + (\mathbf{G}.\mathbf{b})(\mathbf{b}.\mathbf{G})] \tag{2.65}$$

with

$$\beta_1 = 2J^{-1}[\frac{\partial W}{\partial I_2} I_2 + \frac{\partial W}{\partial I_3} I_3], \qquad \beta_2 = 2J^{-1}\frac{\partial W}{\partial I_1},$$
$$\beta_3 = -2J^{-1}\frac{\partial W}{\partial I_2} I_3, \quad \beta_7 = 2J^{-1}\frac{\partial W}{\partial I_7}, \quad \beta_8 = 2J^{-1}\frac{\partial W}{\partial I_8} \tag{2.66}$$

By following the same procedure for the magnetization vector, Eq. (2.52) can be expressed as:

$$\mathbf{m} = -\beta_6 \mathbf{b} - \beta_7 \mathbf{G}.\mathbf{b} - \beta_8 \mathbf{G}^2.\mathbf{b} \tag{2.67}$$

with

$$\beta_6 = 2J^{-1}\frac{\partial W}{\partial I_6} \tag{2.68}$$

For the case in which the medium is subject to a magnetic field only in the absence of the mechanical loading, Eq. (2.67) can be expressed in the following form:

$$\mathbf{m} = -(\beta_6 |_{\mathbf{F}=\mathbf{I}} + \beta_7 |_{\mathbf{F}=\mathbf{I}} + \beta_8 |_{\mathbf{F}=\mathbf{I}})\mathbf{b} \tag{2.69}$$

In the above relation, the magnetostriction is negligible, i.e. $\mathbf{F} = \mathbf{I}$.

Comparing the above relation with purely magnetic relations permits the identification of the material unknowns in the stored-energy density function. By combining Eqs. (1.53) and (1.54), defined for a linear magnetic material, the magnetization can be expressed as:

$$\mathbf{m} = \frac{\chi}{\mu_0(1+\chi)}\mathbf{b} \tag{2.70}$$

Subsequently, by making an analogy between Eqs. (2.69) and (2.70), the following relation can be accomplished:

$$\beta_6 |_{\mathbf{F}=\mathbf{I}} + \beta_7 |_{\mathbf{F}=\mathbf{I}} + \beta_8 |_{\mathbf{F}=\mathbf{I}} = -\frac{\chi}{2\mu_0(1+\chi)} \tag{2.71}$$

Now, let us focus on the case in which only a mechanical loading is exerted to the body. From Eq. (2.65), in the absence of the magnetic field, $\mathbf{b} = \mathbf{0}$, the Cauchy stress tensor may be expressed as:

$$\boldsymbol{\sigma} = \beta_1 |_{\mathbf{b}=\mathbf{0}} \mathbf{I} + \beta_2 |_{\mathbf{b}=\mathbf{0}} \mathbf{G} + \beta_3 |_{\mathbf{b}=\mathbf{0}} \mathbf{G}^{-1} \tag{2.72}$$

The above relation is identical to the Cauchy stress tensor developed for hyperelastic materials [6] and as expected the stress tensor is symmetric. The above stress relation facilitates the development of a constitutive equation for the MAE and estimations of material unknowns from the mechanical deformation alone. It should be noted that the constitutive relation for MAEs in the present study is derived on the basis of the traditional material models of hyperelastic materials.

2.3.3 Incompressible Deformable Magnetic Medium

This section deals with the constitutive equations for the incompressible MAEs. The incompressibility condition requires that the determinant of the deformation is equal to one, J=1. This implies the unity value of the third invariant of the Cauchy-Green deformation tensor, I_3=1. Consequently, for the incompressible case, the energy density is a function of the invariants I_1, I_2, I_6, I_7 and I_8, such that:

$$W = W(I_1, I_2, I_6, I_7, I_8) - p(J-1) \tag{2.73}$$

where p plays the role of the Lagrange multiplier and must be determined by solving the associated problem. By following the procedure described for the compressible MAE in 2.3.2, the stress tensor for the incompressible medium can be obtained as:

$$\begin{aligned} \boldsymbol{\sigma} = &-p\mathbf{I} + 2([\frac{\partial W}{\partial I_1} + \frac{\partial W}{\partial I_2} I_1]\mathbf{G} - \frac{\partial W}{\partial I_2}\mathbf{G}^2 + \frac{\partial W}{\partial I_7}(\mathbf{G}.\mathbf{b})\mathbf{b} \\ &+ \frac{\partial W}{\partial I_8}[(\mathbf{G}^2.\mathbf{b})\mathbf{b} + (\mathbf{G}.\mathbf{b})(\mathbf{b}.\mathbf{G})]) \end{aligned} \tag{2.74}$$

An alternate form of the above relation further obtained using the Cayley-Hamilton theorem as:

$$\boldsymbol{\sigma} = -\overline{p}\mathbf{I} + \overline{\beta}_2\mathbf{G} + \overline{\beta}_3\mathbf{G}^{-1} + \overline{\beta}_7(\mathbf{G}.\mathbf{b})\mathbf{b} + \overline{\beta}_8[(\mathbf{G}^2.\mathbf{b})\mathbf{b} + (\mathbf{G}.\mathbf{b})(\mathbf{b}.\mathbf{G})] \tag{2.75}$$

where

$$\bar{\beta}_1 = 2\frac{\partial W}{\partial I_2} I_2, \quad \bar{\beta}_2 = 2\frac{\partial W}{\partial I_1}, \quad \bar{\beta}_3 = -2\frac{\partial W}{\partial I_2}, \quad \bar{\beta}_7 = 2\frac{\partial W}{\partial I_7}, \quad \bar{\beta}_8 = 2\frac{\partial W}{\partial I_8} \tag{2.76}$$

For an incompressible magnetic deformable solid, Eq. (2.67) can also be expressed in the following form:

$$\mathbf{m} = -\bar{\beta}_6 \mathbf{b} - \bar{\beta}_7 \mathbf{G}.\mathbf{b} - \bar{\beta}_8 \mathbf{G}^2.\mathbf{b} \tag{2.77}$$

with

$$\bar{\beta}_6 = 2\frac{\partial W}{\partial I_6} \tag{2.78}$$

In a manner similar to the compressible medium, the stress tensor and the magnetization vector for the incompressible MAE in the absence of the magnetic field and the deformation, respectively, are obtained as:

$$\boldsymbol{\sigma} = -\bar{p}\mathbf{I} + \bar{\beta}_2 |_{\mathbf{b}=\mathbf{0}} \mathbf{G} + \bar{\beta}_3 |_{\mathbf{b}=\mathbf{0}} \mathbf{G}^{-1} \tag{2.79}$$

$$\mathbf{m} = -(\bar{\beta}_6 |_{\mathbf{F}=\mathbf{I}} + \bar{\beta}_7 |_{\mathbf{F}=\mathbf{I}} + \bar{\beta}_8 |_{\mathbf{F}=\mathbf{I}})\mathbf{b} \tag{2.80}$$

The coefficients β_i $(i = 6,7,8)$ in Eq. (2.80) are related to magnetic susceptibility, as:

$$\bar{\beta}_6 |_{\mathbf{F}=\mathbf{I}} + \bar{\beta}_7 |_{\mathbf{F}=\mathbf{I}} + \bar{\beta}_8 |_{\mathbf{F}=\mathbf{I}} = -\frac{\chi}{2\mu_0(1+\chi)} \tag{2.81}$$

Equations (2.79) and (2.81) are used for identifying the material unknowns for the incompressible MAEs.

2.4 Experimental Study

In the present study, an experiment is designed to measure the torque-deflection characteristics of an isotropic MAE. The magnetic permeability imposed in the MAE is also characterized and the measured data is used to identify unknown constants in the proposed material model. For the purpose of experiments, cylindrical MAE sample was fabricated in the laboratory. The fabrication and experimental method are discussed in the following sub-section

2.4.1 Fabrication of MAE

An isotropic MAE with 15% volume fraction of iron particles was fabricated in the laboratory using the method described in [106]. Briefly, the silicon rubber Ecoflex 00-50, shown

in Figure 2-2, with 100% modulus of 12 psi was used as the matrix. The soft carbonyl iron powder (diameter changes from 3.9 to 5 μm), shown in Figure 2-3, are taken as the iron particles. Samples of pure rubbers were also fabricated for characterizing the properties of the rubbers. For this purpose, the Ecoflex 00-50, was mixed with the curing agent (ratio 1:1) and then the mixture was degassed and poured in a mold. The mixture was permitted to cure for several hours in the ambient condition. Subsequently, the MAE sample was fabricated by mixing the iron powder in Ecoflex 00-50 together with curing agent. In order to avoid the hysteric magnetic behavior in this work the soft iron particles were used for fabrication of MAEs. The fraction of iron particles was limited to 15% by volume. After thoroughly mixing, the mixture was degassed in a vacuum chamber and permitted to cure in mold under ambient condition. Samples of rubbers and MAE were cut from the respective cured component (diameter = 20 *mm*; thickness = 6 *mm*). The mass density of the MAE was estimated using two approaches. In the first approach, the mass density of MAE, ρ_{MAE}, was computed from those of the constituents as

$$\rho_{MAE} = 0.85\rho_{Rubber} + 0.15\rho_{Iron} = 2090.6 \ \ kg/m^3 \tag{2.82}$$

where $\rho_{Rubber} = 1070 \ kg/m^3$ and $\rho_{Iron} = 7874 \ \ kg/m^3$ are the mass density of silicone rubber and iron particles, respectively. The mass density of the MAE was also estimated through direct measurement of the sample volume and mass which revealed the mass density of about $\rho_{MAE} = 2000 \ \ kg/m^3$. The two approaches are considered to yield comparable mass density with distinction of 4.5%.

Figure 2-2. Parts A and B of the silicone rubber Ecoflex 00-50.

Figure 2-3. Carbonyl iron powder.

2.4.2 Measurement of Magnetic Permeability

An experiment was initially designed for measuring the relative permeability of the MAE with 15% volume fraction of carbonyl iron particle (CIP). An electromagnet was used to induce the desired magnetic field on the MAE. A finite element model of the circular cylinder MAE was developed to evaluate distribution of the magnetic field induction inside the MAE. The distribution of the magnetic field induction along the y-direction is illustrated in Figure 2-4. As it can be seen, the magnetic field inside the material is homogenous. The circular cylinder geometry with the chosen orientation permitted uniform magnetic field distribution. The homogenous magnetization induced inside the MA sample with circular cross-section also permits evaluation of its permeability experimentally by measurement of the magnetic field induction and the magnetic field strength inside the material.

The two probes, labelled A and B, were positioned on the left and top surfaces of the cylindrical sample as shown in Figure 2-4 for measurement of magnetic field induction and strength. Both the probes were positioned in the vicinity of the bounding surface of the cylindrical MAE, for measuring the magnetic field in the gap surrounding the MAE. It should be noted that the relation $\mathbf{b} = \mu_0 \mathbf{h}$ holds for the air. Probe A measures the magnetic field strength of the air in the direction of y-axis, while probe B measures the vertical magnetic field induction of the air in the neighborhood of the cylinder. Considering the magnetic boundary condition stated in Eq. (2.22), the quantity measured by probe A is the vertical magnetic field strength in the magnetic medium. Furthermore, Eq. (2.21) states that the normal component of magnetic field induction is the same at the magnetic boundaries, which permits evaluation of the magnetic induction in the medium along the y-axis. Considering homogenous magnetic parameters, as

discussed above, and assuming that there is a linear relation between magnetic field induction and the magnetic field strength as given in Eq. (2.17) the relative permeability of the medium can be evaluated from $\mu^r = \mu_0^{-1} b / h$ using known values of b and h. For MAE with 15% volume fraction of CIP, the measurements were repeated under varying levels of the magnetic field. The results revealed nearly constant value of relative permeability under different magnetic fields. The mean value was obtained as $\mu^r = 1.5$.

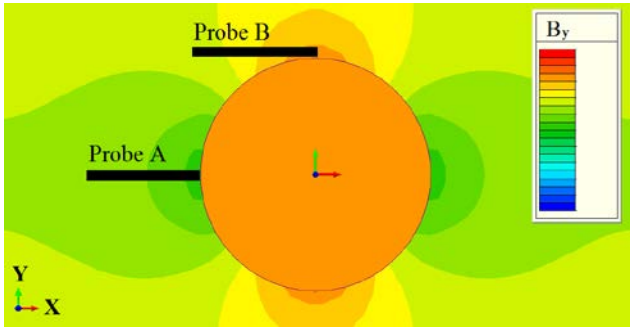

Figure 2-4. Distribution of the magnetic field induction for a right circular cylinder obtained from the FE analysis.

2.4.3 Measurement of Torsion Characteristics of the MAE

Experiments were performed to characterize torque-deflection response of the MAE subject to finite torsion (shear) loading and different levels of the magnetic field. The measured data are used to identify the material unknowns in the proposed constitutive model, as described in the following section. The experiments were performed using the magneto-rheometer from TA instrument (Discovery Hybrid Rheometer-HR-3) equipped with an electromagnet for characterizing coupled magneto-mechanical behavior of the MAE. The maximum torque, the torque resolution and the displacement resolution are respectively 200 N. mm, 50 nN. mm and 2 nrad for the DHR instrument. The rheometer has been widely used for characterization of magnetorheological fluids/elastomers in the presence of magnetic field up to 1 T and temperature in the -10 °C to 170 °C range [95, 107]. The main advantage of the magneto-rheometer is its integrated control system, which permits application of controlled magnetic field over the deformation of the sample. The closed-loop control ensures constant magnetic field applied to

the sample during the mechanical deformation. The main components of the magnetic cell used in the rheometer are shown in Figure 2-5.

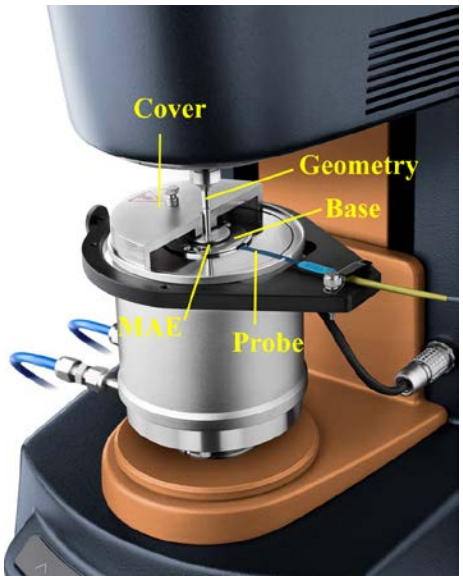

Figure 2-5. Main components of a magneto-rheometer.

For the purpose of the designed experiments, uniform cylindrical samples of MAE (diameter 20 mm; height 6 mm) were cut from the fabricated MAE. A sample was then placed between the base and upper geometry of the rheometer, as shown in Figure 2-5. Sufficient normal compressive force was applied to ensure no-slip condition during the test and the deformation due to the loading was very negligible. The rheometer applies oscillatory mechanical loading in the shear direction. The height of the MAE thus remains constant. The MAE is subjected to torsion, as the upper geometry rotates and induces an external torque. The upper surface of the cylindrical MAE undergoes angular deformation, which directly related to angular displacement of the geometry. It should be noted that the lower surface is fixed due to no-slip condition between the MAE sample and the base, as shown in Figure 2-6. A Hall probe was also located just under the sample for measurement of the central vertical magnetic field. The measurements were reported under different levels of magnetic field density, ranging from 0 to 0.4 T, which the amplitude of angular deformation (twist) was held as 0.39 rad (22 degrees). All experiments were conducted at a temperature of about 20° C. The oscillatory rotations were generated at a very low frequency of 0.1 Hz, and the load-deflection (torque-twist angle) response

corresponding to each applied magnetic field was recorded. In carrying out the experiments, measures associated with the calibration of the rheometer were taken into account. Additionally, tests were repeated at least twice in each case in order to verify the accuracy of the measured data.

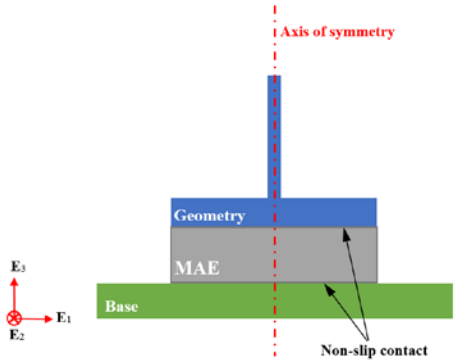

Figure 2-6. Schematic of the MAE subject to torsion in the oscillatory rotation.

2.4.4 Measured Torque-Deflection Responses of the MAE

Figure 2-7 (b) to Figure 2-7 (d) illustrate the torque-deflection (twist) response of the MAE subject to different levels of the magnetic flux density. The torque-deflection response of the pure rubber sample was also measured, and shown in Figure 2-7 (a). The figures also show linear torque-deflection characteristics, obtained from tangent lines in the vicinity of 0 deflection. These permit the assessment of the deviation of the MAE's responses from the linear response. The results suggest that an increase in the magnetic flux density yields increasing deviation of the MAE's response from the linear characteristics. Moreover, the torque corresponding to maximum deflection increases considerably with the application of the magnetic field when compared with the rubber sample. The magnitude of the torque increases with increase in the magnetic field density, as shown in Figure 2-8, leading to higher effective stiffness of the MAE. Additionally, it should be noted that the magnetoactive effects are considerably dependent on the stiffness of a rubber used as matrix.

The measurements were also performed under a very small angular deformation of the MAE (amplitude = 0.04 degree). The measured torque-deflection responses as function of the magnetic flux density are presented in Figure 2-9. The data are used to identify nominal shear modulus of the MAE as a function of the applied magnetic flux density, which are summarized in Table 2-1.

The measured data are also used to verify the material model developed for small deformation analysis, presented in section 2.5.

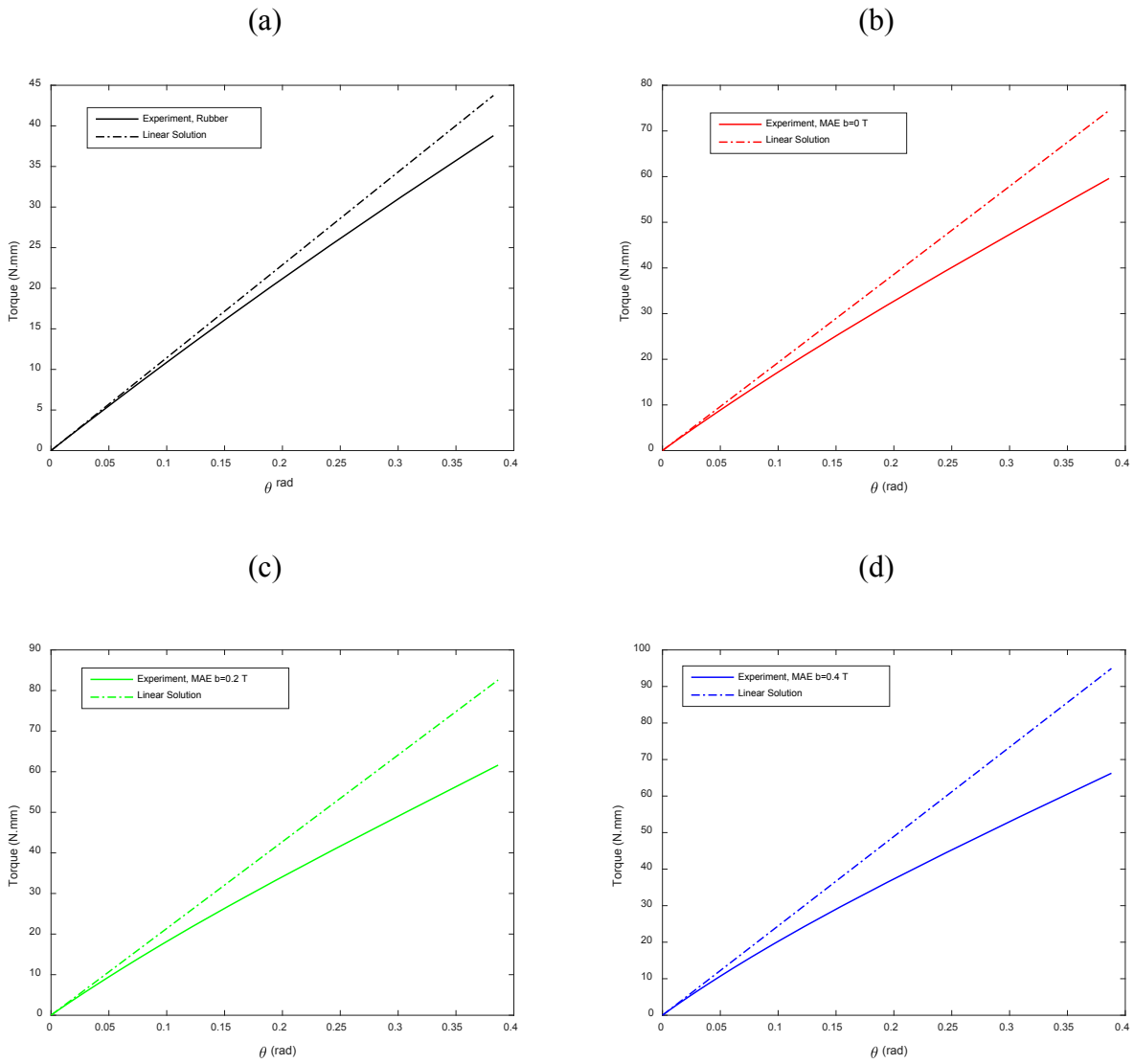

Figure 2-7. Torque-deflection response of (a) pure rubber sample; (b) MAE in B=0 T, (c) MAE in B=0.2 T, (d) MAE in B=0.4 T.

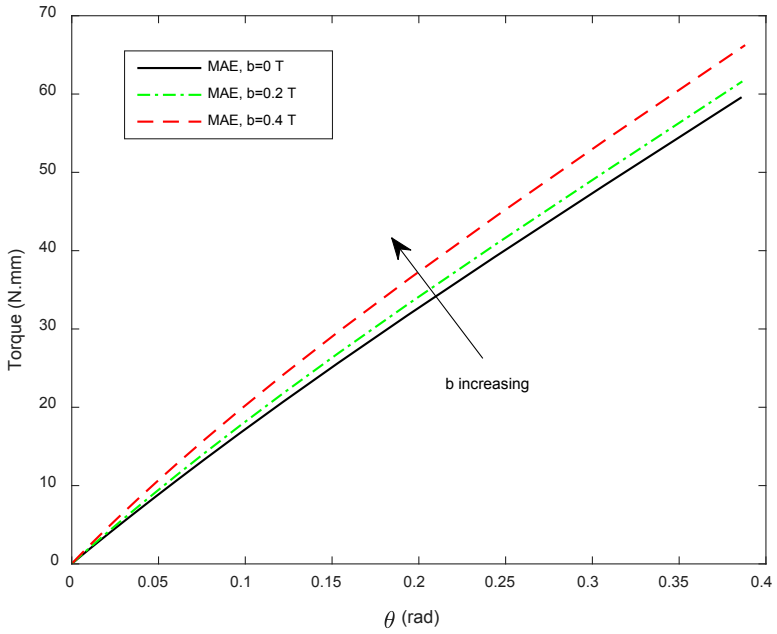

Figure 2-8. Effect of magnetic flux density (b) on the torque-deflection characteristics of the MAE.

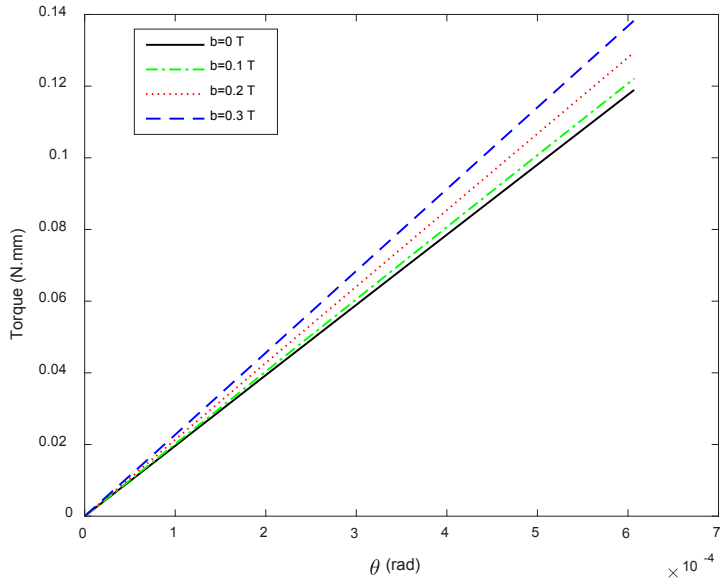

Figure 2-9. Torque-twist angle response for various magnetic fields.

Table 2-1. Nominal shear modulus of the MAE obtained from measured torque-deflection characteristics, under a very small deformation and different levels of magnetic field density.

	Magnetic Field induction b (mT)			
	0	100	200	300
Nominal Shear Modulus G^* (kPa)	74.31	77.60	82.42	87.53

2.5 Small Deformation Analysis

In this section, the framework and the formulation associated with the small-deformation analysis of the MAE are presented and a material model is proposed.

2.5.1 Decomposition of Magnetic Parameters

The governing equations for the small deformation analysis are formulated by decomposing the magnetic parameters in the deformed configuration into two parts, which related to those for the rigid-body state and the corresponding variations, see Figure 2-10. In the following formulation, the upper case letters are used for the magnetic variables in the rigid-body state, while the lower case letters describe the variables for the perturbed state. The spatial magnetic parameters $\{\mathbf{b},\mathbf{h},\mathbf{m}\}$ are decomposed into two constituents involving the initial fields $\{\mathbf{B},\mathbf{H},\mathbf{M}\}$ and the corresponding variations $\{\hat{\mathbf{b}},\hat{\mathbf{h}},\hat{\mathbf{m}}\}$, as [66]:

$$\mathbf{b} = \mathbf{B} + \hat{\mathbf{b}}, \tag{2.83}$$

$$\mathbf{h} = \mathbf{H} + \hat{\mathbf{h}}, \tag{2.84}$$

$$\mathbf{m} = \mathbf{M} + \hat{\mathbf{m}} \tag{2.85}$$

For the rigid-body state, the relationship among **B**, **H** and **M** is obtained from Eq. (2.15), as:

$$\mathbf{B} = \mu_0 (\mathbf{H} + \mathbf{M}) \tag{2.86}$$

Substituting Eqs. (2.83)-(2.85) into Eq. (2.15) yields the following relation among the parameters describing the variations in the magnetic parameters:

$$\hat{\mathbf{b}} = \mu_0 \left(\hat{\mathbf{h}} + \hat{\mathbf{m}} \right) \tag{2.87}$$

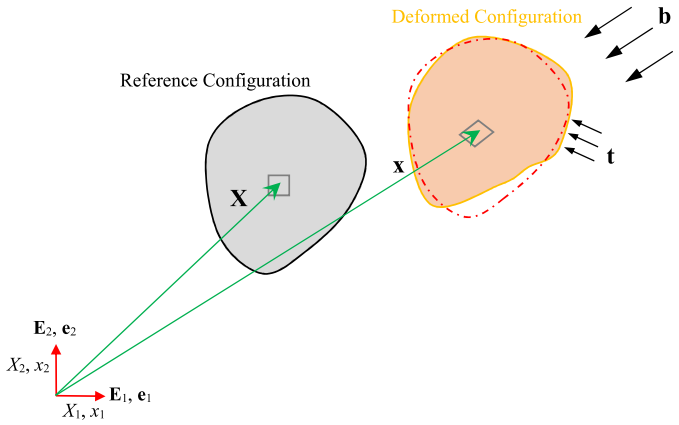

Figure 2-10. Reference and deformed configurations of a body as well as the rigid-body state.

2.5.2 A Material Model for Small-Strain Deformation of MAEs

Considering a rigid medium and a linear relation between the magnetic field and the magnetization, Eq. (2.45) yields:

$$\mathbf{M} = -\frac{\partial W}{\partial \tilde{\mathbf{B}}}\Big|_{\mathbf{F}=\mathbf{I}} \tag{2.88}$$

The above relation is obtained assuming negligible magnetostriction effect and the magnetic field being below the saturation limit. The proposed relation in Eq. (2.88) facilitates identification of the material unknowns in the energy density function through its comparison with the magnetization-magnetic induction relation for the magnetic material. Considering Eqs. (1.51) and (1.52), which are valid for the magnetic materials, the relation between the magnetization and magnetic induction can be obtained as:

$$\mathbf{m} = \frac{\chi}{\mu_0 (1+\chi)} \mathbf{b} \tag{2.89}$$

Considering that $\mathbf{m} = \mathbf{M}$ and $\mathbf{b} = \mathbf{B}$ for the rigid-body state, comparison of Eqs. (2.88) and (2.89) yields:

$$\frac{\partial W}{\partial \tilde{\mathbf{B}}}|_{\mathbf{F}=\mathbf{I}} = \frac{\chi}{\mu_0 (1+\chi)} \tag{2.90}$$

Additionally, when the body is subject to only the mechanical load, the stress tensor, $\boldsymbol{\sigma}$, in Eq. (2.44) can be rewritten as:

$$\boldsymbol{\sigma} = J^{-1}\mathbf{F}.\frac{\partial W}{\partial \mathbf{E}}|_{\mathbf{b}=0}.\mathbf{F}^{\mathrm{T}} \tag{2.91}$$

The above relation is identical to the Cauchy stress tensor developed for the Saint Venant-Kirchhoff materials in terms of the Green-Lagrange strain tensor [6].

For the development of the linear material model, the general constitutive equation for a medium under finite deformation, as stated in Eq. (2.46), has been utilized, which is followed by a linearization scheme conducted about the rigid-body state. It must be pointed out that the magnetostriction effect is assumed negligible in comparison with the deformation due to the applied mechanical loading. Thus, in the rigid-body state, the strain and the magnetic field tensors can be simplified to [66]:

$$\mathbf{E}^0 = \mathbf{0}, \qquad \tilde{\mathbf{B}}^0 = \mathbf{B} \tag{2.92}$$

The superscript 0 in the above relations refers to the rigid-body state.

Using the Taylor series expansion and considering Eq. (2.92) in the rigid-body state, the linearized terms of $\frac{\partial W}{\partial \mathbf{E}}$ and $\frac{\partial W}{\partial \tilde{\mathbf{B}}}$ in Eq. (2.46) can be written as:

$$\left(\frac{\partial W}{\partial \mathbf{E}}\right)^L = \left(\frac{\partial W}{\partial \mathbf{E}}\right)^0 + \left(\frac{\partial^2 W}{\partial \mathbf{E}\partial \mathbf{E}}\right)^0 \left(\mathbf{E}-\mathbf{E}^0\right) + \left(\frac{\partial^2 W}{\partial \tilde{\mathbf{B}}\partial \mathbf{E}}\right)^0 \left(\tilde{\mathbf{B}}-\tilde{\mathbf{B}}^0\right), \tag{2.93}$$

$$\left(\frac{\partial W}{\partial \tilde{\mathbf{B}}}\right)^L = \left(\frac{\partial W}{\partial \tilde{\mathbf{B}}}\right)^0 + \left(\frac{\partial^2 W}{\partial \mathbf{E}\partial \tilde{\mathbf{B}}}\right)^0 \left(\mathbf{E}-\mathbf{E}^0\right) + \left(\frac{\partial^2 W}{\partial \tilde{\mathbf{B}}\partial \tilde{\mathbf{B}}}\right)^0 \left(\tilde{\mathbf{B}}-\tilde{\mathbf{B}}^0\right). \tag{2.94}$$

Furthermore, for the deformation analysis, the tensors $\mathbf{E}$ and $\tilde{\mathbf{B}}$ in the above equations can be approximated as:

$$\mathbf{E} \approx \mathbf{e} = \frac{1}{2}\left(\nabla \mathbf{u} + \mathbf{u}\nabla\right) \tag{2.95}$$

$$\tilde{\mathbf{B}} \approx \mathbf{B} + \hat{\mathbf{b}} + \mathbf{u}\nabla^T.\mathbf{B} + \mathbf{u}\nabla^T.\hat{\mathbf{b}} \tag{2.96}$$

where **e** denotes the so-called infinitesimal strain tensor. Moreover, it is noted that the relation $J^{-1} = 1 - tr(\mathbf{u}\nabla)$ holds, which is used later in the linearization scheme of the stress tensor.

Eqs. (2.93) and (2.94) comprise derivatives of the energy density, which should be evaluated in the rigid-body state. An energy density function for the isotropic MAE is employed, such that:

$$W = \frac{\lambda^*}{2}[tr(\mathbf{E})]^2 + G^*\mathbf{E}:\mathbf{E} + \frac{\gamma}{2}\tilde{\mathbf{B}}.\tilde{\mathbf{B}} \tag{2.97}$$

where λ^*, G^* and γ are unknowns, which are identified from the measured data.

The stress tensor for the MAE subject to small deformation is obtained by substituting for the derivatives of the W described in Eqs. (2.93) and (2.94) into Eq. (2.46). Assuming negligible variation in the magnetic field and linear approximations, the simplified form of the stress tensor is obtained as:

$$\boldsymbol{\sigma} = \lambda^* tr(\mathbf{e})\mathbf{I} + 2G^*\mathbf{e} + \gamma\mathbf{B}\mathbf{B} + \gamma(\mathbf{e}.\mathbf{B})\mathbf{B} \tag{2.98}$$

The unknowns λ^* and G^*, are also referred to as nominal Lamé's parameters, which are expressed as a function of the magnetic field induction.

The magnetization vector **m** is obtained following the same procedure as the Cauchy stress tensor and considering Eq. (2.45) as:

$$\mathbf{m} = -\gamma(\mathbf{B} + (\mathbf{u}\nabla).\mathbf{B}) \tag{2.99}$$

The energy density for the small-deformation analysis can be obtained by the linearization scheme employed for the stress tensor in Eq. (2.98), which yields:

$$W = \frac{\lambda^*}{2}[tr(\mathbf{e})]^2 + G^*\mathbf{e}:\mathbf{e} + \frac{\gamma}{2}\tilde{\mathbf{B}}.\tilde{\mathbf{B}} \tag{2.100}$$

The above relation suggests that the energy density is a quadratic function of the variables **e** and $\tilde{\mathbf{B}}$.

Let us focus on the material unknowns present in the small-deformation stress tensor, Eq. (2.98), for the pure mechanical case. In the absence of a magnetic field, Eq. (2.98) must be equivalent to the Hooke's law. Accordingly, it is concluded that

$$\lambda^*|_{\mathbf{b}=\mathbf{0}} = \lambda, \qquad G^*|_{\mathbf{b}=\mathbf{0}} = G \tag{2.101}$$

where λ and G are Lamé's constants. Furthermore, Eq. (2.99) must be true for the case in which no external mechanical loading is applied. Accordingly:

$$\mathbf{M} = -\gamma|_{\mathbf{F}=\mathbf{I}}\,\mathbf{B} \tag{2.102}$$

In the derivation of the small-deformation stress, it was supposed that the parameter γ is not dependent upon a kinematic parameter and it is deduced that $\gamma|_{\mathbf{F}=\mathbf{I}} = \gamma$. Furthermore, Eqs. (1.53) and (1.54) together with Eq. (2.102) yield the following relation for γ in terms of μ^r:

$$\gamma = -\frac{1}{\mu_0}\frac{\chi}{1+\chi} = \frac{1-\mu^r}{\mu_0\mu^r} \tag{2.103}$$

The small strains and nearly incompressible nature of MAEs yield [108]:

$$J = 1 \quad \text{and} \quad tr(\mathbf{e}) = 0 \tag{2.104}$$

For the incompressible MAEs, Eq. (2.98) can thus be rewritten as:

$$\boldsymbol{\sigma} = -p\mathbf{I} + 2G^*\mathbf{e} + \gamma\mathbf{B}\mathbf{B} + \gamma(\mathbf{e}.\mathbf{B})\mathbf{B} \tag{2.105}$$

where the parameter p is related to incompressibility of the material and can be obtained from the boundary condition of the body. Additionally, the energy density for the incompressible MAE is given by:

$$W = -ptr(\mathbf{e}) + G^*\mathbf{e}:\mathbf{e} + \frac{\gamma}{2}\tilde{\mathbf{B}}.\tilde{\mathbf{B}} \tag{2.106}$$

2.5.3 Analytical Solution to Small-deformation Torsion of a Cylinder

The material unknowns in the linearized constitutive equation proposed for the small deformation analysis of the magnetoactive elastomers are identified using the experimental data obtained for the cylindrical MAE, as described in section 2.4.4. For small-deformation torsion of the sample, in the rectangular coordinate system as shown in Figure 2-11, the components of the displacement vector may be written as [109]:

$$u_1 = -\kappa x_2 x_3, \qquad u_2 = \kappa x_1 x_3, \qquad u_3 = 0 \tag{2.107}$$

where $\kappa = \theta / x_3$ is the angle of twist per unit length. As shown in Figure 2-12, the bottom of the cylinder is fixed and the coordinate system is located at the center of the bottom surface, while the axis x_3 is along the axis of the cylinder. As it can be realized, the displacement components in

Eq. (2.107) satisfy the boundary condition associated with the constrained bottom surface of the cylinder.

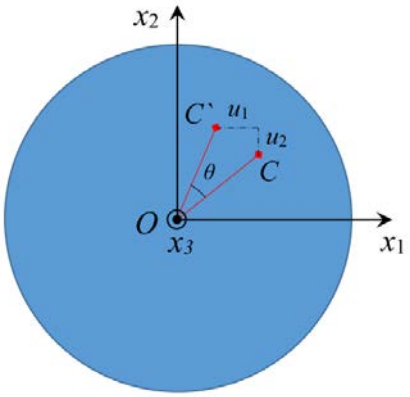

Figure 2-11. Circular cross section of the MAE along with the coordinate system.

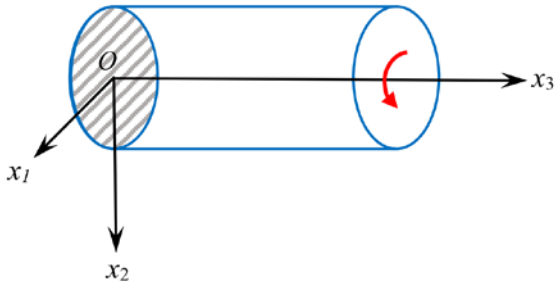

Figure 2-12. A right circular cylinder under torsion.

Given the definition of the infinitesimal strain tensor, $e_{ij} = \frac{1}{2}\left(\frac{\partial u_i}{\partial x_j} + \frac{\partial u_j}{\partial x_i}\right)$, and using Eq. (2.107), the expressions for non-vanishing strains are obtained as:

$$e_{13} = -\frac{1}{2}\kappa x_2, \qquad e_{23} = \frac{1}{2}\kappa x_1, \tag{2.108}$$

Substituting for the strain components presented in Eq. (2.108) into Eq. (2.105) and considering that the magnetic field induction is constant and it occurs along the x_3-axis, the non-zero components of the stress tensor $\boldsymbol{\sigma}$ are obtained, as:

$$\sigma_{11} = -p \tag{2.109}$$

$$\sigma_{22} = -p \tag{2.110}$$

$$\sigma_{33} = -p \tag{2.111}$$

$$\sigma_{13} = [2G^* + \gamma B_3^{\,2}]e_{13} \tag{2.112}$$

$$\sigma_{31} = 2G^* e_{13} \tag{2.113}$$

$$\sigma_{23} = \left[2G^* + \gamma B_3^{\,2}\right]e_{23} \tag{2.114}$$

$$\sigma_{32} = 2G^* e_{23} \tag{2.115}$$

The above stress field should satisfy the linear and angular momentum, Eqs. (2.10) and (2.11), respectively. Considering negligible particles accelerations under the quasi-static deformation and assuming uniform and homogenous magnetic field and negligible mechanical body force, the conservation of the linear momentum, Eq. (2.10), yields:

$$\sigma_{11,1} + \sigma_{21,2} + \sigma_{31,3} = 0 \tag{2.116}$$

$$\sigma_{12,1} + \sigma_{22,2} + \sigma_{32,3} = 0 \tag{2.117}$$

$$\sigma_{13,1} + \sigma_{23,2} + \sigma_{33,3} = 0 \tag{2.118}$$

Employing Eqs. (2.109) to (2.115), the static equilibrium equations can be rewritten as:

$$-p_{,1} + \left(2G^* e_{31}\right)_{,3} = 0 \tag{2.119}$$

$$-p_{,2} + \left(2G^* e_{32}\right)_{,3} = 0 \tag{2.120}$$

$$(\left[2G^* + \gamma B_3^{\,2}\right]e_{13})_{,1} + (\left[2G^* + \gamma B_3^{\,2}\right]e_{23})_{,2} - p_{,3} = 0 \tag{2.121}$$

The simultaneous solution of the above equations yields an expression for p.

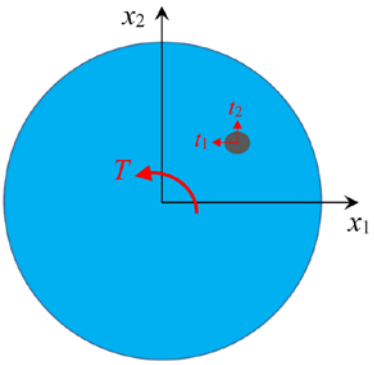

Figure 2-13. In-plane tractions and associated applied torque.

For the magnetic field acting solely in the axial direction, the stress field is consistent with the conservation of angular momentum, described in Eq. (2.11).

The mechanical tractions developed at the top surface of the cylinders are obtained considering the boundary conditions. It should be noted that the lateral surface of the cylinder is free of mechanical tractions, while the bottom surface is fully constrained. The top surface of the cylinder is subjected to a mechanical torque. Using the mechanical boundary condition defined in Eq. (2.20), see Figure 2-13, the mechanical tractions **t** developed on the top surface can be expressed as:

$$t_1 = \left(\sigma_{31} - [\![\sigma_{31}^S]\!]\right) \tag{2.122}$$

$$t_2 = \left(\sigma_{32} - [\![\sigma_{32}^S]\!]\right) \tag{2.123}$$

Moreover, using Eq. (2.23), the components of the stress tensor $\boldsymbol{\sigma}^S$ are obtained as:

$$[\![\sigma_{31}^S]\!] = [\![\sigma_{31}^S]\!] = 0 \tag{2.124}$$

Consequently, the applied tractions can be formulated as:

$$t_1 = 2G^* e_{31}, \qquad t_2 = 2G^* e_{32} \tag{2.125}$$

The magnitude of the applied torsion T can be obtained by taking the moment of the applied tractions on the top surface of the MAE, such that:

$$T = \int_A \left(x_1 t_2 - x_2 t_1\right) \mathrm{d}A \tag{2.126}$$

where the domain of integration A defines the cross sectional area of the MAE cylinder.

Substituting for the non-vanishing strains, e_{31} and e_{32}, from Eq. (2.108) in Eq. (2.125), and applying the resulting tractions into Eq. (2.126) yields the following relation for the applied torque:

$$T = G^* I \kappa \qquad \text{with} \qquad I = \int_A \left(x_1^{\,2} + x_2^{\,2}\right) \mathrm{d}A \tag{2.127}$$

where I is the polar moment of inertia of the cross section, which for the circular section with radius of R is $I = \pi R^4 / 2$. The above relation implies that the slope of T/I-κ is indeed equivalent to the term G^*. The experimental results, however, revealed that the value of nominal shear modulus varies with the external magnetic field (Table 2-1). The dependence of the modulus on the magnetic field is considered by assuming that the magnetic field inside the material is homogenous and occurs in the vertical direction only, which automatically satisfies the Maxwell

equations, Eqs. (2.13) and (2.14). It needs to be emphasized that the magneto-rheometer applies controlled magnetic field to the MAE, which remains constant during the sample's deformation.

In the proposed material model for small-deformation of MAEs, the shear modulus is considered to vary quadratically with the magnetic field induction, as it is observed for the energy density and the stress in Eqs. (2.106) and (2.105), respectively. Furthermore, Figure 2-14 shows the variation in nominal shear modulus of the MAE with B_3^2, obtained from the experiments.

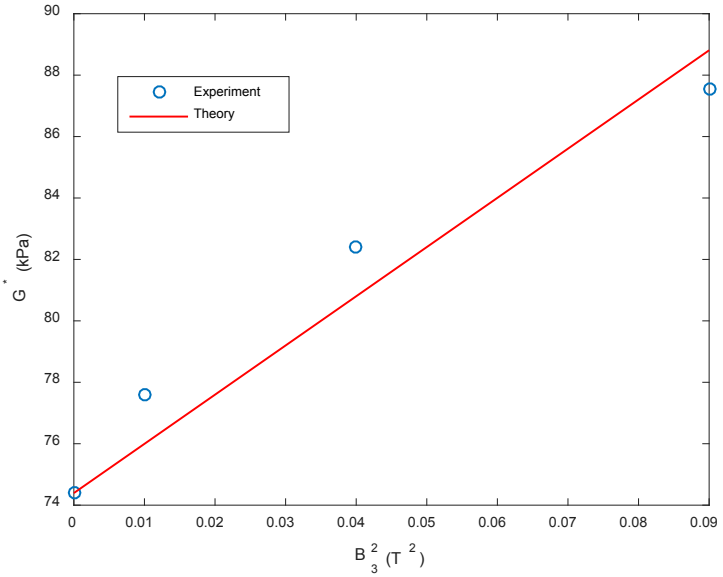

Figure 2-14. Nominal shear modulus versus B_3^2.

The following relation is subsequently proposed to describe the variation in the nominal shear modulus with respect to the magnetic induction:

$$G^* = G\left[1+\eta tr\left(\mathbf{BB}\right)\right] \tag{2.128}$$

where G is the shear modulus of the material in the absence of the magnetic field, which was obtained as 74.31 kPa from the measured data under small deformation (Table 2-1). The material constant η is identified by minimizing the error between the model predicted and the measured modulus. The error minimization converged to η of 2.153 $1/T^2$. The variation in the nominal shear modulus predicted from the proposed model has been shown in Figure 2-14, which compares reasonably well with the measured data. Also, to compare quantitatively the theoretical results with the experimental data, use is made of the most general definition of the coefficient of

determination which is described by the relation $R^2 = 1 - \sum_i (G_i^{*EXP} - G_i^{*THEOR})^2 / \sum_i (G_i^{*EXP} - \bar{G}_i^{*EXP})^2$, where $\bar{G}_i^{*EXP} = \sum_i G_i^{*EXP} / n_p$ and n_p stands for the number of experimental points. R^2 is found to be over 93% in the range of considered applied magnetic fields, confirming that the proposed relation in Eq. (2.128) can reasonably predict the field-dependent nominal shear modulus under relatively low to moderate magnetic fields.

For the current problem, the value of p is estimated from the fact that the lateral surface of the cylinder is free from the mechanical tractions. Using Eqs. (2.108), and (2.119) to (2.121) and (2.128) and considering the homogeneity of the magnetic field, it is found that:

$$p_{,1} = 0, \qquad p_{,2} = 0, \qquad p_{,3} = 0 \tag{2.129}$$

The above implies that the p is not a function of x_1, x_2 and x_3. The pressure, however, can be estimated from the mechanical tractions developed on the lateral surface of the cylinder, which are obtained from Eq. (2.20), as:

$$t_1 = \left(\sigma_{11} - [\![\sigma_{11}^S]\!]\right) n_1 + \left(\sigma_{21} - [\![\sigma_{21}^S]\!]\right) n_2 \tag{2.130}$$

$$t_2 = \left(\sigma_{12} - [\![\sigma_{12}^S]\!]\right) n_1 + \left(\sigma_{22} - [\![\sigma_{22}^S]\!]\right) n_2 \tag{2.131}$$

$$t_3 = \left(\sigma_{13} - [\![\sigma_{13}^S]\!]\right) n_1 + \left(\sigma_{23} - [\![\sigma_{23}^S]\!]\right) n_2 \tag{2.132}$$

By taking advantage of the stress field presented in Eqs. (2.109) to (2.115) and employing Eq. (2.23), the above tractions are simplified as:

$$t_1 = \left(\sigma_{11} - [\![\sigma_{11}^S]\!]\right) n_1 + \sigma_{21} n_2 \tag{2.133}$$

$$t_2 = \sigma_{12} n_1 + \left(\sigma_{22} - [\![\sigma_{22}^S]\!]\right) n_2 \tag{2.134}$$

$$t_3 = \sigma_{13} n_1 + \sigma_{23} n_2 \tag{2.135}$$

For a polar coordinate system defined with respect to the axes x_1 and x_2, the following relations hold for a point on the circumference of the circle:

$$x_1 = R\cos\alpha, \qquad x_2 = R\sin\alpha, \qquad n_1 = \cos\alpha, \qquad n_2 = \sin\alpha \tag{2.136}$$

where α is the angle with respect to the positive direction of x_1-axis. The above relations help to define the tractions on the lateral surface in a simple manner. The x_3-component of the traction on the lateral surface is subsequently derived from Eqs. (2.112), (2.114) and (2.108), as:

$$t_3 = -\left[2G^* + \gamma B_3^{\,2}\right]\kappa R\sin\alpha\cos\alpha + \left[2G^* + \gamma B_3^{\,2}\right]\kappa R\cos\alpha\sin\alpha = 0 \tag{2.137}$$

which automatically satisfies the traction boundary condition in the corresponding direction. The expressions for t_1 and t_2 are also obtained, following the same procedure, as

$$t_1 = \left(-p - [\![\sigma_{11}^S]\!]\right)n_1 = 0 \tag{2.138}$$

$$t_2 = \left(-p - [\![\sigma_{22}^S]\!]\right)n_2 = 0 \tag{2.139}$$

where

$$[\![\sigma_{11}^S]\!] = [\![\sigma_{22}^S]\!] = -\frac{1}{2\mu_0}B_3^+ B_3^+ - \left(M_3^- B_3^- - \frac{1}{2\mu_0}B_3^- B_3^-\right) \tag{2.140}$$

From Eqs. (2.138) and (2.139), it can be concluded that

$$p = -[\![\sigma_{11}^S]\!] \tag{2.141}$$

The parameter p is thus defined with respect to the magnetic variables.

2.6 Analytical Solution to Finite Torsion of a Cylindrical MAE

In this section, the torsion response of the cylindrical MAE is obtained analytically, and an energy density function is proposed. The material constants are estimated through comparison of the analytical solution with the experimental data.

2.6.1 General Solution

Figure 2-15 illustrates the right cylinder of radius R together with the coordinate system. The thickness of the cylinder is described by L between the two rigid disks and remains constant during the angular deformation. The bottom surface of the cylinder is constrained, while the upper one is subject to angular deformation and is able to rotate about its axis, as it is shown for the experimental setup in Figure 2-6. In the assigned Cartesian coordinate system, shown in Figure 2-15, X_1X_2-plane is normal to the axis of the cylinder, the axis X_3 is parallel to the cylinder axis and the origin of the coordinate system is located at the center of the bottom cross section. The deformation of the cylinder subjected to the toque at the upper face can be described by [6]:

$$\begin{aligned} x_1 &= X_1\cos(\theta(X_3)) - X_2\sin(\theta(X_3)),\\ x_2 &= X_1\sin(\theta(X_3)) + X_2\cos(\theta(X_3)),\\ x_3 &= X_3, \end{aligned} \tag{2.142}$$

where θ is the rotation of every cross section and is a function of X_3 alone. Additionally, it is supposed that the torsion angle changes linearly along the X_3 direction, such that

$$\theta = \kappa X_3 \tag{2.143}$$

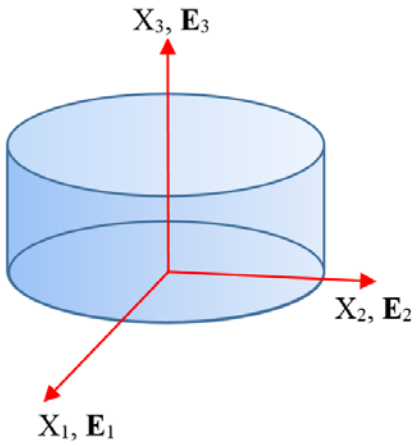

Figure 2-15. A right circular cylinder along with the coordinate system.

in which κ is a constant that defines the angle of twist per unit length. The height of the cylinder does not vary during the torsion, and the angle of twist at the bottom of the cylinder is zero. The chosen conditions are consistent with those used in the experiments described in section 2.4.4.

There exists one underlying point which must be addressed herein. The torsion of a circular cylinder and the simple shear of a slab under a finite deformation involve different boundary conditions and applied loads. The analytical solution obtained for the simple shear, however, is equally valid for finite torsion, provided that the torque-twist response is linear even for large rotations [6]. In this case, the stress and strain fields of a point on the lateral surface of the cylinder are analogous to those obtained for the simple shear test. The magneto-rheometer tests report the stress-strain response characteristics under the assumption that the distribution of the shear stress is a linear function of the radius and the angular deformation is very small. For elastomers exhibiting nonlinear torque-twist response, these assumptions, however, are not valid. The measured torque-twist responses are thus used instead of the shear stress-strain data.

As for the magnetic parameters, it is assumed the magnetic field induction is solely present in the X_3 direction, and is homogenous and uniform during the deformation of the cylinder. Consequently, we can write:

$$\mathbf{b} = b\mathbf{e}_3 \tag{2.144}$$

Using the expression for the deformation, defined in Eq. (2.142), the deformation gradient tensor can be obtained as:

$$\mathbf{F} = \cos\theta\mathbf{e}_1\mathbf{E}_1 - \sin\theta\mathbf{e}_1\mathbf{E}_2 - x_2\kappa\mathbf{e}_1\mathbf{E}_3 + \sin\theta\mathbf{e}_2\mathbf{E}_1 + \cos\theta\mathbf{e}_2\mathbf{E}_2 + x_1\kappa\mathbf{e}_2\mathbf{E}_3 + \mathbf{e}_3\mathbf{E}_3 \tag{2.145}$$

Since the determinant of the tensor above is one ($J = 1$), the volume of the body does not change during the deformation, irrespective of the compressibility of the material.

From the above relation together with Eqs. (1.5) and (1.10), the right and left Cauchy-Green deformation tensors can be obtained as follows:

$$\begin{aligned}\mathbf{C} &= \mathbf{E}_1\mathbf{E}_1 + \kappa(x_1\sin\theta - x_2\cos\theta)\mathbf{E}_1\mathbf{E}_3 + \mathbf{E}_2\mathbf{E}_2 + \kappa(x_1\cos\theta + x_2\sin\theta)\mathbf{E}_2\mathbf{E}_3 \\ &+\kappa(x_1\sin\theta - x_2\cos\theta)\mathbf{E}_3\mathbf{E}_1 + \kappa(x_1\cos\theta + x_2\sin\theta)\mathbf{E}_3\mathbf{E}_2 + [\kappa^2(x_1^{\,2} + x_2^{\,2}) + 1]\mathbf{E}_3\mathbf{E}_3\end{aligned} \tag{2.146}$$

and

$$\begin{aligned}\mathbf{G} &= [1 + x_2^{\,2}\kappa^2]\mathbf{e}_1\mathbf{e}_1 - x_1x_2\kappa^2\mathbf{e}_1\mathbf{e}_2 - x_2\kappa\mathbf{e}_1\mathbf{e}_3 - x_1x_2\kappa^2\mathbf{e}_2\mathbf{e}_1 + [1 + x_1^{\,2}\kappa^2]\mathbf{e}_2\mathbf{e}_2 \\ &+x_1\kappa\mathbf{e}_2\mathbf{e}_3 - x_2\kappa\mathbf{e}_3\mathbf{e}_1 + x_1\kappa\mathbf{e}_3\mathbf{e}_2 + \mathbf{e}_3\mathbf{e}_3\end{aligned} \tag{2.147}$$

The inverse of the left Cauchy-Green deformation tensor can also be written as:

$$\begin{aligned}\mathbf{G}^{-1} &= \mathbf{e}_1\mathbf{e}_1 + x_2\kappa\mathbf{e}_1\mathbf{e}_3 + \mathbf{e}_2\mathbf{e}_2 - x_1\kappa\mathbf{e}_2\mathbf{e}_3 + x_2\kappa\mathbf{e}_3\mathbf{e}_1 - x_1\kappa\mathbf{e}_3\mathbf{e}_2 \\ &+[1 + (x_1^{\,2} + x_2^{\,2})\kappa^2]\mathbf{e}_3\mathbf{e}_3\end{aligned} \tag{2.148}$$

From the above relations, the invariants are obtained as follows, which are used later in the formulation of the smart hyperelastic material model:

$$I_1 = 3 + \kappa^2(x_1^{\,2} + x_2^{\,2}) \tag{2.149}$$

$$I_2 = 3 + \kappa^2(x_1^{\,2} + x_2^{\,2}) \tag{2.150}$$

$$I_3 = 1 \tag{2.151}$$

$$I_7 = b^2 \tag{2.152}$$

Application of the constitutive equations developed earlier yields a relation for the stress in terms of the deformation tensors and the invariants. Assuming that the energy density of the incompressible material has no dependency on the invariants I_6 and I_8, the stress tensor, presented in Eq. (2.75) reduces to:

$$\boldsymbol{\sigma} = -\overline{p}\mathbf{I} + \overline{\beta}_2\mathbf{G} + \overline{\beta}_3\mathbf{G}^{-1} + \overline{\beta}_7\left(\mathbf{G}.\mathbf{b}\right)\mathbf{b} \tag{2.153}$$

Moreover, considering Eq. (2.77), the magnetization vector can be expressed as:

$$\mathbf{m} = -\overline{\beta}_7 \mathbf{G}.\mathbf{b} \tag{2.154}$$

Upon substituting for the kinematic tensors from Eqs. (2.147) and (2.148) in Eq. (2.153), the expressions for the nonzero stresses are derived as:

$$\begin{aligned}
&\sigma_{11} = -\overline{p} + \overline{\beta}_2\left(1+\kappa^2 {x_2}^2\right) + \overline{\beta}_3 = -\overline{p} + \overline{\beta}_2 + \overline{\beta}_3 + \overline{\beta}_2\kappa^2 {x_2}^2 \\
&\sigma_{12} = \sigma_{21} = -\overline{\beta}_2\kappa^2 x_1 x_2 \\
&\sigma_{13} = -\overline{\beta}_2\kappa x_2 + \overline{\beta}_3\kappa x_2 = \left(\overline{\beta}_3 - \overline{\beta}_2\right)\kappa x_2 - \overline{\beta}_7 x_2 \kappa b^2 \\
&\sigma_{31} = -\overline{\beta}_2\kappa x_2 + \overline{\beta}_3\kappa x_2 = \left(\overline{\beta}_3 - \overline{\beta}_2\right)\kappa x_2 \\
&\sigma_{22} = -\overline{p} + \overline{\beta}_2\left(1+\kappa^2 {x_1}^2\right) + \overline{\beta}_3 = -\overline{p} + \overline{\beta}_2 + \overline{\beta}_3 + \overline{\beta}_2\kappa^2 {x_1}^2 \\
&\sigma_{23} = \overline{\beta}_2\kappa x_1 - \overline{\beta}_3\kappa x_1 = \left(\overline{\beta}_2 - \overline{\beta}_3\right)\kappa x_1 + \overline{\beta}_7 x_1 \kappa b^2 \\
&\sigma_{32} = \overline{\beta}_2\kappa x_1 - \overline{\beta}_3\kappa x_1 = \left(\overline{\beta}_2 - \overline{\beta}_3\right)\kappa x_1 \\
&\sigma_{33} = -\overline{p} + \overline{\beta}_2 + \overline{\beta}_3\left[1+\kappa^2\left({x_1}^2 + {x_2}^2\right)\right] = -\overline{p} + \overline{\beta}_2 + \overline{\beta}_3 + \overline{\beta}_3\kappa^2\left({x_1}^2 + {x_2}^2\right) + \overline{\beta}_7 b^2
\end{aligned} \tag{2.155}$$

The solution to the finite torsion problem of a right circular cylinder made of a magnetoactive material subject to a magnetic field, presented in Eq. (2.142), must satisfy the conservation of linear momentum stated in Eq. (2.10). For this torsion problem, the mechanical body force is assumed to be negligible ($\overline{\mathbf{f}} = \mathbf{0}$). The magnetic body force is also taken as zero ($\mathbf{f} = \mathbf{0}$), considering homogeneity of the magnetic field inside the material together with two relations in Eqs. (2.144) and (2.18).

Before addressing the conservation of the linear momentum, let us consider the angular momentum law. As shown above, the stress tensor is not symmetric based on the stress field. The components of dual of the couple **l** in Eq. (2.11) can be expressed as:

$$\boldsymbol{\eta} = \frac{\overline{\beta}_5}{2} x_2 \kappa b^2 \mathbf{e}_1\mathbf{e}_3 - \frac{\overline{\beta}_5}{2} x_1 \kappa b^2 \mathbf{e}_2\mathbf{e}_3 - \frac{\overline{\beta}_5}{2} x_2 \kappa b^2 \mathbf{e}_3\mathbf{e}_1 + \frac{\overline{\beta}_5}{2} x_1 \kappa b^2 \mathbf{e}_3\mathbf{e}_2 \tag{2.156}$$

From the above relation the components of the body couple vector are obtained as:

$$l_1 = -\overline{\beta}_5 x_1 \kappa b^2, \qquad l_2 = -\overline{\beta}_5 x_2 \kappa b^2, \qquad l_3 = 0 \tag{2.157}$$

Furthermore, using the magnetization vector in Eq. (2.154) and the body couple vector in Eq. (2.18), the couple **l** reduces to:

$$\mathbf{l} = -\overline{\beta}_5\left(\mathbf{G}.\mathbf{b}\right)\times\mathbf{b}, \tag{2.158}$$

By substituting for the tensor **G** and magnetic field induction **b** from Eq. (2.147) and Eq. (2.144), respectively, in the above relation, it can be shown that the body couple above is similar to that presented in Eq. (2.157), which proves that the conservation law of the angular momentum is fully conserved.

The law of conservation of the linear momentum results in:

$$\nabla_{\mathbf{x}}.\boldsymbol{\sigma} = \mathbf{0} \tag{2.159}$$

Substituting for the stresses from Eq. (2.155) in Eq. (2.159) yields:

$$-\frac{\partial \overline{p}}{\partial x_1}+\frac{\partial \overline{\beta}_2}{\partial x_1}+\frac{\partial \overline{\beta}_3}{\partial x_1}+\frac{\partial \overline{\beta}_2}{\partial x_1}\kappa^2 {x_2}^2-\frac{\partial \overline{\beta}_2}{\partial x_2}\kappa^2 x_1 x_2-\overline{\beta}_2\kappa^2 x_1+(\frac{\partial \overline{\beta}_3}{\partial x_3}-\frac{\partial \overline{\beta}_2}{\partial x_3})\kappa x_2=0 \tag{2.160}$$

$$-\frac{\partial \overline{\beta}_2}{\partial x_1}\kappa^2 x_1 x_2-\overline{\beta}_2\kappa^2 x_2-\frac{\partial \overline{p}}{\partial x_2}+\frac{\partial \overline{\beta}_2}{\partial x_2}+\frac{\partial \overline{\beta}_3}{\partial x_2}+\frac{\partial \overline{\beta}_2}{\partial x_2}\kappa^2 {x_1}^2+(\frac{\partial \overline{\beta}_2}{\partial x_3}-\frac{\partial \overline{\beta}_3}{\partial x_3})\kappa x_1=0 \tag{2.161}$$

$$(\frac{\partial \overline{\beta}_3}{\partial x_1}-\frac{\partial \overline{\beta}_2}{\partial x_1})\kappa x_2+(\frac{\partial \overline{\beta}_2}{\partial x_2}-\frac{\partial \overline{\beta}_3}{\partial x_2})\kappa x_1-\frac{\partial \overline{p}}{\partial x_3}+\frac{\partial \overline{\beta}_2}{\partial x_3}+\frac{\partial \overline{\beta}_3}{\partial x_3}+\frac{\partial \overline{\beta}_3}{\partial x_3}\kappa^2({x_1}^2+{x_2}^2)+\frac{\partial \overline{\beta}_7}{\partial x_3}b^2=0 \tag{2.162}$$

In the above relations, the variable $\overline{p}$ is obtained from the boundary condition related to the lateral surface of the right circular cylinder, which is free from an external mechanical traction. By allowing for Eq. (2.20) and the normal vector to the lateral surface, $\overline{\mathbf{n}} = n_1\mathbf{e}_1 + n_2\mathbf{e}_2$, tractions on the surface are obtained as:

$$t_1^{(\overline{\mathbf{n}})} = (\sigma_{11} - [\![\sigma_{11}^S]\!])n_1 + (\sigma_{21} - [\![\sigma_{21}^S]\!])n_2 = 0 \tag{2.163}$$

$$t_2^{(\overline{\mathbf{n}})} = (\sigma_{12} - [\![\sigma_{12}^S]\!])n_1 + (\sigma_{22} - [\![\sigma_{22}^S]\!])n_2 = 0 \tag{2.164}$$

$$t_3^{(\overline{\mathbf{n}})} = (\sigma_{13} - [\![\sigma_{13}^S]\!])n_1 + (\sigma_{23} - [\![\sigma_{23}^S]\!])n_2 = 0 \tag{2.165}$$

Furthermore, the non-zero components of $\boldsymbol{\sigma}^S$ are deduced from Eq. (2.23) as:

$$\sigma_{11}^S = m_3 b_3 - \frac{{b_3}^2}{2\mu_0}, \qquad \sigma_{22}^S = m_3 b_3 - \frac{{b_3}^2}{2\mu_0}, \qquad \sigma_{33}^S = \frac{{b_3}^2}{2\mu_0} \tag{2.166}$$

Also, since the air surrounding the MAE is not magnetized, the jump in the stress tensor, $\boldsymbol{\sigma}^S$, on the lateral surface can be expressed as:

$$[\![\sigma_{11}^S]\!] = [\![\sigma_{22}^S]\!] = -\frac{b_3^{+2}}{2\mu_0} - m_3^- b_3^- + \frac{b_3^{-2}}{2\mu_0}, \qquad [\![\sigma_{33}^S]\!] = \frac{b_3^{+2}}{2\mu_0} - \frac{b_3^{-2}}{2\mu_0} \tag{2.167}$$

Now, for simplification purposes, a cylindrical coordinate system is adopted in order to simplify the above-stated formulas. The coordinate system is located at the center of bottom face of the MAE, which yields:

$$x_1 = r\cos\varphi, \qquad x_2 = r\sin\varphi` \tag{2.168}$$

where $r = \sqrt{x_1^2 + x_2^2}$ is the radial distance between a particle and the center, and φ is for the angle with respect the axis x_1. Additionally, it is evident that $n_1 = \cos\varphi$ and $n_2 = \sin\varphi$.

For the given stress field for the MAE subject to a finite torsion, Eq. (2.165) is automatically satisfied and Eqs. (2.163) and (2.164) can be rewritten as

$$t_1^{(\bar{\mathbf{n}})} = (\sigma_{11} - [\![\sigma_{11}^S]\!])n_1 + \sigma_{21}n_2 = 0 \tag{2.169}$$

$$t_2^{(\bar{\mathbf{n}})} = \sigma_{12}n_1 + (\sigma_{22} - [\![\sigma_{22}^S]\!])n_2 = 0 \tag{2.170}$$

We addressed the boundary condition associated with the bottom surface of the cylinder previously. The torque developed at the top surface of the cylinder can be obtained from integration of the applied in-plane mechanical tractions on the surface with $\mathbf{n} = \mathbf{e}_3$. The mechanical tractions developed at the top surface can be obtained from Eq. (2.20), as:

$$t_1^{(\mathbf{e}_3)} = \sigma_{31} - [\![\sigma_{31}^S]\!] = \sigma_{31} \tag{2.171}$$

$$t_2^{(\mathbf{e}_3)} = \sigma_{32} - [\![\sigma_{32}^S]\!] = \sigma_{32} \tag{2.172}$$

where use has been made of $[\![\sigma_{31}^S]\!] = [\![\sigma_{32}^S]\!] = 0$.

Using the expressions for the stresses in Eq. (2.155), the above expressions for the tractions can be expressed in the cylindrical coordinate system as

$$t_r^{(\mathbf{e}_3)} = 0 \tag{2.173}$$

$$t_\varphi^{(\mathbf{e}_3)} = (\bar{\beta}_2 - \bar{\beta}_3)\kappa r \tag{2.174}$$

The applied torque is subsequently obtained from:

$$T = \int_A r t_\varphi^{(\mathbf{e}_3)} dA = \int_A (\bar{\beta}_2 - \bar{\beta}_3)\kappa r^2 dA \tag{2.175}$$

where the domain of integration A defines the area of the top surface of the cylinder.

As mentioned earlier, the magnetic field is assumed to be homogenous in the cylinder, which satisfies the Maxwell's equations.

2.6.2 Formulation of the Material Model

Let us raise one underlying point on hyperelastic models allowing for finite torsion of the cylinder addressed before. The widely used constitutive equations such as, neo-Hookean and Mooney-Rivlin models exhibit a linear relation between the torque and the twist angle [6]. The measured torque-deflection characteristics of the rubber and the MAE, shown in Figure 2-7, however show notably nonlinear properties. In the study, the I_1-based energy density function, proposed by Lopez-Pamies [25], is applied to describe the observed nonlinearity. In fact, the simulation associated with the torsion test based on the model has the potential for being nonlinear considering the experimental observations. Next, the reported energy density function is modified for the deformable magnetic medium, as:

$$W = \sum_{i=1}^{m} \frac{3^{1-\alpha_i}}{2\alpha_i} G_i^* (I_1^{\alpha_i} - 3^{\alpha_i}) + f(I_7) \tag{2.176}$$

with

$$G_i^* = G_i(1+\gamma_i I_7), \qquad f(I_7) = \eta I_7 \tag{2.177}$$

where G_i, γ_i, α_i and η are material constants to be considered from the experimental data, and m is an integer. It is also assumed that the material constants obtained for the case involving pure mechanical loading are a function of the magnetic field inside the material, which implies that the stiffness of the material alters under the application of a magnetic field. Additionally, given the fact that terms proposed for G_i^* and $f(I_7)$ are linear functions with respect to I_7, the material model is efficient at fields below average ones.

It should be noted that in the absence of the magnetic field, the proposed density function presented in Eq. (2.176) is identical to the original material model proposed by Lopez-Pamies [25], which is also very similar to the constitutive equation proposed for large elastic deformation of rubbers by Arruda and Boyce [14]. For the purely magnetic loading case, the energy is equivalent to that for a rigid ferromagnetic material. In this case, using Eq. (2.81), it can be shown that $\frac{\partial W}{\partial I_7}|_{\mathbf{F}=\mathbf{I}} = \eta = -\frac{\mu_r - 1}{2\mu_0\mu_r}$. Furthermore, the stored energy vanishes in the absence of both the mechanical and magnetic loadings.

The parameters of the general constitutive equation, namely $\overline{\beta}_2$, $\overline{\beta}_3$ and $\overline{\beta}_7$, for the incompressible MAE, are identified considering the stored energy function proposed in Eq. (2.176), such that

$$\overline{\beta}_2 = \sum_{i=1}^{m} 3^{1-\alpha_i} G_i^* {I_1}^{\alpha_i - 1} \tag{2.178}$$

$$\overline{\beta}_3 = 0 \tag{2.179}$$

$$\overline{\beta}_7 = \sum_{i=1}^{m} \frac{3^{1-\alpha_i}}{\alpha_i} G_i \gamma_i ({I_1}^{\alpha_i} - 3^{\alpha_i}) + \eta \tag{2.180}$$

Using the above relations in Eq. (2.175) yields an expression for the applied torque, as:

$$T = \sum_{i=1}^{m} 3^{1-\alpha_i} \int_A G_i^* (3 + \kappa^2 r^2)^{\alpha_i - 1} \kappa r^2 dA = 2\pi \sum_{i=1}^{m} 3^{1-\alpha_i} G_i^* \int_0^R (3 + \kappa^2 r^2)^{\alpha_i - 1} \kappa r^3 dr \tag{2.181}$$

By using integration by parts, the above integral reduces to:

$$\int_0^R (3 + \kappa^2 r^2)^{\alpha_i - 1} \kappa r^3 dr = \frac{(3 + \kappa^2 R^2)^{\alpha_i} (\alpha_i R^2 \kappa^2 - 3) + 3^{\alpha_i + 1}}{2\alpha_i (\alpha_i + 1)\kappa^3} \tag{2.182}$$

and the applied torque is subsequently obtained, as:

$$T = \frac{\pi}{\kappa^3} \sum_{i=1}^{m} G_i^* \frac{3^{1-\alpha_i} (3 + \kappa^2 R^2)^{\alpha_i} (\alpha_i R^2 \kappa^2 - 3) + 3^2}{\alpha_i (\alpha_i + 1)} \tag{2.183}$$

Using the relations for parameters, $\overline{\beta}_2$, $\overline{\beta}_3$ and $\overline{\beta}_7$, in Eqs (2.178)-(2.180), together with the invariants presented in Eqs. (2.149) to (2.151), the equilibrium equations, Eqs. (2.160) to (2.162), for the proposed material model can be written as:

$$-\frac{\partial \overline{p}}{\partial x_1} + \frac{\partial \overline{\beta}_2}{\partial x_1} + \frac{\partial \overline{\beta}_2}{\partial x_1} \kappa^2 {x_2}^2 - \frac{\partial \overline{\beta}_2}{\partial x_2} \kappa^2 x_1 x_2 - \overline{\beta}_2 \kappa^2 x_1 = 0 \tag{2.184}$$

$$-\frac{\partial \overline{\beta}_2}{\partial x_1} \kappa^2 x_1 x_2 - \overline{\beta}_2 \kappa^2 x_2 - \frac{\partial \overline{p}}{\partial x_2} + \frac{\partial \overline{\beta}_2}{\partial x_2} + \frac{\partial \overline{\beta}_2}{\partial x_2} \kappa^2 {x_1}^2 = 0 \tag{2.185}$$

$$-\frac{\partial \overline{\beta}_2}{\partial x_1} \kappa x_2 + \frac{\partial \overline{\beta}_2}{\partial x_2} \kappa x_1 - \frac{\partial \overline{p}}{\partial x_3} = 0 \tag{2.186}$$

where Eq. (2.186) yields:

$$\frac{\partial \overline{p}}{\partial x_3} = 0 \tag{2.187}$$

indicating that $\overline{p}$ is not a function of x_3. Moreover, the derivative of parameter $\overline{p}$ with respect to the cylindrical coordinates, r and φ, can be obtained as:

$$\frac{\partial \overline{p}}{\partial \varphi} = \frac{\partial \overline{p}}{\partial x_1}\frac{\partial x_1}{\partial \varphi} + \frac{\partial \overline{p}}{\partial x_2}\frac{\partial x_2}{\partial \varphi} = 0 \tag{2.188}$$

$$\frac{d\overline{p}}{dr} = \frac{\partial \overline{p}}{\partial x_1}\frac{\partial x_1}{\partial r} + \frac{\partial \overline{p}}{\partial x_2}\frac{\partial x_2}{\partial r} = \sum_{i=1}^{m} 3^{1-\alpha_i} G_i^* \kappa^2 r[-(3+\kappa^2 r^2)^{\alpha_i - 1} + 2(\alpha_i - 1)(3+\kappa^2 r^2)^{\alpha_i - 2}] \tag{2.189}$$

From the above relations, it is deduced that the parameter $\overline{p}$ is only a function of r. Performing integration on both sides of Eq. (2.189) with respect to r leads to an expression for $\overline{p}$, as:

$$\overline{p} = \sum_{i=1}^{m} 3^{1-\alpha_i} G_i^* [(3+\kappa^2 r^2)^{\alpha_i} / 2\alpha_i + (3+\kappa^2 r^2)^{\alpha_i - 1}] + C \tag{2.190}$$

where C is the constant of integration, which is determined considering boundary condition related to the lateral surface of the cylinder (r=R). Using the traction defined in Eqs. (2.169) and (2.170), together with the stress field and the normal vector to the surface in the cylindrical coordinate system, yields:

$$\overline{p} = \overline{\beta}_2^{\,*} - [\![\sigma_{11}^S]\!] \tag{2.191}$$

where

$$\overline{\beta}_2^* = \sum_{i=1}^{m} 3^{1-\alpha_i} G_i \left(1+\gamma_i b^2\right)\left(3+\kappa^2 R^2\right)^{\alpha_i - 1} \tag{2.192}$$

The material constants of the proposed stored energy function in Eq. (2.176), namely G_i and α_i are estimated using the load-deflection curve and the shear modulus obtained from the experiments, and the methodology reported in [29].

The curve-fitting process is initially applied to the relation in Eq. (2.183) considering the zero magnetic field. From Figure 2-8, it is evident that the curve is concave down first and then straight. Consequently, two terms in the torque relation in Eq. (2.183) (m=2) are considered sufficient, as suggested in [29]. The values of G_1, G_2, α_1 and α_2 are identified following the curve-fitting procedure as:

$$G_1 = 62.640\ kPa, \quad G_2 = 12\ kPa, \quad \alpha_1 = 0.6, \quad \alpha_2 = -100, \tag{2.193}$$

The effectiveness of the proposed model is examined by comparison of the model-predicted torque-deflection characteristics with the measured data. Figure 2-16 compares the torque-twist result obtained from the proposed formulation with the experimental data in the absence of the applied magnetic field. The comparison suggests very good agreement between the analytical solution and the experimental data. The dependence of the material properties on the applied

magnetic field is characterized by the constants γ_1 and γ_2 in the proposed material model. These are obtained from the curve-fitting processes, as:

$$\gamma_1 = 0.522\ 1/T^2, \qquad \gamma_2 = 3.100\ 1/T^2 \tag{2.194}$$

Figure 2-16 further compares the model-predicted torque-deflection responses with the measured data for two different values of the induced magnetic field (b = 0.2 T; b = 0.4 T). The comparisons suggest good agreements between the theory and the experiment in the presence of applied magnetic fields. Additionally, the coefficient of determination calculated based on the relation $R^2 = 1 - \sum_i (T_i^{EXP} - T_i^{THEOR})^2 / \sum_i (T_i^{EXP} - \bar{T}_i^{EXP})^2$ with $\bar{T}_i^{EXP} = \sum_i \bar{T}_i^{EXP} / n_p$ (n_p is the number of experimental points) for the fields of 0 T, 0.2 T and 0.4 T, respectively, is 99.92%, 99.98% and 99.95%.

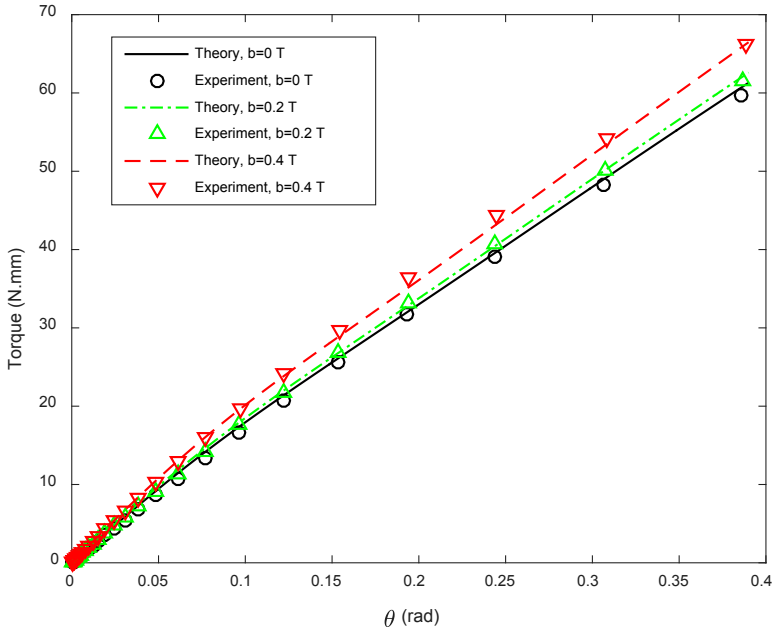

Figure 2-16. Comparison of theoretical and experimental results for MAE at various magnetic fields.

2.7 Summary

In the present chapter, a general formulation was presented for the finite deformation analysis of isotropic magnetoactive elastomers. Upon presenting principles of mechanics along with

magnetism for a deformable body, a general stored energy function defined with respect to some invariants was introduced. Laboratory experiments were performed to measure the permeability of the MAE fabricated with 15% volume fraction of carbonyl iron particles and the torque-deflection response of the right circular cylindrical MAE sample for various applied magnetic fields. Subsequently, a linear model of the MAE was developed on the basis of experimental observations, and the model constants were estimated through curve-fitting of the measured data. Furthermore, the experimental results and the analytical solution for the finite torsion of a cylinder were used to propose a material model for large deformation of the MAEs. The comparison of the model-predicted torque-deflection responses of the MAE with the measured data showed very good agreement with the experimental results.

CHAPTER 3

ANISOTROPIC MAGNETOACTIVE ELASTOMERS AT LARGE DEFORMATIONS

3.1 Introduction

The current chapter is concerned with the development of novel constitutive equations for the anisotropic magnetoactive elastomers (MAEs) considering the chain-like structure of the iron particles in the medium resulting in anisotropy in the mechanical and magnetic properties. The constitutive equations are formulated for anisotropic MAEs on the basis of the framework used for the isotropic elastomers in the previous chapter. A hyperelastic material model is subsequently proposed for the incompressible magnetoelastic medium representing transversely-isotropic MAEs to investigate its response behaviour in the presence of the applied magnetic field while undergoing finite deformations. Constants of the proposed material model are estimated using the laboratory measured torque-deflection responses. For this purpose, the transversely-isotropic MAE samples in circular cylindrical geometry with 15% iron particle volume fraction were fabricated and experiments were designed to measure the permeability and torque-twist response of the MAE. The experimental results are utilized to identify the parameters in the proposed material model. The effectiveness of the proposed constitutive equations is demonstrated through comparison of the model-predicted and measured torque-deflection responses under different levels of the magnetic field.

3.2 Constitutive Equation

In this section, the general form of the constitute equation is presented for the compressible and incompressible anisotropic magnetoactive elastomers.

3.2.1 Compressible Transversely Isotropic MAE

What distinguishes the transversely isotropic MAE from their isotropic counterpart is the formation of the chain of iron particles in the direction of the applied magnetic field, which essentially leads to both mechanical and magnetic anisotropy. To develop a material model for this class of materials, we take advantage of the strategy implemented in modelling of purely mechanical anisotropic elastomers. First, suppose that **A** is a unit vector aligned with the chain direction of the MAE in the reference configuration, which is also denoted as the axis of the transverse isotropy. Following the mechanical deformation, $d\mathbf{x} = \mathbf{F}.d\mathbf{X}$, the vector, **A**, from the reference configuration deforms to the vector, **a**, in the deformed configuration, such that:

$$\mathbf{a} = \mathbf{F}.\mathbf{A} \tag{3.1}$$

where the magnitude of the vector **a** is not necessarily unity.

Based on the approach adopted by Spencer [56] for developing the finite constitutive equations for an anisotropic medium and also for satisfying the principle of material objectivity (material frame indifference), the energy density can be described in terms of the right Cauchy-Green deformation tensor, $\mathbf{C} = \mathbf{F}^T.\mathbf{F}$, the Lagrangian magnetic field, $\tilde{\mathbf{B}} = \mathbf{F}^T.\mathbf{b}$ (pull back of the magnetic field induction from current to reference configuration) and the unit chain vector, **A**. Thus, the stored energy function would be related to **C**, $\tilde{\mathbf{B}}$ and **A** as $W = W\left(\mathbf{C}, \tilde{\mathbf{B}}, \mathbf{A}\right)$ for the class of deformable anisotropic magnetic media. The material magnetic field induction is essential for satisfying the material objectivity. Dependency of the energy density on the chain direction is mainly due to anisotropy of the MAEs addressed herein. As it is conventional in the finite deformation of elastomers, here a general stored energy which is dependent on some invariants associated with the above-mentioned tensors is proposed as:

$$W = W(I_1, I_2, I_3, I_4, I_5, I_6, I_7, I_8, I_9, I_{10}) \tag{3.2}$$

where the most of the invariants have been introduced in Eqs. (1.6)-(1.8), (1.28), (1.29) and (2.47)-(2.49), and

$$I_9 = \mathbf{A}.(\tilde{\mathbf{B}}\tilde{\mathbf{B}}).\mathbf{A} = \mathbf{a}.(\mathbf{b}\mathbf{b}).\mathbf{a} \tag{3.3}$$

$$I_{10} = \mathbf{A}.((\mathbf{C}.\tilde{\mathbf{B}})(\mathbf{C}.\tilde{\mathbf{B}})).\mathbf{A} = \mathbf{a}.((\mathbf{G}.\mathbf{b})(\mathbf{G}.\mathbf{b})).\mathbf{a} \tag{3.4}$$

In the above, I_1-I_3 are invariants of the tensor **C** and I_4 and I_5 are invariants associated with transversely isotropic hyperelasticity. Furthermore, I_6, I_7 and I_8 are concerned with the isotropic

magneto-mechanical behavior, while I_9 and I_{10} are considered in the model to capture the coupled anisotropic magneto-mechanical property of the medium. It is noted that $\mathbf{G} = \mathbf{F}.\mathbf{F}^T$ is the left Cauchy-Green deformation tensor. Additionally, it is worth noting that the invariants I_4, I_5, I_9 and I_{10} remain unaltered when the direction of the chain is reversed.

Now, considering Eqs. (2.35) and (3.2)-(3.4), and using the chain rule differentiation, the Cauchy stress tensor can be described in the following form:

$$\boldsymbol{\sigma} = J^{-1}\sum_{p=1}^{10}\frac{\partial W}{\partial I_p}\mathbf{F}.(\frac{\partial I_p}{\partial \mathbf{F}})^T \tag{3.5}$$

Next, by taking advantage of Eqs. (2.53)-(2.61) along with the following relations

$$\frac{\partial I_4}{\partial \mathbf{C}} = \mathbf{A}\mathbf{A}, \tag{3.6}$$

$$\frac{\partial I_5}{\partial \mathbf{C}} = \mathbf{A}(\mathbf{C}.\mathbf{A}) + (\mathbf{C}.\mathbf{A})\mathbf{A} \tag{3.7}$$

$$\frac{\partial I_9}{\partial \mathbf{F}} = 2(\mathbf{b}.\mathbf{a})\mathbf{b}\mathbf{A}, \tag{3.8}$$

$$\frac{\partial I_{10}}{\partial \mathbf{F}} = 2[(\mathbf{G}.\mathbf{b})(\mathbf{a}.\mathbf{G}.\mathbf{b})\mathbf{A} + \mathbf{a}(\mathbf{a}.\mathbf{G}.\mathbf{b})(\mathbf{b}.\mathbf{F}) + \mathbf{b}(\mathbf{a}.\mathbf{G}.\mathbf{b})(\mathbf{a}.\mathbf{F})] \tag{3.9}$$

$$\frac{\partial I_9}{\partial \mathbf{b}} = 2(\mathbf{b}.\mathbf{a})\mathbf{a} \tag{3.10}$$

$$\frac{\partial I_{10}}{\partial \mathbf{b}} = 2\mathbf{a}.\mathbf{G}(\mathbf{a}.\mathbf{G}.\mathbf{b}) \tag{3.11}$$

and employing the Cayley-Hamilton theorem, the Cauchy stress tensor can be expressed as follows:

$$\begin{aligned}\boldsymbol{\sigma} = \bar{\boldsymbol{\sigma}} + \beta_7(\mathbf{G}.\mathbf{b})\mathbf{b} + \beta_8\{(\mathbf{G}^2.\mathbf{b})\mathbf{b} + (\mathbf{b}.\mathbf{G})(\mathbf{G}.\mathbf{b})\} + \beta_9(\mathbf{b}.\mathbf{a})\mathbf{a}\mathbf{b} + \\ \beta_{10}[\mathbf{a}(\mathbf{a}.\mathbf{G}.\mathbf{b})(\mathbf{G}.\mathbf{b}) + (\mathbf{G}.\mathbf{a})(\mathbf{a}.\mathbf{G}.\mathbf{b})\mathbf{b} + (\mathbf{G}.\mathbf{b})(\mathbf{a}.\mathbf{G}.\mathbf{b})\mathbf{a}]]\end{aligned} \tag{3.12}$$

where the symmetric tensor $\bar{\boldsymbol{\sigma}}$ is:

$$\bar{\boldsymbol{\sigma}} = \beta_1\mathbf{I} + \beta_2\mathbf{G} + \beta_3\mathbf{G}^{-1} + \beta_4\mathbf{a}\mathbf{a} + \beta_5[\mathbf{a}(\mathbf{G}.\mathbf{a}) + (\mathbf{G}.\mathbf{a})\mathbf{a}] \tag{3.13}$$

with

$$\begin{aligned}&\beta_1 = \frac{2}{\sqrt{I_3}}[\frac{\partial W}{\partial I_3}I_3 + I_2\frac{\partial W}{\partial I_2}], \quad \beta_2 = \frac{2}{\sqrt{I_3}}\frac{\partial W}{\partial I_1}, \quad \beta_3 = -2\sqrt{I_3}\frac{\partial W}{\partial I_2}, \quad \beta_4 = \frac{2}{\sqrt{I_3}}\frac{\partial W}{\partial I_4} \\ &\beta_5 = \frac{2}{\sqrt{I_3}}\frac{\partial W}{\partial I_5}, \quad \beta_7 = \frac{2}{\sqrt{I_3}}\frac{\partial W}{\partial I_7}, \quad \beta_8 = \frac{2}{\sqrt{I_3}}\frac{\partial W}{\partial I_8}, \quad \beta_9 = \frac{2}{\sqrt{I_3}}\frac{\partial W}{\partial I_9}, \quad \beta_{10} = \frac{2}{\sqrt{I_3}}\frac{\partial W}{\partial I_{10}}\end{aligned} \tag{3.14}$$

With respect to the magnetization vector, by following the same procedure as the stress tensor and bearing in mind Eq. (2.45), we have:

$$Jm_i = -\sum_{p=1}^{10} \frac{\partial W}{\partial I_p} \frac{\partial I_p}{\partial b_i} \tag{3.15}$$

which after undertaking some mathematical operations, one can write:

$$\mathbf{m} = -(\beta_6 \mathbf{b} + \beta_7 \mathbf{G}.\mathbf{b} + \beta_8 \mathbf{G}^2.\mathbf{b} + \beta_9 (\mathbf{b}.\mathbf{a})\mathbf{a} + \beta_{10} (\mathbf{a}.\mathbf{G}.\mathbf{b})(\mathbf{a}.\mathbf{G})) \tag{3.16}$$

in which β_7, β_8, β_9 and β_{10} are defined in Eq. (3.14) and β_6 can be obtained as:

$$\beta_6 = \frac{2}{\sqrt{I_3}} \frac{\partial W}{\partial I_6} \tag{3.17}$$

3.2.2 Incompressible Transversely Isotropic MAE

In this study, we restrict ourselves to incompressible transversely isotropic magnetoactive elastomers. By applying the incompressibility condition, i.e. $I_3 = 1$, the energy density function can be expressed as:

$$W = W(I_1, I_2, I_4, I_5, I_6, I_7, I_8, I_9, I_{10}) - p(J-1) \tag{3.18}$$

where p stands for the Lagrange multiplier.

Using the same procedure described in the preceding section for deriving the Cauchy stress tensor for the compressible transversely isotropic magnetoelastic medium, one can find:

$$\begin{aligned} \boldsymbol{\sigma} = \overline{\boldsymbol{\sigma}} + \overline{\beta}_7 (\mathbf{G}.\mathbf{b})\mathbf{b} + \overline{\beta}_8 \{(\mathbf{G}^2.\mathbf{b})\mathbf{b} + (\mathbf{b}.\mathbf{G})(\mathbf{G}.\mathbf{b})\} + \overline{\beta}_9 (\mathbf{b}.\mathbf{a})(\mathbf{a})\mathbf{b} + \\ \overline{\beta}_{10} [(\mathbf{a})((\mathbf{a}).\mathbf{G}.\mathbf{b})(\mathbf{G}.\mathbf{b}) + (\mathbf{G}.(\mathbf{a}))((\mathbf{a}).\mathbf{G}.\mathbf{b})\mathbf{b} + (\mathbf{G}.\mathbf{b})((\mathbf{a}).\mathbf{G}.\mathbf{b})(\mathbf{a})]] \end{aligned} \tag{3.19}$$

where

$$\overline{\boldsymbol{\sigma}} = -\overline{p}\mathbf{I} + \overline{\beta}_2 \mathbf{G} + \overline{\beta}_3 \mathbf{G}^{-1} + \overline{\beta}_4 \mathbf{a}\mathbf{a} + \overline{\beta}_5 [\mathbf{a}(\mathbf{G}.\mathbf{a}) + (\mathbf{G}.\mathbf{a})\mathbf{a}] \tag{3.20}$$

in which $\overline{p} = p - \overline{\beta}_1$ and $\overline{\beta}_i$ are described as:

$$\begin{aligned} &\overline{\beta}_1 = 2I_2 \frac{\partial W}{\partial I_2}, \quad \overline{\beta}_2 = 2\frac{\partial W}{\partial I_1}, \quad \overline{\beta}_3 = -2\frac{\partial W}{\partial I_2}, \quad \overline{\beta}_4 = 2\frac{\partial W}{\partial I_4} \\ &\overline{\beta}_5 = 2\frac{\partial W}{\partial I_5}, \quad \overline{\beta}_7 = 2\frac{\partial W}{\partial I_7}, \quad \overline{\beta}_8 = 2\frac{\partial W}{\partial I_8}, \quad \overline{\beta}_9 = 2\frac{\partial W}{\partial I_9}, \quad \overline{\beta}_{10} = 2\frac{\partial W}{\partial I_{10}} \end{aligned} \tag{3.21}$$

In view of the magnetization for the incompressible magnetoactive elastomers, we have

$$\mathbf{m} = -(\overline{\beta}_6\mathbf{b} + \overline{\beta}_7\mathbf{G}.\mathbf{b} + \overline{\beta}_8\mathbf{G}^2.\mathbf{b} + \overline{\beta}_9(\mathbf{b}.\mathbf{a})\mathbf{a} + \overline{\beta}_{10}(\mathbf{a}.\mathbf{G}.\mathbf{b})(\mathbf{a}.\mathbf{G})) \tag{3.22}$$

where

$$\overline{\beta}_6 = 2\frac{\partial W}{\partial I_6} \tag{3.23}$$

3.2.3 Transversely Isotropic Ferromagnetic Materials with Negligible Magnetostriction

MAEs used for vibration control and isolation applications generally show negligible magnetostriction effect due to the usage of rather stiff base elastomer during the fabrication process. In the present section, we aim at constructing a relation between the magnetic parameters for an anisotropic magnetic medium for which the magnetostriction is negligible. As addressed in the first chapter, i.e. Eq. (1.52), for a fully anisotropic case we have

$$\mathbf{m} = \boldsymbol{\chi}.\mathbf{h} \quad \text{or} \quad m_i = \chi_{ij}h_j \tag{3.24}$$

where $\boldsymbol{\chi} = \chi_{ij}\mathbf{e}_i\mathbf{e}_j$ is the second-order susceptibility tensor. In what follows, there is attempt to simplify the above relation given the chain of iron particles. To this aim, suppose that **Q** is an orthogonal transformation tensor defined between two coordinate systems. In the new coordinate system, represented by the superscript prime and obtained by applying the tensor **Q**, we have

$$m'_i = \chi'_{ij}h'_j \tag{3.25}$$

Additionally, the following relations among components of **m** and **h** in the two coordinate systems can be constructed [110]:

$$m'_i = Q_{ij}m_j, \qquad m_i = Q_{ji}m'_j \tag{3.26}$$

$$h'_i = Q_{ij}h_j, \qquad h_i = Q_{ji}h'_j \tag{3.27}$$

and consequently

$$\chi_{ij} = Q_{mi}Q_{nj}\chi'_{mn} \quad \text{or} \quad \chi'_{ij} = Q_{im}Q_{jn}\chi_{mn} \tag{3.28}$$

For a transversely isotropic material with a chain along the axis x_3, the transformation tensor can be represented by:

$$[Q_{ij}] = \begin{bmatrix} \cos\phi & \sin\phi & 0 \\ -\sin\phi & \cos\phi & 0 \\ 0 & 0 & 1 \end{bmatrix} \tag{3.29}$$

where ϕ is an arbitrary value. Thus, by choosing two values of ϕ (0 and π), it is deduced that the nonzero components of the susceptibility tensor are χ_{11}, χ_{22} and χ_{33}, and the relation $\chi_{11} = \chi_{22}$ holds. As a result, Eq. (3.24) reduces to

$$m_1 = \chi_{11} h_1, \qquad m_2 = \chi_{11} h_2, \qquad m_3 = \chi_{33} h_3 \tag{3.30}$$

Additionally, by substituting Eq. (3.30) in Eq. (2.15), we have:

$$b_1 = \mu_0 (1 + \chi_{11}) h_1, \qquad b_2 = \mu_0 (1 + \chi_{11}) h_2, \qquad b_3 = \mu_0 (1 + \chi_{33}) h_3 \tag{3.31}$$

and equivalently

$$b_1 = \mu_0 \mu_{11}^r h_1, \qquad b_2 = \mu_0 \mu_{22}^r h_2, \qquad b_3 = \mu_0 \mu_{33}^r h_3 \tag{3.32}$$

where

$$\mu_{11}^r = \mu_{22}^r = (1 + \chi_{11}), \qquad \mu_{33}^r = (1 + \chi_{33}) \tag{3.33}$$

It must be remarked that Eq. (3.32) can be accomplished by making use of Eq. (1.51) and carrying out the same procedure as the one used for simplifying the susceptibility tensor.

Assuming that there exists an energy function that can be defined with respect to the magnetic field induction and the unit vector of symmetry for the transversely isotropic material, the magnetization vector can be attained from derivative of the energy function with respect to the magnetic field. Thus, we have

$$m_i = -\frac{\partial \psi^{mag}}{\partial b_i} \tag{3.34}$$

The magnetic energy can be expressed by [56]:

$$\psi^{mag} = -\xi_1 b_i b_i - \xi_2 A_i A_j b_i b_j \tag{3.35}$$

where ξ_1 and ξ_2 are two unknown constants that must be evaluated experimentally.

With the knowledge of the magnetic energy density and taking derivative with respect to the magnetic field induction, we have

$$m_i = 2\xi_1 b_i + 2\xi_2 A_k b_k A_i \tag{3.36}$$

Now let us investigate ξ_1 and ξ_2 in terms of the constants of the relative magnetic permeability and susceptibility tensors. Assuming that the chains of iron particles are aligned with x_3-axis of the rectangular coordinate system, consequently $\mathbf{A} = \{0,0,1\}^T$, Eq. (3.36) yields:

$$m_1 = 2\xi_1 b_1, \qquad m_2 = 2\xi_1 b_2, \qquad m_3 = 2(\xi_1 + \xi_2) b_3 \tag{3.37}$$

By combining Eqs. (3.30) and (3.31), we are able to extract relations between m_i and b_i. Accordingly, by making an analogy between the relations and Eq. (3.37), the following relations are accomplished:

$$\xi_1 = \frac{1}{2\mu_0}\frac{\chi_{11}}{(1+\chi_{11})} = \frac{1}{2\mu_0}\frac{\mu_{11}^r - 1}{\mu_{11}^r}, \qquad \xi_2 = \frac{1}{2\mu_0}\frac{\chi_{33} - \chi_{11}}{(1+\chi_{11})(1+\chi_{33})} = \frac{1}{2\mu_0}\frac{\mu_{33}^r - \mu_{11}^r}{\mu_{11}^r \mu_{33}^r} \tag{3.38}$$

Also, the above relations are derived using the expressions for the relative permeability, presented in Eq. (3.33). As can be verified, the unknowns in the magnetic energy density have been expressed with respect to the components of the susceptibility and permeability tensors for a transversely isotropic magnetic material.

3.3 Incompressible Transversely Isotropic Hyperelastic Model for MAEs

It is customary in the literature of anisotropic elastomers that some new mixed invariants defined with respect to the direction of fibers as well as deformation tensors (such as left and right Cauchy-Green deformation tensors) are utilized. In fact some terms are appended to the traditional models implemented into the isotropic hyperelasticity. In the present section, the intent is to introduce a nonlinear material model for a transversely isotropic magnetoactive elastomer. To this aim, the isotropic hyperelastic model developed by Lopez-Pamies [25] is employed and tailored for the anisotropic MAE. It must be also pointed out that Moreira and Nunes [50] presented a transversely isotropic material model given Lopez-Pamies' model and successfully validated the predictive results using experimental reports of a soft fiber-reinforced composite under the simple shear test. The adaption of the nonlinear elastic model to the MAE with chains of iron particles can be addressed in two phases. First, the model must be modified with respect to the transverse isotropy and afterwards the energy connected with magnetic contribution must be appended to it. As for the first process, as explained in detail in the introduction, it is obligatory to use not only I_4 but also I_5 on the account of compatibility with transversely isotropic linear elasticity, please see [33] for more information. With respect to the

magnetic properties, the counterpart of the energy density presented in Eq. (3.35) for a deformable magnetic material by making use of the invariants I_7 and I_9 should be added to the energy density. It is assumed that the incompressibility constraint of elastomeric materials is still valid for MAEs and it results in the fact that the third invariant of the Cauchy-Green deformation tensor is unity. All in all, the following energy density is employed in the present contribution:

$$W = \sum_{i=1}^{m} \frac{3^{1-\alpha_i}}{2\alpha_i} G_i^* (I_1^{\alpha_i} - 3^{\alpha_i}) + \omega_1^* (2I_4 - I_5 - 1) + \omega_2^* (I_4 - 1)^2 - \xi_1 I_7 - \xi_2 I_9 \tag{3.39}$$

where for the sake of simplicity the overscript of W has been dropped and α_i, ξ_1 and ξ_2 are some constants and it is further assumed that G_i^*, ω_1^* and ω_2^* are a linear function of I_7 so that

$$G_i^* = G_i(1+\eta_i I_7), \qquad \omega_1^* = \omega_1(1+\gamma_1 I_7), \qquad \omega_2^* = \omega_2(1+\gamma_2 I_7) \tag{3.40}$$

Notice that the above supposition is consistent with fields below enough the magnetic saturation due to the linearity of the functions with respect to I_7.

3.4 Experiments

All information associated with the fabrication and experimental analysis of the MAE is presented in the present section.

3.4.1 Fabrication of MAE

In this section, the process associated with the fabrication of the anisotropic MAE is introduced briefly. As explained before, the MAE has two main constituents involving a rubbery matrix and iron particles. As for the matrix, the rubber Ecoflex 00-50 is adopted. This rubber has two parts called parts A and B in the fluid form and after mixing them by ratio 1A:1B (weight or volume) the final product which is very soft and stretchy is obtained. With respect to the iron particles, BASF soft carbonyl iron powder is used similar to the isotropic case. For the fabrication of transversely isotropic MAE with the volume fraction of 15%, parts A and B of the rubber Ecoflex 00-50 with the same volume ratio are mixed with proper amount of the iron powder in appropriate time, subsequent to degassing, the fluid mixture is poured in the tube-form molds shown in Figure 3-1 and finally the molds are placed between two poles of the electromagnetic represented in Figure 3-2 with the applied field of 1 T which is big enough to achieve the chains of iron particles that are the reason of both the mechanical and magnetic

anisotropy. Two types of the cylindrical sample with the diameter of 20 mm are produced called Type-I and Type-II, see Figure 3-3. In Type-I samples the iron-particle chains of MAE are parallel to the cylinder axis, while in Type-II samples the chains are transverse to the central axis. In addition, it is pointed out that the tube has been utilized for fabrication purposes has inner diameter of 20 mm and outer diameter of 25 mm and its length is 38 mm.

Figure 3-1. Tube used as mold.

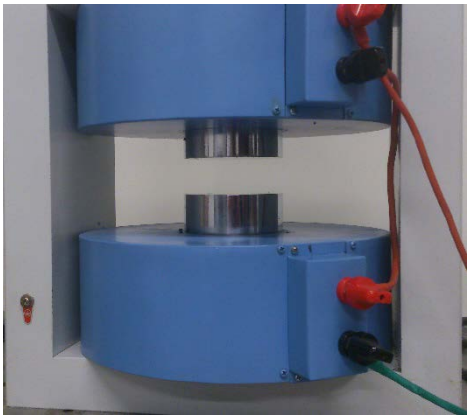

Figure 3-2. Electromagnet used for fabrication of the anisotropic MAE.

3.4.2 Measurement of MAE Magnetic Permeability

For the fabricated MAEs, the magnetic properties of the material are not constant in all directions. The presence of chains of iron particles in the medium leads to the anisotropic magnetic behavior of the material. Also, by assuming a transversely isotropic model, there exist two constants associated with the magnetic second-order permeability tensor. To explore these

two values, indicating the ability of the material to be magnetized under the application of an external magnetic field, two types of sample are taken into account involving Type-I and Type-II MAEs, see Figure 3-3. As pointed out before, the chains are aligned with the axis of the cylinder in the former, but they are transverse to the axis of symmetry of cylinder for the latter. By exploiting the homogeneity of the magnetic parameters over the cross section for a cylinder in which the external magnetic field is normal to its axis, types I and II, we are able to estimate the permeability of the MAE. To this end, the magnetic fields inside the body are measured under low fields so that the linear relations between the magnetic parameters are still valid and magnetostriction is negligible.

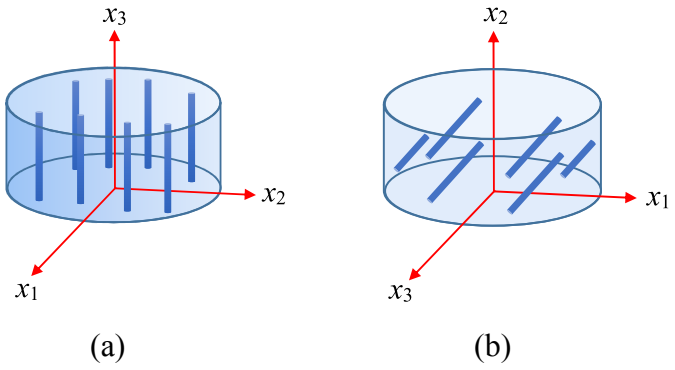

Figure 3-3 Schematic of (a) Type-I and (b) Type-II samples.

From type-I MAE, we are able to estimate the magnetic permeability with respect to x_1-axis or x_2-axis. Notice that the axis x_3 is along the chains of iron particles. To this aim, analogous to the procedure conducted for the isotropic MAE, magnetic field induction and strength inside the material in the direction of x_1-axis can be obtained from probes B and A, respectively. With the knowledge of b_1 and h_1 and Eq. (3.32), the relative permeability can be obtained from

$$\mu_{11}^{r} = \mu_0^{-1} \frac{b_1}{h_1} \tag{3.41}$$

Similarly, for Type-II sample, by taking advantage of the homogeneity of the internal magnetic fields, the following relation is implemented to find the magnetic constant:

$$\mu_{33}^{r} = \mu_0^{-1} \frac{b_3}{h_3} \tag{3.42}$$

As has been depicted in Figure 3-4 and Figure 3-5, two probes have been utilized to measure the magnetic fields in the small neighborhood of the sample. It should be remarked that what is

reported by the probes is indeed the magnetic fields in the air surrounding the sample and by taking advantage of the boundary conditions associated with a magnetic medium the probes A and B, respectively, indicate the vertical magnetic field strength and induction in the anisotropic MAE. Based on the experiments conducted, the following values have been obtained $\mu_{11}^{r}=1.35$ and $\mu_{33}^{r}=2.3$. As expected, the relative permeability in the chain direction is higher than the transverse direction. It is also valuable to mention that the relative permeability of the isotropic sample with the similar constituents is about 1.5.

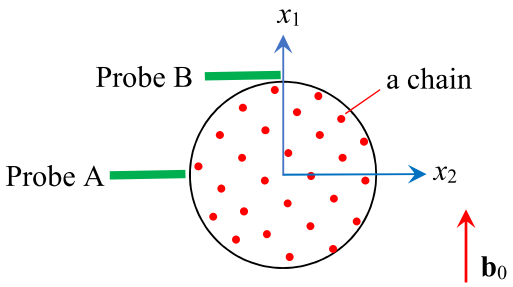

Figure 3-4. Cross section of type-I MAE.

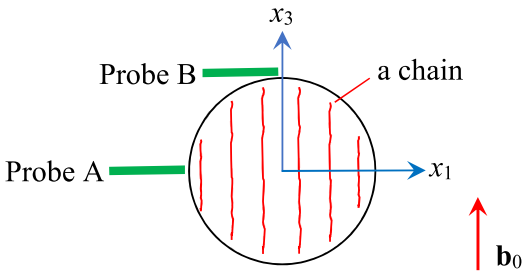

Figure 3-5. Cross section of type-II MAE.

3.4.3 Torsion of a Right Circular Cylinder

In this chapter, use is made of the circular cylinder, addressed previously, to carry out some tests in order to explore the coupled magneto-mechanical features of the transversely isotropic material. It is also worth noting that the sample has the diameter of 20 mm and the length of 6.4 mm so that the ratio of the length to radius is L/R=0.64.

To accomplish the so-called torque-twist diagrams for the MAE, some magneto-mechanical tests are conducted on type-I samples. More precisely, the MA right circular cylinders are twisted under the application of an external torque on the top surface in the presence and absence of the magnetic field which is originally parallel to the cylinder axis. Similar to the isotropic case, a magneto-rheometer is utilized to conduct the experiments. A detailed description of the magneto-rheometer, shown in Figure 3-6, has been addressed in the previous chapter. It is also worthwhile mentioning that the test condition is completely similar to the isotropic case. For the purpose of the brevity, the information is not dealt with herein.

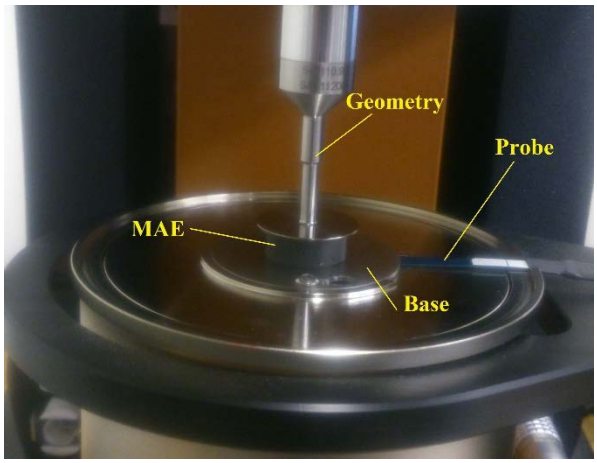

Figure 3-6 MAE under torsion test.

3.5 Analytical Solution for Torsion of a Cylinder

For the anisotropic MAE, the same analytical solution as the isotropic one is adopted. Indeed, for the case in which the iron chains are parallel to the cylinder axis, use can be made of the deformation field presented in Eq. (2.142), see Figure 3-3 (a). Simply, the kinematic relations developed in the previous chapter, i.e. Eqs. (2.142), (2.143) and (2.145)-(2.148) are used. Additionally, analogous to the isotropic case, it is supposed the dominant magnetic field is in the axial direction which is the direction of the original magnetic field. Consequently, the invariants presented in Eqs. (1.6)-(1.8), (1.28), (1.29), (2.47)-(2.49), (3.3) and (3.4) for this deformation are

$$I_1 = 3 + \kappa^2 r^2 \tag{3.43}$$

$$I_2 = 3 + \kappa^2 r^2 \tag{3.44}$$

$$I_3 = 1 \tag{3.45}$$

$$I_4 = 1 + \kappa^2 r^2 \tag{3.46}$$

$$I_5 = (1 + \kappa^2 r^2)^2 + \kappa^2 r^2 \tag{3.47}$$

$$I_6 = b^2 \tag{3.48}$$

$$I_7 = b^2 \tag{3.49}$$

$$I_8 = b^2(\kappa^2 r^2 + 1) \tag{3.50}$$

$$I_9 = b^2 \tag{3.51}$$

$$I_{10} = b^2(\kappa^2 r^2 + 1)^2 \tag{3.52}$$

As it can be realized for the finite torsion based on the proposed deformation field the third invariant of the right Cauchy-Green deformation tensor is equal to unity which is consistent with the assumption made on the incompressibility of the material.

In addition, it must be pointed out that the energy density proposed in the previous section depends on the invariants I_1, I_4, I_5, I_7 and I_9. By bearing this information along with Eqs. (3.19), (3.20) and (3.22) in mind, the Cauchy stress tensor and the magnetization vector find the following forms:

$$\boldsymbol{\sigma} = \overline{\boldsymbol{\sigma}} + \overline{\beta}_7(\mathbf{G}.\mathbf{b})\mathbf{b} + \overline{\beta}_9(\mathbf{b}.\mathbf{a})\mathbf{a}\mathbf{b} \tag{3.53}$$

in which

$$\overline{\boldsymbol{\sigma}} = -\overline{p}\mathbf{I} + \overline{\beta}_2\mathbf{G} + \overline{\beta}_4\mathbf{a}\mathbf{a} + \overline{\beta}_5[\mathbf{a}(\mathbf{G}.\mathbf{a}) + (\mathbf{G}.\mathbf{a})\mathbf{a}] \tag{3.54}$$

and

$$\mathbf{m} = -(\overline{\beta}_7\mathbf{G}.\mathbf{b} + \overline{\beta}_9(\mathbf{b}.\mathbf{a})\mathbf{a}) \tag{3.55}$$

Now by substituting **G**, **b** and **a** into the constitutive equation for the stress above, the components of the stress field can be obtained as:

$$\sigma_{11} = -\overline{p} + \overline{\beta}_2(1 + x_2{}^2\kappa^2) + \overline{\beta}_4 x_2{}^2\kappa^2 + \overline{\beta}_5(4x_2{}^2\kappa^2 + 2x_1{}^2x_2{}^2\kappa^4 + 2x_2{}^4\kappa^4) \tag{3.56}$$

$$\sigma_{22} = -\overline{p} + \overline{\beta}_2(1 + x_1{}^2\kappa^2) + \overline{\beta}_4 x_1{}^2\kappa^2 + \overline{\beta}_5(4x_1{}^2\kappa^2 + 2x_1{}^2x_2{}^2\kappa^4 + 2x_1{}^4\kappa^4) \tag{3.57}$$

$$\sigma_{33} = -\overline{p} + \overline{\beta}_2 + \overline{\beta}_4 + \overline{\beta}_5(2x_2{}^2\kappa^2 + 2x_1{}^2\kappa^2 + 2) + \overline{\beta}_7 b^2 + \overline{\beta}_9 b^2 \tag{3.58}$$

$$\sigma_{12} = -\overline{\beta}_2(x_1x_2\kappa^2) - \overline{\beta}_4(x_1x_2\kappa^2) + \overline{\beta}_5(-2x_1{}^3x_2\kappa^4 - 2x_1x_2{}^3\kappa^4 - 4x_1x_2\kappa^2) \tag{3.59}$$

$$\sigma_{21} = -\overline{\beta}_2(x_1x_2\kappa^2) - \overline{\beta}_4(x_1x_2\kappa^2) + \overline{\beta}_5(-2x_1{}^3x_2\kappa^4 - 2x_1x_2{}^3\kappa^4 - 4x_1x_2\kappa^2) \tag{3.60}$$

$$\sigma_{13} = -\overline{\beta}_2(x_2\kappa) + \overline{\beta}_4(-x_2\kappa) + \overline{\beta}_5(-2x_1{}^2x_2\kappa^3 - 2x_2{}^3\kappa^3 - 3x_2\kappa) + \overline{\beta}_7(-x_2\kappa)b^2 + \overline{\beta}_9(-x_2\kappa)b^2 \tag{3.61}$$

$$\sigma_{31} = -\overline{\beta}_2(x_2\kappa) + \overline{\beta}_4(-x_2\kappa) + \overline{\beta}_5(-2x_1{}^2x_2\kappa^3 - 2x_2{}^3\kappa^3 - 3x_2\kappa) \tag{3.62}$$

$$\sigma_{23} = \overline{\beta}_2(x_1\kappa) + \overline{\beta}_4(x_1\kappa) + \overline{\beta}_5(2x_1{x_2}^2\kappa^3 + 2{x_1}^3\kappa^3 + 3x_1\kappa) + \overline{\beta}_7(x_1\kappa)b^2 + \overline{\beta}_9(x_1\kappa)b^2 \tag{3.63}$$

$$\sigma_{32} = \overline{\beta}_2(x_1\kappa) + \overline{\beta}_4(x_1\kappa) + \overline{\beta}_5(2x_1{x_2}^2\kappa^3 + 2{x_1}^3\kappa^3 + 3x_1\kappa) \tag{3.64}$$

As expected, the stress tensor is not symmetric.

Now let us apply the boundary condition associated with the lateral surface of the cylinder for which normal to the surface has a null component along the x_3 axis, n_3=0. It is noted that the lateral surface is free from any mechanical surface tractions and consequently based on Eq. (2.20), the following can be written:

$$t_1 = n_1\sigma_{11} + n_2\sigma_{21} - n_1[\![\sigma_{11}^S]\!] - n_2[\![\sigma_{21}^S]\!] \tag{3.65}$$

$$t_2 = n_1\sigma_{12} + n_2\sigma_{22} - n_1[\![\sigma_{12}^S]\!] - n_2[\![\sigma_{22}^S]\!] \tag{3.66}$$

$$t_3 = n_1\sigma_{13} + n_2\sigma_{23} - n_1[\![\sigma_{13}^S]\!] - n_2[\![\sigma_{23}^S]\!] \tag{3.67}$$

Considering the related stress field components on the lateral surface and using Eqs. (3.65) and (3.66), it is concluded that:

$$\overline{p}(r=R) = \overline{\beta}_2(r=R) + \overline{\beta}_3(r=R) - [\![\sigma_{22}^S]\!] \tag{3.68}$$

where $[\![\sigma_{22}^S]\!] = -\frac{\mu_0}{2} m_3 m_3$ and R is the radius of the cylinder. Also, it should be remarked that the stress field satisfies Eq. (3.67).

Now with respect to the applied mechanical tractions on the top surface in which $n_1 = n_2 = 0$ and $n_3 = 1$, the following can be expressed:

$$t_1 = \sigma_{31} \tag{3.69}$$

$$t_2 = \sigma_{32} \tag{3.70}$$

Afterwards, by integration over the area the applied torque along the axis of the cylinder can be obtained by undertaking some mathematical manipulations as:

$$T_3 = \int_A [(\overline{\beta}_2 + \overline{\beta}_4)r^2\kappa + \overline{\beta}_5(2r^4\kappa^3 + 3r^2\kappa)]dA \tag{3.71}$$

To attain an explicit expression for the applied torque, $\overline{\beta}_2$, $\overline{\beta}_4$ and $\overline{\beta}_5$ should be explored using the proposed stored energy presented in Eq. (3.39). Thus substituting Eq. (3.39) in Eq. (3.21) yields:

$$\overline{\beta}_2 = \sum_{i=1}^{m} 3^{1-\alpha_i} G_i^* {I_1}^{\alpha_i - 1} = \sum_{i=1}^{m} 3^{1-\alpha_i} G_i^* (3 + \kappa^2 r^2)^{\alpha_i - 1} \tag{3.72}$$

$$\overline{\beta}_4 = 4[\omega_1^* + \omega_2^*(I_4 - 1)] = 4[\omega_1^* + \omega_2^* \kappa^2 r^2] \tag{3.73}$$

$$\overline{\beta}_5 = -2\omega_1^* \tag{3.74}$$

Subsequently, by inserting the above equations in Eq. (3.71) and conducting some mathematical operations, an expression for the applied torque can be obtained as:

$$T_3 = 2\pi\{\sum_{i=1}^{m} G_i^* \frac{3^{1-\alpha_i}(3+\kappa^2 R^2)^{\alpha_i}(\alpha_i \kappa^2 R^2 - 3) + 3^2}{2\alpha_i(\alpha_i + 1)\kappa^3} + \frac{2}{3}(\omega_2^* - \omega_1^*)\kappa^3 R^6 - \frac{1}{2}\omega_1^* \kappa R^4\} \tag{3.75}$$

It is worth noting that the above equation will be implemented to identify the unknowns associated with the material model later.

Next, the conservation of the linear momentum for the torsion problem in the present work is investigated. Given Eq. (2.10) and in the absence of the mechanical body force and the magnetic body force, due to the assumption that the internal magnetic field is homogenous, the equilibrium equation can be written as

$$\sigma_{11,1} + \sigma_{21,2} + \sigma_{31,3} = 0 \tag{3.76}$$

$$\sigma_{12,1} + \sigma_{22,2} + \sigma_{32,3} = 0 \tag{3.77}$$

$$\sigma_{13,1} + \sigma_{23,2} + \sigma_{33,3} = 0 \tag{3.78}$$

Upon inserting the stress field presented in Eqs. (3.56)-(3.64), in the above equations, it can be found from last equation above, Eq. (3.78), that the parameter $\overline{p}$ is not a function of x_3. Additionally, derivatives of $\overline{p}$ with respect to x_1 and x_2 can be attained using Eqs. (3.76) and (3.77), respectively. Subsequently, using the chain rule operation and considering that $x_1 = r\cos\varphi$ and $x_2 = r\sin\varphi$, it is feasible to find the derivative of $\overline{p}$ based on the cylindrical coordinates r and φ as:

$$\frac{\partial \overline{p}}{\partial \varphi} = \frac{\partial \overline{p}}{\partial x_1}\frac{\partial x_1}{\partial \varphi} + \frac{\partial \overline{p}}{\partial x_2}\frac{\partial x_2}{\partial \varphi} = -r\frac{\partial \overline{p}}{\partial x_1}\sin\varphi + r\frac{\partial \overline{p}}{\partial x_2}\cos\varphi = 0 \tag{3.79}$$

$$\frac{d\overline{p}}{dr} = \frac{\partial \overline{p}}{\partial x_1}\frac{\partial x_1}{\partial r} + \frac{\partial \overline{p}}{\partial x_2}\frac{\partial x_2}{\partial r} = \frac{\partial \overline{p}}{\partial x_1}\cos\varphi + \frac{\partial \overline{p}}{\partial x_2}\sin\varphi \tag{3.80}$$

which infers that $\overline{p}$ is independent of φ. Now, with the knowledge of the derivative of $\overline{p}$ with respect to x_1 and x_2, as discussed previously, Eq. (3.80) can be restated as:

$$\begin{aligned}\frac{d\overline{p}}{dr} &= \sum_{i=1}^{m} 3^{1-\alpha_i} G_i^*[2\kappa^2 r(\alpha_i - 1)(3+\kappa^2 r^2)^{\alpha_i - 2} - \kappa^2 r(3+\kappa^2 r^2)^{\alpha_i - 1}] \\ &+ 4\kappa^2 r[\kappa^2 r^2(\omega_1 - \omega_2) + \omega_1]\end{aligned} \tag{3.81}$$

Integration of Eq. (3.81) with respect to *r*, results in the following expression for $\overline{p}$:

$$\begin{aligned}\overline{p} &= \sum_{i=1}^{m} 3^{1-\alpha_i} G_i^* [(3+\kappa^2 r^2)^{\alpha_i - 1} - \frac{1}{2\alpha_i}(3+\kappa^2 r^2)^{\alpha_i}] \\ &+\kappa^4 r^4 (\omega_1 - \omega_2) + 2\kappa^2 r^2 \omega_1 + C\end{aligned} \tag{3.82}$$

The constant of integration, *C*, in Eq. (3.82) can be accomplished using the expression for $\overline{p}$ in Eq. (3.68) and can be expressed as:

$$C = \sum_{i=1}^{m} 3^{1-\alpha_i} G_i^* \frac{1}{2\alpha_i}(3+\kappa^2 R^2)^{\alpha_i} - \kappa^4 R^4 (\omega_1^* - \omega_2^*) - 2\kappa^2 R^2 \omega_1^* - [\![\sigma_{22}^S]\!] \tag{3.83}$$

Subsequent to the conservation of the linear momentum, satisfaction of the principle of the angular momentum must be verified. To accomplish this, firstly, the components of the magnetization vector are derived using Eq. (3.55) as:

$$m_1 = (\overline{\beta}_7 + \overline{\beta}_9) b x_2 \kappa \tag{3.84}$$

$$m_2 = -(\overline{\beta}_7 + \overline{\beta}_9) b x_1 \kappa \tag{3.85}$$

$$m_3 = (\overline{\beta}_7 + \overline{\beta}_9) b \tag{3.86}$$

where

$$\begin{aligned}\overline{\beta}_7 &= \sum_{i=1}^{m} \frac{3^{1-\alpha_i}}{\alpha_i} G_i \eta_1 (I_1^{\alpha_i} - 3^{\alpha_i}) + 2\omega_1 \eta_2 (2I_4 - I_5 - 1) + 2\omega_2 \eta_3 (I_4 - 1)^2 - 2\xi_1 \\ &= \sum_{i=1}^{m} \frac{3^{1-\alpha_i}}{\alpha_i} G_i \eta_1 (I_1^{\alpha_i} - 3^{\alpha_i}) + 2\omega_1 \eta_2 (2I_4 - I_5 - 1) + 2\omega_2 \eta_3 (I_4 - 1)^2 - 2\xi_1\end{aligned} \tag{3.87}$$

$$\overline{\beta}_9 = -2\xi_2 \tag{3.88}$$

are obtained by making use of the energy density function in Eq. (3.39) and its substitution in Eq. (3.21).

Allowing for Eq. (2.19) and the magnetization vector and the magnetic field for the finite torsion of the MAE, parts of the body couple vector are

$$l_1 = m_2 b \tag{3.89}$$

$$l_2 = -m_1 b \tag{3.90}$$

$$l_3 = 0 \tag{3.91}$$

As mentioned before, the stress field must satisfy the equations associated with the conservation of the angular momentum, i.e. Eq. (2.11), which can now be explained as

$$\sigma_{23} - \sigma_{32} = -l_1 \tag{3.92}$$
$$\sigma_{31} - \sigma_{13} = -l_2 \tag{3.93}$$
$$\sigma_{12} - \sigma_{21} = -l_3 \tag{3.94}$$

By employing the stress and the body couple fields presented in Eqs. (3.56)-(3.64) and (3.89)-(3.91) in Eqs. (3.92)-(3.94), the satisfaction of the principle of the angular momentum can be achieved. All in all, the assigned deformation field is consistent with the angular and linear momentum. It is also concluded that the proposed deformation field is admissible. Additionally, by supposing that the magnetic fields are homogenous the Maxwell equations are satisfied as well.

An explicit relation for the torsion-twist response of an incompressible transversely isotropic cylindrical MAE as given in Eq. (3.75) was previously derived. Considering only two terms in the summation part in Eq. (3.75) and considering Eq. (3.40), there are 10 unknown material parameters in the developed analytical relation which are G_1, G_2, α_1, α_2, ω_1, ω_2, η_1, η_2, γ_1 and γ_2. These parameters have been identified using least-square minimization approach by minimizing the error between simulation and experimental results and are found to be

$$\begin{aligned} &G_1 = 6.5 \text{ kpa}, \quad G_2 = 58.5 \text{ kpa}, \quad \alpha_1 = 0.6, \quad \alpha_2 = -600, \\ &\omega_1 = -32.5 \text{ kpa}, \quad \omega_2 = 3.125 \text{ kpa}, \quad \eta_1 = 16.6665 \text{ 1/T}^2, \\ &\eta_2 = 16.6666 \text{ 1/T}^2, \quad \gamma_1 = 8.333 \text{ 1/T}^2, \quad \gamma_2 = 33.333 \text{ 1/T}^2 \end{aligned} \tag{3.95}$$

Figure 3-7 shows the comparison of analytical results with those obtained experimentally. As it can be realized, good agreement exists between the theory and the experiment. Also, the value of $R^2 = 1 - \sum_i (T_{3i}^{EXP} - T_{3i}^{THEOR})^2 / \sum_i (T_{3i}^{EXP} - \overline{T}_{3i}^{EXP})^2$, that $\overline{T}_{3i}^{EXP} = \sum_i \overline{T}_{3i}^{EXP} / n_p$ and n_p is the length of the data set, is 99.35% in the absence of the field and 97.79% for the field of 0.2 T.

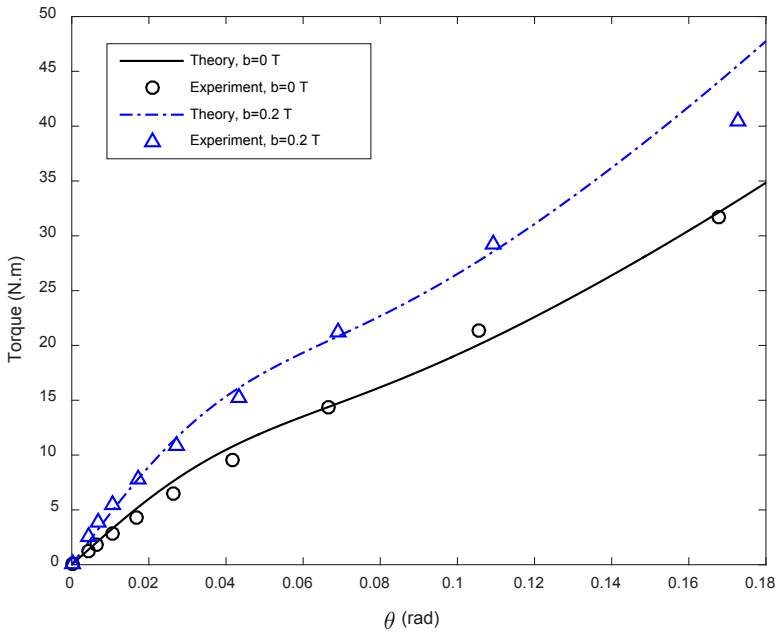

Figure 3-7 Torque-twist response of the MAE.

3.6 Summary

The present chapter was centered on developing a material model for the anisotropic magnetoactive elastomers. After presenting constitutive equations based on some invariants, a novel material model was proposed for the finite deformation of transversely isotropic elastomers. Experimental studies were undertaken on the fabricated samples with the volume fraction 15% in order to find the magnetic and mechanical constants of the MAE. Subsequently, by solving the finite torsion of the anisotropic MAE analytically given the proposed energy density function for the medium and comparing it with experimental results, it was demonstrated that there exists a good consistency between the theoretical analysis and the experimental observations.

CHAPTER 4

CONTRIBUTIONS, CONCLUSIONS AND RECOMMENDATIONS FOR FUTURE WORKS

4.1 Highlights and Major Contributions

Novel Frameworks for finite and small deformation analysis of isotropic and anisotropic MAEs have been presented in the dissertation building upon the continuum mechanics. Constitutive equations for the stress tensor and the magnetization vector have been derived with respect to energy density functions delineated in terms of invariants associated with some parameters. These factors are the right Cauchy-Green deformation tensor and the magnetic field induction vector for the isotropic MAE. With respect to the transversely isotropic medium, there is a dependency on the isotropy unit vector in addition to the aforestated tensors. For both media, a novel energy density function, featuring prominently in the continuum-based approach, which is able to simulate the experimental observations has been proposed. For experimental investigation, isotropic and anisotropic MAEs with the iron volume fraction of 15 per cent have been fabricated in the lab. Afterwards, permeabilities of the MAEs have been successfully measured. Furthermore, experimental data required for estimation of the material unknowns of the constitutive equations has been extracted from the magneto-rheometer via the torsion tests on cylindrical MA elastomers. Then, by making an analogy between the theory and the experiments, it has been illustrated that the formulations associated with the continuum-based approach are in excellent agreement with empirical observations. All in all, the fundamental contributions of the thesis can be outlined as follows:

1. Constitutive equations for finite deformation of the isotropic MAE.
2. Linearization of the general constitutive relations, then elaboration of a linear model for deformation of isotropic magnetoactive elastomers.

3. An energy density function has been recommended for large deformation of MAEs allowing for experimental observations.
4. Fabrication of 15% iron volume fraction MAEs in cylindrical forms, measuring the permeability of the isotropic MAE and conducting torsion tests on isotropic MAEs rigorously and finding the torque-twist response under various magnetic fields by utilization of the magneto-rheometer.
5. The invariant-based formulation for the transversely isotropic magnetoactive elastomer.
6. Proposing an energy density function for finite deformation of the anisotropic MAE based on the experiments.
7. Producing cylindrical MAEs with chains of iron particles resulting in both mechanical and magnetic anisotropy, experimental investigation into measurement of permeabilities of the anisotropic medium, and obtaining the torque-twist response of the transversely isotropic MAEs by taking advantage of the magneto-rheometer.

Furthermore, the outcomes of the PhD dissertation are three articles listed below:

- Beheshti, A., Sedaghati, R., Rakheja, S., Development of a small-deformation material model for an isotropic magnetoactive elastomer, Acta Mechanica, 2020, DOI: 10.1007/s00707-020-02647-1.
- Beheshti, A., Sedaghati, R., Rakheja, S., Finite deformation analysis of isotropic magnetoactive elastomers, Continuum Mechanics and Thermodynamics, 2020, under review.
- Beheshti, A., Sedaghati, R., Rakheja, S., Transversely isotropic magnetoactive elastomers: theory and experiments, Smart Materials and Structures, 2020, under review.

4.2 Conclusions

The main conclusions of the PhD thesis can be summarized as follows:

1. The formulation associated with the continuum-based approach for finite deformation of isotropic MAEs is able to predict mechanical behaviors of the MAEs accurately.

2. The linearized constitutive equations given the decomposition of the magnetic parameters into rigid-body and perturbation states can successfully simulate the empirical observations.
3. The framework for large deformation of the transversely isotropic magnetoactive elastomers and more importantly the energy density function recommended for this smart material are robust and in agreement with experimental data.

4.3 Recommendations for Future Works

The followings are recommended for future research:

1. The research undertaken herein is based on the quasi-static deformation. This work can be extended to dynamic deformation in which a visco-magneto-mechanical material model should be developed on the account of the rate-dependent behavior of this class of materials for both isotropic and transversely isotropic MAEs.
2. Allowing for thermal effects in constitutive equations and the energy density is also a potential research topic.
3. Nonlinear finite element analysis of MAEs is suggested for upcoming studies due to the fact that the analytical solutions are just available to us for simple geometries and loadings.
4. Building upon the proposed framework, a homogenization scheme can be elaborated for not only the isotropic MAE but also the transversely isotropic magnetoactive elastomer.

REFERENCES

[1] Carpi, F., De Rossi, D., Kornbluh, R., Pelrine, R., Sommer-Larsen, P.: Dielectric Elastomers as Electromechanical Transducers Fundamentals Materials Devices Models and Applications of an Emerging Electroactive Polymer Technology. Elsevier Science (2008)

[2] Siboni, M.H., Ponte Castañeda, P.: Macroscopic response of particle-reinforced elastomers subjected to prescribed torques or rotations on the particles. Journal of the Mechanics and Physics of Solids. **91**, 240-264 (2016)

[3] Rudykh, S., Bertoldi, K.: Stability of anisotropic magnetorheological elastomers in finite deformations: A micromechanical approach. Journal of the Mechanics and Physics of Solids. **61**(4), 949-967 (2013)

[4] Harvey, J.A., *Smart Materials*, in *Mechanical Engineers' Handbook: Materials and Mechanical Design*, M. Kutz, Editor. 2005, John Wiley & Sons, Inc. p. 401-418.

[5] Lanotte, L., Ausanio, G., Hison, C., Iannotti, V., Luponio, C., Luponio, C.: State of the art and development trends of novel nanostructured elastomagnetic composites. Journal of Optoelectronics and Advanced Materials. **6**(2), 523-532 (2004)

[6] Batra, R.C.: Elements of continuum mechanics. AIAA education series (2006)

[7] Gurtin, M.E., Fried, E., Anand, L.: The Mechanics and Thermodynamics of Continua. New York: Cambridge University Press (2010)

[8] Ogden, R.W.: Large Deformation Isotropic Elasticity: On the Correlation of Theory and Experiment for Compressible Rubberlike Solids. Proceedings of the Royal Society A: Mathematical, Physical and Engineering Sciences. **328**(1575), 567-583 (1972)

[9] Kankanala, S.V., Triantafyllidis, N.: On finitely strained magnetorheological elastomers. Journal of the Mechanics and Physics of Solids. **52**(12), 2869-2908 (2004)

[10] Dorfmann, A., Ogden, R.W.: Nonlinear magnetoelastic deformations of elastomers. Acta Mechanica. **167**(1-2), 13-28 (2004)

[11] Muhr, A.H.: Modeling the Stress-Strain Behavior of Rubber. Rubber Chemistry and Technology. **78**(3), 391-425 (2005)

[12] Treloar, L.R.G.: Physics of Rubber Elasticity. Oxford University Press

[13] Marckmann, G., Verron, E.: Comparison of Hyperelastic Models for Rubber-Like Materials. Rubber Chemistry and Technology. **79**(5), 835-858 (2006)

[14] Arruda, E.M., Boyce, M.C.: A three-dimensional constitutive model for the large stretch behavior of rubber elastic materials. Journal of the Mechanics and Physics of Solids. **41**(2), 389-412 (1993)

[15] Ball, R.C., Doi, M., Edwards, S.F., Warner, M.: Elasticity of entangled networks. Polymer. **22**(8), 1010-1018 (1981)

[16] Kaliske, M., Heinrich, G.: An Extended Tube-Model for Rubber Elasticity: Statistical-Mechanical Theory and Finite Element Implementation. Rubber Chemistry and Technology. **72**(4), 602-632 (1999)

[17] Amin, A.F.M.S., Lion, A., Sekita, S., Okui, Y.: Nonlinear dependence of viscosity in modeling the rate-dependent response of natural and high damping rubbers in compression and shear: Experimental identification and numerical verification. International Journal of Plasticity. **22**(9), 1610-1657 (2006)

[18] Amin, A.F.M.S., Wiraguna, S.I., Bhuiyan, A.R., Okui, Y.: Hyperelasticity model for finite element analysis of natural and high damping rubbers in compression and shear. Journal of Engineering Mechanics. **132**(1), 54-64 (2006)

[19] Treloar, L.R.G.: Stress-Strain Data for Vulcanized Rubber under Various Types of Deformation. Rubber Chemistry and Technology. **17**(4), 813-825 (1944)

[20] Steinmann, P., Hossain, M., Possart, G.: Hyperelastic models for rubber-like materials: consistent tangent operators and suitability for Treloar's data. Archive of Applied Mechanics. **82**(9), 1183-1217 (2012)

[21] Hasanpour, K., Ziaei-Rad, S., Mahzoon, M.: A large deformation framework for compressible viscoelastic materials: Constitutive equations and finite element implementation. International Journal of Plasticity. **25**(6), 1154-1176 (2009)

[22] Niroomandi, S., Alfaro, I., Cueto, E., Chinesta, F.: Model order reduction for hyperelastic materials. International Journal for Numerical Methods in Engineering. **81**(9), 1180-1206 (2010)

[23] Yeoh, O.H.: Some Forms of the Strain-Energy Function for Rubber. Rubber Chemistry and Technology. **66**(5), 754-771 (1993)

[24] Gent, A.N.: A new constitutive relation for rubber. Rubber Chemistry and Technology. **69**(1), 59-61 (1996)

[25] Lopez-Pamies, O.: A new I-1-based hyperelastic model for rubber elastic materials. Comptes Rendus Mécanique. **338**(1), 3-11 (2010)

[26] Rivlin, R.S., Saunders, D.W.: Large Elastic Deformations of Isotropic Materials. VII. Experiments on the Deformation of Rubber. Philosophical Transactions of the Royal Society A: Mathematical, Physical and Engineering Sciences. **243**(865), 251-288 (1951)

[27] Mooney, M.: A Theory of Large Elastic Deformation. Journal of Applied Physics. **11**(9), 582-592 (1940)

[28] Gent, A.N., Thomas, A.G.: Forms for the stored (strain) energy function for vulcanized rubber. Journal of Polymer Science. **28**(118), 625-628 (1958)

[29] Ogden, R.W.: Large Deformation Isotropic Elasticity - On the Correlation of Theory and Experiment for Incompressible Rubberlike Solids. Proceedings of the Royal Society A: Mathematical, Physical and Engineering Sciences. **326**(1567), 565-584 (1972)

[30] Simo, J.C., Taylor, R.L.: Penalty function formulations for incompressible nonlinear elastostatics. Computer Methods in Applied Mechanics and Engineering. **35**(1), 107-118 (1982)

[31] Simo, J.C., Pister, K.S.: Remarks on Rate Constitutive-Equations for Finite Deformation Problems - Computational Implications. Computer Methods in Applied Mechanics and Engineering. **46**(2), 201-215 (1984)

[32] Hartmann, S., Neff, P.: Polyconvexity of generalized polynomial-type hyperelastic strain energy functions for near-incompressibility. International Journal of Solids and Structures. **40**(11), 2767-2791 (2003)

[33] Murphy, J.G.: Transversely isotropic biological, soft tissue must be modelled using both anisotropic invariants. European Journal of Mechanics - A/Solids. **42**, 90-96 (2013)

[34] Merodio, J., Ogden, R.W.: Mechanical response of fiber-reinforced incompressible non-linearly elastic solids. International Journal of Non-Linear Mechanics. **40**(2-3), 213-227 (2005)

[35] Weiss, J.A., Maker, B.N., Govindjee, S.: Finite element implementation of incompressible, transversely isotropic hyperelasticity. Computer Methods in Applied Mechanics and Engineering. **135**(1-2), 107-128 (1996)

[36] Qiu, G.Y., Pence, T.J.: Remarks on the behavior of simple directionally reinforced incompressible nonlinearly elastic solids. Journal of Elasticity. **49**(1), 1-30 (1997)

[37] Merodio, J., Ogden, R.W.: Material instabilities in fiber-reinforced nonlinearly elastic solids under plate deformation. Arch. Mech. **54** ((5-6)), 525-552 (2002)

[38] Merodio, J., Ogden, R.W.: Instabilities and loss of ellipticity in fiber-reinforced compressible non-linearly elastic solids under plane deformation. International Journal of Solids and Structures. **40**(18), 4707-4727 (2003)

[39] Horgan, C.O., Saccomandi, G.: A new constitutive theory for fiber-reinforced incompressible nonlinearly elastic solids. Journal of the Mechanics and Physics of Solids. **53**(9), 1985-2015 (2005)

[40] Kassianidis, F., Ogden, R.W., Merodio, J., Pence, T.J.: Azimuthal Shear of a Transversely Isotropic Elastic Solid. Mathematics and Mechanics of Solids. **13**(8), 690-724 (2008)

[41] Horgan, C.O., Murphy, J.G.: Torsion of Incompressible Fiber-Reinforced Nonlinearly Elastic Circular Cylinders. Journal of Elasticity. **103**(2), 235-246 (2010)

[42] Horgan, C.O., Murphy, J.G.: Finite extension and torsion of fiber-reinforced non-linearly elastic circular cylinders. International Journal of Non-Linear Mechanics. **47**(2), 97-104 (2012)

[43] Destrade, M., Donald, B.M., Murphy, J.G., Saccomandi, G.: At least three invariants are necessary to model the mechanical response of incompressible, transversely isotropic materials. Computational Mechanics. **52**(4), 959-969 (2013)

[44] Destrade, M., Horgan, C.O., Murphy, J.G.: Dominant negative Poynting effect in simple shearing of soft tissues. Journal of Engineering Mathematics. **95**(1), 87-98 (2014)

[45] Hamdaoui, M.E., Merodio, J., Ogden, R.W., Rodríguez, J.: Finite elastic deformations of transversely isotropic circular cylindrical tubes. International Journal of Solids and Structures. **51**(5), 1188-1196 (2014)

[46] Polignone, D.A., Horgan, C.O.: Cavitation for incompressible anisotropic nonlinearly elastic spheres. Journal of Elasticity. **33**(1), 27-65 (1993)

[47] Lu, J., Zhang, L.: Physically motivated invariant formulation for transversely isotropic hyperelasticity. International Journal of Solids and Structures. **42**(23), 6015-6031 (2005)

[48] Feng, Y., Okamoto, R.J., Namani, R., Genin, G.M., Bayly, P.V.: Measurements of mechanical anisotropy in brain tissue and implications for transversely isotropic material models of white matter. Journal of the Mechanical Behavior of Biomedical Materials. **23**, 117-32 (2013)

[49] Horgan, C.O., Murphy, J.G.: Reverse Poynting Effects in the Torsion of Soft Biomaterials. Journal of Elasticity. **118**(2), 127-140 (2014)

[50] Moreira, C.S., Nunes, L.C.S.: Effects of fiber orientation in a soft unidirectional fiber-reinforced material under simple shear deformation. International Journal of Non-Linear Mechanics. **111**, 72-81 (2019)

[51] Bonet, J., Burton, A.J.: A simple orthotropic, transversely isotropic hyperelastic constitutive equation for large strain computations. Computer Methods in Applied Mechanics and Engineering. **162**(1-4), 151-164 (1998)

[52] Itskov, M., Aksel, N.: A class of orthotropic and transversely isotropic hyperelastic constitutive models based on a polyconvex strain energy function. International Journal of Solids and Structures. **41**(14), 3833-3848 (2004)

[53] Itskov, M., Ehret, A.E., Mavrilas, D.: A polyconvex anisotropic strain-energy function for soft collagenous tissues. Biomech Model Mechanobiol. **5**(1), 17-26 (2006)

[54] Gasser, T.C., Ogden, R.W., Holzapfel, G.A.: Hyperelastic modelling of arterial layers with distributed collagen fibre orientations. Journal of the Royal Society Interface. **3**(6), 15-35 (2006)

[55] Guo, Z.Y., Peng, X.Q., Moran, B.: A composites-based hyperelastic constitutive model for soft tissue with application to the human annulus fibrosus. Journal of the Mechanics and Physics of Solids. **54**(9), 1952-1971 (2006)

[56] Spencer , A.J.M.: Continuum Theory of the Mechanics of Fibre-Reinforced Composites. Wien: Springer-Verlag (1984)

[57] Feng, Y., Okamoto, R.J., Genin, G.M., Bayly, P.V.: On the accuracy and fitting of transversely isotropic material models. Journal of the Mechanical Behavior of Biomedical Materials. **61**, 554-566 (2016)

[58] Pao, Y.-H., *Electromagnetic forces in deformable continua*, in *Mechanics today*, S. Nevat-Nasser, Editor. 1978, Pergamon Press, Inc.: New York p. 209-305.

[59] Krupka, J.: Measurement of the complex permittivity, initial permeability, permeability tensor and ferromagnetic linewidth of gyromagnetic materials. Measurement Science and Technology. **29**(9), 092001 (2018)

[60] Toupin, R.: The Elastic Dielectric. Journal of Rational Mechanics and Analysis. **5**(6), 849-915 (1956)

[61] Toupin, R.A.: A dynamical theory of elastic dielectrics. International Journal of Engineering Science. **1**(1), 101-126 (1963)

[62] Tiersten, H.F.: Coupled Magnetomechanical Equations for Magnetically Saturated Insulators. Journal of Mathematical Physics. **5**(9), 1298-1318 (1964)

[63] Tiersten, H.F.: Variational Principle for Saturated Magnetoelastic Insulators. Journal of Mathematical Physics. **6**(5), 779-787 (1965)

[64] Jordan, N.F., Eringen, A.C.: On the static nonlinear theory of electromagnetic thermoelastic solids—II. International Journal of Engineering Science. **2**(1), 97-114 (1964)

[65] Maugin, G.A., Eringen, A.C.: Deformable Magnetically Saturated Media. I. Field Equations. Journal of Mathematical Physics. **13**(2), 143-155 (1972)

[66] Pao, Y.-H., Yeh, C.-S.: A linear theory for soft ferromagnetic elastic solids. International Journal of Engineering Science. **11**(4), 415-436 (1973)

[67] Hutter, K., Pao, Y.H.: A dynamic theory for magnetizable elastic solids with thermal and electrical conduction. Journal of Elasticity. **4**(2), 89-114 (1974)

[68] Tiersten, H.F., Tsai, C.F.: On the Interaction of the Electromagnetic Field with Heat Conducting Deformable Insulators. Journal of Mathematical Physics. **13**(3), 361-378 (1972)

[69] Brown, W.F.: Magnetoelastic Interactions. Springer-Verlag Berlin. Heidelberg New York, (1966)

[70] Eringen, A.C., Maugin, G.A.: Electrodynamics of Continua I Foundations and Solid Media. Springer-Verlag New York Inc., (1990)

[71] Kovetz, A.: Electromagnet Theory. Oxford University Press. New York: Oxford University Press (2000)

[72] Pao, Y.-H., Hutter, K.: Electrodynamics for moving elastic solids and viscous fluids. Proceedings of the IEEE. **63**(7), 1011-1021 (1975)

[73] Dorfmann, A., Ogden, R.W.: Magnetoelastic modelling of elastomers. European Journal of Mechanics a-Solids. **22**(4), 497-507 (2003)

[74] Dorfmann, A., Ogden, R.W.: Nonlinear magnetoelastic deformations. The Quarterly Journal of Mechanics and Applied Mathematics. **57**(4), 599-622 (2004)

[75] Dorfmann, A., Ogden, R.W.: Some problems in nonlinear magnetoelasticity. Zeitschrift für angewandte Mathematik und Physik. **56**(4), 718-745 (2005)

[76] Brigadnov, I.A., Dorfmann, A.: Mathematical modeling of magneto-sensitive elastomers. International Journal of Solids and Structures. **40**(18), 4659-4674 (2003)

[77] Bustamante, R., Dorfmann, A., Ogden, R.W.: Universal relations in isotropic nonlinear magnetoelasticity. Quarterly Journal of Mechanics and Applied Mathematics. **59**(3), 435-450 (2006)

[78] Bustamante, R.: Mathematical modelling of boundary conditions for magneto-sensitive elastomers: variational formulations. Journal of Engineering Mathematics. **64**(3), 285-301 (2008)

[79] Bustamante, R.: Transversely isotropic nonlinear magneto-active elastomers. Acta Mechanica. **210**(3-4), 183-214 (2009)

[80] Bustamante, R., Dorfmann, A., Ogden, R.W.: On Variational Formulations in Nonlinear Magnetoelastostatics. Mathematics and Mechanics of Solids. **13**(8), 725-745 (2008)

[81] Bustamante, R., Ogden, R.W.: Nonlinear magnetoelastostatics: Energy functionals and their second variations. Mathematics and Mechanics of Solids. **18**(7), 760-772 (2012)

[82] Bustamante, R., Rajagopal, K.R.: Implicit constitutive relations for nonlinear magnetoelastic bodies. Proc Math Phys Eng Sci. **471**(2175), 20140959 (2015)

[83] Saxena, P., Hossain, M., Steinmann, P.: A theory of finite deformation magneto-viscoelasticity. International Journal of Solids and Structures. **50**(24), 3886-3897 (2013)

[84] Danas, K., Kankanala, S.V., Triantafyllidis, N.: Experiments and modeling of iron-particle-filled magnetorheological elastomers. Journal of the Mechanics and Physics of Solids. **60**(1), 120-138 (2012)

[85] Saxena, P., Hossain, M., Steinmann, P.: Nonlinear magneto-viscoelasticity of transversally isotropic magneto-active polymers. Proc Math Phys Eng Sci. **470**(2166), 20140082 (2014)

[86] Spieler, C., Metsch, P., Kastner, M., Ulbricht, V.: Microscale Modeling of Magnetoactive Composites Undergoing Large Deformations. TECHNISCHE MECHANIK. **34**(1), 12 (2014)

[87] Kalina, K.A., Metsch, P., Kästner, M.: Microscale modeling and simulation of magnetorheological elastomers at finite strains: A study on the influence of mechanical preloads. International Journal of Solids and Structures. **102-103**, 286-296 (2016)

[88] Kallio, M.: The elastic and damping properties of magnetorheological elastomers. VTT publications, (2005)

[89] Vicente, J.d., Bossis, G., Lacis, S., Guyot, M.: Permability measurements in cobalt ferrite and carbonyl iron powders and suspensions. Journal of Magnetism and Magnetic Materials. **251**(1), 9 (2002)

[90] An, Y.X., Shaw, M.T.: Actuating properties of soft gels with ordered iron particles: basis for a shear actuator. Smart Materials & Structures. **12**(2), 157-163 (2003)

[91] Lokander, M., Stenberg, B.: Improving the magnetorheological effect in isotropic magnetorheological rubber materials. Polymer Testing. **22**(6), 677-680 (2003)

[92] Dishovsky, N., Ruskova, K., Radulov, I.: "In situ" magnetic modification of polar elastomers. Materials Research Bulletin. **36**(1-2), 35-45 (2001)

[93] Martin, J.E., Venturini, E., Odinek, J., Anderson, R.A.: Anisotropic magnetism in field-structured composites. Physical Review E. **61**(3), 2818-2830 (2000)

[94] Carlson, J.D., Jolly, M.R.: MR fluid, foam and elastomer devices. Mechatronics. **10**(4-5), 555-569 (2000)

[95] Lokander, M., Stenberg, B.: Performance of isotropic magnetorheological rubber materials. Polymer Testing. **22**(3), 245-251 (2003)

[96] Jiles, D.: Introduction to Magnetism and Magnetic Materials. Chapman and Hall (1991)

[97] Guan, X., Dong, X., Ou, J.: Magnetostrictive effect of magnetorheological elastomer. Journal of Magnetism and Magnetic Materials. **320**(3-4), 158-163 (2008)

[98] Boczkowska, A., Awietj, S.: Microstructure and Properties of Magnetorheological Elastomers. Boczkowska A. (Ed.), Advanced Elastomers – Technology, Properties and Applications, InTech, (2012)

[99] Farshad, M., Benine, A.: Magnetoactive elastomer composites. Polymer Testing. **23**(3), 347-353 (2004)

[100] Coquelle, E., Bossis, G.: Mullins effect in elastomers filled with particles aligned by a magnetic field. International Journal of Solids and Structures. **43**(25-26), 7659-7672 (2006)

[101] Chen, L., Gong, X.L., Li, W.H.: Microstructures and viscoelastic properties of anisotropic magnetorheological elastomers. Smart Materials and Structures. **16**(6), 2645-2650 (2007)

[102] Jolly, M.R., Carlson, J.D., Munoz, B.C.: A model of the behaviour of magnetorheological materials. Smart Materials & Structures. **5**(5), 607-614 (1996)

[103] Varga, Z., Filipcsei, G., Zrínyi, M.: Magnetic field sensitive functional elastomers with tuneable elastic modulus. Polymer. **47**(1), 227-233 (2006)

[104] Bellan, C., Bossis, G.: Field Dependence of Viscoelastic Properties of Mr Elastomers. International Journal of Modern Physics B. **16**(17n18), 2447-2453 (2012)

[105] Bodelot, L., Voropaieff, J.P., Pössinger, T.: Experimental investigation of the coupled magneto-mechanical response in magnetorheological elastomers. Experimental Mechanics. **58**(2), 207-221 (2017)

[106] Gong, X.L., Zhang, X.Z., Zhang, P.Q.: Fabrication and characterization of isotropic magnetorheological elastomers. Polymer Testing. **24**(5), 669-676 (2005)

[107] Kordonski, W., Gorodkin, S.: The behavior of a magnetorheological (MR) fluid under compressive deformation. Journal of Rheology. **60**(1), 129-139 (2016)

[108] Eringen, A.C., Suhubi, E.S.: Elastodynamics, Linear theory. Vol. Volume 2. Academic Press (1975)

[109] Sokolnikoff, I.S.: Mathematical Theory of Elasticity. McGraw-Hill Book Company (1946)

[110] Sadd, M.H.: ELASTICITY Theory, Applications, and Numerics. Elsevier Butterworth–Heinemann (2005)